AN INVESTIGATION OF TENSILE BEHAVIOR OF CMC'S AT ROOM AND ELEVATED TEMPERATURES

by

Shaojin Zhang

A Dissertation Submitted To The Graduate Faculty In Engineering In Partial Fulfillment Of The Requirements For The Degree Of Doctor Of Philosophy, The City University of New York

1995

This manuscript has been read and accepted for the Graduate Faculty in Engineering in satisfaction of the dissertation requirement for the degree of Doctor of Philosophy.

4/17/95
Date

Chair of Examining Committee

4/18/95
Date

Executive Officer

Professor F. Delale

Professor B. M. Liaw

Professor A. M. Sadegh
Supervisory Committee

THE CITY UNIVERSITY OF NEW YORK

Abstract

AN INVESTIGATION OF TENSILE BEHAVIOR OF CMC'S
AT ROOM AND ELEVATED TEMPERATURES

by

Shaojin Zhang

Adviser: Professor Feridun Delale

Tensile behavior has been widely recognized as one of the most important properties for ceramic matrix composites. In this study, the tensile failure mechanisms of ceramic matrix composites were investigated experimentally and analytically.

First, unidirectional Nicalon/CAS II tensile specimens with fiber volume fractions of 30% and 40% were tested at room as well as elevated temperatures. All tests exhibited a non-linear stress-strain behavior. Using an innovative in-situ testing technique [1], damages to the specimens at different temperatures and at different loading levels were identified and correlated with the failure behavior of the composites. Matrix crack density was introduced and used to characterize the damage behavior of the composite. The effects of fiber volume fraction and temperature on the failure behavior were also studied. Matrix crack initiation stress showed an increase with increasing fiber volume fraction. However, temperature effect was found not quite significant within the temperature range tested (from room temperature to 700 °C). Specimen size effect was noted and discussed.

Then, two analytical models, one using the singular integral equation technique and the other using finite element method were developed. Both models assume that the composite consists of equally spaced fiber strips in a matrix material and the actual problems were simplified as two dimensional. In the singular integral equation model, a variety of single row H-shaped crack geometries were used to study the singular behavior at the crack tips. In the finite element model, a multiple row H-shaped crack geometry was adopted to simulate the non-linear stress strain behavior. The stress intensity factors and strain energy release rates were calculated for various crack geometries and used to explain the failure behavior of the composite. The results from the singular integral equation formulation predict that once the matrix cracks are formed, they will propagate to the fiber/matrix interface. This behavior conforms with the observed behavior. The results from the finite element model compared well with the experimental results.

ACKNOWLEDGMENTS

I am indebted to my advisor, Professor Feridun Delale for his guidance and support. His advice and support are greatly appreciated. I am very grateful to Professor Ben Liaw for his helpful instruction on the experimentation. I would like to dedicate this work to my father, my wife and my brothers for their encouragement and enduring support. This work was partially supported by AFOSR under grant AFOSR-90-0341.

TABLE OF CONTENTS

LIST OF TABLES

LIST OF FIGURES

NOMENCLATURE

H_1	- half width of the fiber strip
H_2	- half width of the matrix strip
a_1	- transverse crack tip in the fiber medium
a_2	- transverse crack tip in the matrix medium
b_1	- inner interface crack tip
b_2	- outer interface crack tip
V_f	- fiber volume fraction
p_1, p_2	- surface tractions on transverse fiber and matrix cracks
p_3, p_4	- surface tractions on the interface crack (normal and shear components)
E_x, E_x^*	- elastic moduli in x direction for fiber and matrix materials
E_y, E_y^*	- elastic moduli in y direction for fiber and matrix materials
G_{xy}, G_{xy}^*	- shear moduli in x-y plane for fiber and matrix materials
u_i, v_i	- displacements in x and y directions
x_1, y	- coordinates for fiber strip
x_2, y	- coordinates for matrix strip
β_i, β_i^*	- material constants for both fiber and matrix strips
ϕ_i	- crack surface displacement derivatives
ψ_i	- complex surface displacement derivatives
γ_i, γ_i^*	- material constants defined in Appendix B
λ_i, ρ_i	- material constants defined in Appendix B and D

v_{xy}, v^*_{xy}, v_{yx}, v^*_{yx} - material constants for orthotropic materials

$k_i(x_1,\alpha)$, $J_i(x_1,\alpha)$ - kernels related to the fiber crack

$k_i(x_2,a)$, $J_i(x_2,a)$ - kernels related to the matrix crack

$k_i(y,x_1,a)$, $J_i(y,a)$ - kernels related to the interface crack

K_{ij} - the integrand of kernel

K_{ijs} - the integrand of singular kernel

K_{ijf} - the integrand of bounded kernel

$k(a_1)$, $k(a_2)$ - the stress intensity factors at the transverse fiber and matrix crack tips

k_1, k_2 - mode I and mode II stress intensity factors at the interface crack tips

$\frac{\Delta E}{\Delta a}$, G - strain energy release rate

1. INTRODUCTION

The research on ceramic matrix composite materials have intensified in recent years due to some of the appealing features of ceramics, such as great stability and resistance to oxidation under hostile (high temperature or corrosive) environments. In comparison to their metallic and polymer counterparts, ceramics, being brittle and low in tensile strength and fracture toughness, traditionally have had little use in structural applications. However, when reinforced with fibers, ceramic matrix composites exhibit an increase in fracture toughness and tensile strength at room as well as high temperatures [2-3]. A variety of ceramic matrix composite systems have been or are being developed for engineering applications ranging from cutting tools to aerospace structures [4-5]. For example, one can find studies on the following systems of ceramic matrix composites: C/glass [6], C/SiC [7], SiC/glass [8], SiC/LAS glass ceramic [9-14], SiC/BMAS glass-ceramic [14], SiC/alumina [15], SiC/mullite [16], SiC/SiC [17].

In the aforementioned studies, experimental results on damage behaviors of ceramic matrix composites were obtained by failing the specimens with either tensile or three-point bending loading at room or elevated temperatures [10-13]. During the thermomechanical testing, the load *vs.* the displacement (and hence the stress *vs.* the strain) curves were recorded but only the postmortem damage patterns were identified by either a scanning electron or an optical microscope. It is well known that the stress-strain relations of most ceramic matrix composites under thermomechanical loading usually exhibit nonlinear behavior. For such ceramic-matrix composites, the failure mechanisms that cause this nonlinear stress-strain relationship is more complex than that of their monolithic counterparts. These are due to multiple matrix cracking and sequential fiber breaking as a result of weak interfacial bonding between fibers and matrix. The approaches described above although provide important data to the overall understanding of the failure mechanisms of ceramic matrix composites, they fail to correlate the nonlinear stress-strain (and hence the stiffness reduction) behavior with the intermediate damage progression

events inside the ceramic matrix composite specimen. A good experimental approach should provide information on the damage history of the specimen that can be used to correlate the nonlinear stress-strain (and hence the stiffness reduction) behavior with the intermediate causative damage events that occurred in the ceramic matrix composite specimen. Recently, in [18-19], the tensile behavior of a Nicalon/CAS II system was studied. Damage patterns were identified and micrographs were taken to capture the matrix crack propagation. However, these micrographs were not taken at the same location and therefore cannot truly correlate the damage progression with the nonlinear stress-strain behavior. And those studies dealt only with room temperature. In this study, experiments were conducted inside the chamber of a scanning electron microscope equipped with a custom designed tensile/heating substage. This made it possible to directly observe and record *in situ* the progressive tensile damage behavior of the ceramic matrix composites from the very first matrix crack to complete fracture of the specimen at any location in the gage section. Test results for both room and elevated temperatures were obtained. One particular advantage of using SEM is for high temperature testing. Since in SEM, unlike in optical microscope, the electronic lens is always kept at least one inch away from the heated specimen, images can be obtained at magnifications as high as 3000x. without damaging the electronic lens during high temperature testing. This makes the technique very appealing for high temperature testing.

Based on the failure patterns of the composite as observed during the tests, two analytical models have been developed. The thermoelastic properties of the constituents (i.e., the matrix and the fibers), the relative strength of the interface between fibers and matrix, and the volume fraction and arrangement of the fibers are considered in the models. One model utilizes the finite element technique and is based on a periodic multiple-row H-shaped crack configuration. The other uses the singular integral equation method and is based on a variety of single row H-shaped crack configurations. In both models, the real problem is formulated in two dimensional domain.

2. THE EXPERIMENTAL WORK

The experimental work is vital in this study. It provides important insight and data for the understanding of the failure process of this type of composite material. And it also provides the foundation upon which analytical models are based. The technique used in this study is believed to be the first developed in the area of experimental mechanics research.

2.1 THE TESTING PROCEDURE

Figure 2.1 shows a schematic drawing of the experimental set-up which uses a scanning electron microscope equipped with a tensile and heating substage to perform the micromechanical tensile testing of a ceramic matrix composite specimen under high temperature. In this study, a Hitachi S-2400 scanning electron microscope which is equipped with a custom designed E.F. Fullam tensile/heating combined substage is used. The specimen is simple "dog-bone" shaped specimen as shown in Figure 2.2. The actual experimental set-up and tensile/heating substage are shown in Figure 2.3. The material used in this study (Nicalon-fiber/CAS II matrix composite) was obtained from Corning Glass Works. Table 2.1 shows the thermomechanical properties of the constituents of the composite. Specimens of both 30% and 40% fiber volume fractions were tested. To study the size effect, we varied either the thickness or the width of the specimen for specimens with 40% fiber volume fraction. Fibers were unidirectionally aligned with the gage-length direction. The tensile specimens were made by first cutting the large rectangular ceramic matrix composite panel as supplied by Corning Glass Works into smaller rectangular plates using a Leco VC-50 Cari/Cut fine-mesh diamond saw. Then the gage section of the specimens was shaped using the same diamond saw with special a holder. The gage section of the specimens was grounded to its dimensions using a Dremel motorized hand-held grinder with silicon carbide and alumina oxide stones.

Table 2.1 Properties of Nicalon fiber and CAS II matrix

	CAS II Matrix	Nicalon Fiber
Nominal Composition	$CaO\text{-}Al_2O_3\text{-}2SiO_2$	Si_3C_4O
Elastic Modulus Msi(GPa)		
25°C	13.8 (95)	28.3 (195)
1000°C	13.5 (93)	22.9 (158)
1200°C	11.7 (81)	22.5 (155)
Thermal Expansion(10^6/°C)		
	5.0 (25°-1000°C)	3.1 (25°C-200°C)
	--------	4.0 (25°C-1000°C)
Fracture Toughness K_{IC}(MPa $m^{1/2}$)		
25°C	2.16±0.11	--------
1000°C	1.30±0.17	--------
Fiber/Matrix Interfacial Shear Strength		
25°C	15.7±2.0 MPa	

To conduct high temperature testing, the bottom surface of the central part of the specimen, was placed in direct contact with the E.F. Fullam heating element (called heater) which is a rectangular plate made of ceramic material with fuse wire circuit inside. The maximum heated area of the heating element is 0.65"x0.25". It can sustain a maximum working temperature of 1100°C and is equipped with a water-cooled heat sink for continuous operation. Temperature is measured by three platinum 30% rhodium-platinum 6% rhodium thermocouples and controlled by a stand-alone DC power supply with adjustable voltage and current knobs. Since the whole operation is conducted inside the chamber of a scanning electron microscope (in this study a Hitachi S-2400) which is usually vacuumed at $1.5x10^{-6}$ Pa or better, no heat-loss will occur due to thermal

convection. The top surface of the specimen was first polished using fine-grade diamond paste containing 15-, 6-, and 1-micron particles until the surface was well finished and the fibers and matrix could be seen clearly under a Nikon UM-2 microscope. Then the specimen was cleaned using a Bronson ultrasonic cleaner for 10 minutes. Finally the bottom surface of the specimen was coated with silver paint to prevent electric charging and to achieve better image before it was mounted into the E.F. Fullam tensile substage. Because it is very difficult to drill holes in a ceramic composite specimen, the top and bottom ends of the specimen were mounted through stainless steel clamps with serrated teeth to the crossheads of the E.F. Fullam tensile substage. To help in alignment and prevent slippage during testing between the ceramic composite specimen and the serrated clamps, cyanoacrylate-based extra-strength epoxy was also applied on the clamp-specimen interfaces. The clamped specimen was then mounted onto the tensile substage and was left to cure for at least 20 hours to ensure that the epoxy had hardened and was completely dry before testing.

Finally, the specimen together with the tensile/heating assembly was placed inside the chamber of the Hitachi S-2400 scanning electron microscope which is also equipped with a backscatter detector to enhance the image. By using the X-Y staging control of the scanning electron microscope, micrographical patterns within the central gage area can be observed and recorded. The tensile substage is driven by a variable-speed motor which has a maximum speed of 90 rpm. Through a gear mechanism of 100:1 reduction ratio, the crosshead speed can be controlled within 0.127 mm/min (or 0.005 in/min). The tensile stage can provide a tensile load of up to 455 kgs (1000 lbs). The applied load was increased gradually until the specimen failed totally. The damage to the composite as the load increased was first observed on the monitor of the SEM. Then a sequence of micrographs were taken to get hard copies of various microcracking and damage patterns of the specimen at different loading levels. Since the specimen is very thin in thickness (ranges from 1.0 mm to 2.0 mm or 0.04" to .08"), it is assumed that failure will occur

through the thickness. Experimental observation of the failured specimens did indicate that the matrix crack zigzagged through the whole cross section. Thus the recorded micrographs of the surface fracture can represent through-the-thickness failure of the specimen. Quality of the image and hence the quality of the micrographs was further enhanced by transmitting the image signal to a computer which is equipped with an Imaging Technology Advanced Frame Grabber (AFG) digital image analyzer hardware. With the help of the installed software, sharper images were obtained through the contrast and edge enhancement operations. Also text can be added to the micrographs.

The tensile stage is designed in such a way that when the load increases, the top and bottom crossheads move in opposite directions to minimize the shift of the observed site. This is achieved by machining the stainless-steel loading columns into worms of reverse directions. Thus searching and refocusing the damaged zone after each load increment are easily achieved. The applied loads were recorded by a miniature load cell equipped with a digital readout. The relative displacements of the crossheads were measured by a high-precision, strain-gage-type extensometer which is also fitted with a digital readout. The load-displacement data were recorded and converted into a stress-strain curve. The evolution of damage recorded by micrographs were identified with the corresponding stress and strain. Finally the ruptured specimens were observed under a Nikon UM-2 universal measuring microscope for further postmortem examination.

2.2 EXPERIMENTAL RESULTS

2.2.1 Stress-Strain Relations

Typical stress-strain curves for room-temperature, depicting the tensile damage behavior of a Nicalon/CAS II composite with 30% and 40% fiber volume fractions are shown in Figures 2.4 and 2.5 respectively. As depicted in these two figures, the tensile damage behavior of the ceramic matrix composite specimen is characterized by a nonlinear curve made up of three sections. The characteristics are the same for all tests

conducted in this study, even though microscopically these specimens might look quite different. Upon load application, the relation between stress and strain was linear and its slope was equivalent to the stiffness of an intact Nicalon/CAS II specimen (18.15 Msi or 125 GPa for V_f = 30% and 19.6 Msi or 135 GPa for V_f = 40%). For specimens with 30% fiber volume fraction, the slope changed at about 25 ksi (Point A in Figure 2.4). While for 40% fiber volume fraction, the slope changed at about 30 ksi (Point A in Figure 2.5). The first matrix crack is believed to have started at or slightly below of point A in both V_f = 30% and 40% cases. This can be further inferred from the relationship between matrix crack density and tensile stress as will be discussed later in this section. In most cases, matrix cracking initiates either at the edge or at a location where the fiber spacing is maximum. Figure 2.6 shows some micrographs taken during testing. The second micrograph in Figure 2.6 clearly indicates that matrix crack initiated not from the voids but from the location where spacing between two adjacent fibers is the largest. While in Figure 2.7, matrix cracks initiated from both the edge of a fiber and at location where fiber spacing is very large if not the largest. The matrix cracks then propagate perpendicular to the fiber direction throughout the whole width of the gage section to form multiple matrix cracks. Unlike the monolithic materials where failure is controlled by a critical crack size, the failure of the composite goes through a process of damage accumulation. The composite is insensitive to voids and can tolerate very large cracks before failure. At point B (35 ksi for V_f = 30% and 40 ksi for V_f = 40%), the development of multiple matrix cracks reached a saturated stage. Regularly spaced matrix cracks were formed in the whole gage section of the specimen. This happened with only a small increment of tensile stress (about 10 ksi, as can be seen from point A to point B in both Figures 2.4 and 2.5). Further increase of tensile stress creates no or very little additional matrix cracking. Matrix crack opening, fiber debonding, breaking and slipping will dominate the rest of the failure process. Upon reaching point C (about 62 ksi for V_f = 30% and 58 ksi for V_f = 40%), one surface of the matrix cracks in the gage area started to open up with crack opening

displacement far more larger than the rest of the matrix cracks. This then was accompanied by massive fiber breaking and pull-out in that surface. And the eventual separation of the specimen caused the load to drop substantially. Depending on whether the specimen is thin (either in thickness or in width) or thick, there might be a tail in the stress-strain curve at the load drop. Thin specimens tend to have a tail at failure as indicated in Figure 2.5 where both thin and thick specimens were tested. One explanation is that thin specimens are prone to bending during the test. This might be responsible for the lower failure strength and a tail at failure for thin specimens. For thick specimens, failure is always catastrophic. Figure 2.8 shows the progression of damage for a thin specimen. At failure, the specimen (this occurred only for thin specimens) was kept in one piece by the fibers. Further loading after failure was possible as shown in Figure 2.9. Micrographs in Figure 2.10 however, show the catastrophic failure of a thick specimen. Upon reaching the maximum stress value, the specimen fails catastrophically with a very big crack opening at the failure surface. Observation on the failure surfaces of the specimens with 30% and 40% fiber volume fractions, indicated that there are significant differences in both the amount and the length of fiber pull-out between the two specimens. For specimens with V_f = 30%, both the amount and the length of fiber pull-out at failure surface are less than those with V_f = 40% as can be seen from Figures 2.11 and 2.12. The lesser amount of fiber pull-out and the shorter fiber pull-out length is an indication of stronger interfacial bonding strength. This explains why the tensile failure strength of V_f = 30% is slightly higher than that of V_f = 40%. The smoothness of fiber pull-out surface as shown in Figures 2.11 and 2.12 is evidence of non-chemical bonding between fibers and matrix which generally implies weak interfacial bonding strength. It is also noted that the fiber pull-out length and its amount deviated substantially among the same batch of specimens, implying that the fiber/matrix interfacial strength may vary for the same batch of ceramic matrix composite specimens. This is also reflected by the fluctuation of the maximum tensile stresses (Point C) among these tests.

Figure 2.13 is a set of micrographs showing typical damage patterns of the specimen at different magnifications after the stress reached point B in the stress-strain curve. At close-up, one can clearly identify the matrix crack opening, fiber breaking, slipping and fiber bridging of the matrix cracks. Also from Figure 2.13, one can observe the typical "H" shaped crack pattern formed by intersection of the transverse matrix cracks with interface cracks during the failure process. This "H" shaped crack configuration will be used in the analytical models discussed later. Besides the easily identified matrix crack patterns, fiber breaking also exhibits some patterns as shown in Figure 2.14. In Figure 2.14, one fiber breaks at a location away from the matrix cracks first, then a ray of breaking fibers is formed along a line slanted away from the line of matrix cracks. Fiber breaking occurred mostly after the stress reached point B, i.e. after the multiple matrix cracks have been formed.

The stress-strain relations of the Nicalon/CAS II composite at high temperatures will be discussed later.

2.2.2 Matrix Crack Density

Matrix crack density, defined as the number of matrix cracks per 1 mm length in fiber direction, was used to characterize the failure process of the composite. With the help of the scanning electron microscope equipped with a backscatter detector, images reflecting the tensile damage pattern of the composite from the first matrix crack to the eventual failure of the composite were captured. Figures 2.15 and 2.16 are some micrographs showing the development of matrix cracks with increasing stress for V_f = 30% and V_f = 40% respectively. Based on the number of cracks counted in the frame shown in these micrographs and the associated stress level, a matrix crack density versus tensile stress curve was constructed as shown in Figures 2.17 and 2.18 for 30% and 40% fiber volume fractions respectively. From the matrix crack density curves, it is seen that the matrix crack initiation stress is about 25 ksi for V_f = 30% and about 30 ksi for V_f =

40%. These results happen to coincide with point A on the stress-strain curves as shown in both Figures 2.4 and 2.5. As the stress increases, the matrix crack density increases, finally reaching a plateau, meaning that further loading does not result in additional matrix cracking.

2.2.3 Effect of Fiber Volume Fractions

As can be seen from the stress-strain and matrix crack density curves for specimens of both 30% and 40% fiber volume fractions, the fiber volume fraction affects the tensile behavior substantially. Matrix crack initiation stress is less for specimens with less fiber volume fraction (compare points A in Figures 2.4 and 2.5). This result is in agreement with that given in [20-21]. But the tensile failure strength for V_f = 30% is higher than that for V_f = 40% (points C in the stress-strain curves). This might be the result of a relatively stronger interfacial bonding strength for specimens with V_f = 30%. The matrix crack density was found to increase with increasing fiber volume fraction of the specimen. This finding also agrees with that reported in [20-21].

2.2.4 Temperature Effect

The same specimens were tested in the SEM at 250 ^{o}C, 400 ^{o}C, 600 ^{o}C and 700 ^{o}C. Figures 2.19 and 2.20 show the stress-strain curves obtained at higher temperatures for fiber volume fractions 30% and 40% respectively. Within the temperature range tested (room temperature, 250 ^{o}C, 400 ^{o}C, 600 ^{o}C and 700 ^{o}C), no significant changes in ultimate tensile strength have been observed in the stress-strain curves. Figures 2.21 and 2.22 show the temperature effects on the ultimate tensile failure strength of the specimens for both 30% and 40% fiber volume fractions. There was a slight increase in tensile failure strength for V_f = 30% at T = 250 ^{o}C . Micrographs showing the final failure surfaces of the specimens with V_f = 30% at different temperatures were compared. It was observed that both the amount and the length of fiber full-out were the smallest for T = 250 ^{o}C. This might explain why the tensile strength is maximum at T = 250 ^{o}C. For V_f = 40%, this

increase of tensile strength happened at T = 400 ^{o}C. The phenomenon of slight increase of tensile strength might be the result of release of thermal residual stress and changing of interfacial bonding strength due to temperature. Matrix crack density did not show significant changes with temperature. Micrographs in Figure 2.23 show the development of matrix cracks for V_f = 30% taken at T = 600 ^{o}C. And micrographs in Figure 2.24 show the matrix crack development for V_f = 40% taken at T = 400 ^{o}C. Matrix crack initiation stress decreased slightly at high temperatures for V_f = 40%. Micrographs in Figures 2.25 and 2.26 show the fiber breaking and slipping process at high temperatures. Since this composite is basically a glass based material, the stress-strain behavior is expected to be quite different when temperature exceeds over 800 ^{o}C.

2.2.5 Specimen Size Effect

To study the size effect, specimens of 40% fiber volume fraction with different thickness and width combination were used in the tests. It was found that specimens with either relatively thin thickness or width (about 0.0625~0.07") tended to have a quite different failure pattern than thicker ones (greater than 0.0725" in both thickness and width). For thin specimens, first, the tensile strength was quite lower than that of thick specimens; second, when the specimen failed, it had a tail in the stress-strain curve indicating that it still retained some load carrying capability and the specimen was kept in one piece by the fibers. The thick specimens on the other hand always failed catastrophically. A comparison of tensile strength between thin and thick specimens against temperature is shown in Figure 2.27. The discrepancy between the two cases might be the result of bending that might have occurred during the test as explained earlier. For thin Nicalon/CAS II specimens with 40% fiber volume fraction, the stress-strain curves at high temperatures are shown in Figure 2.28.

3. THEORETICAL MODELS

As explained earlier, during experiments, it was found that, after the initiation of transverse matrix cracks at point A (in both Figures 2.4 and 2.5), with increasing load, regularly spaced multiple transverse cracks are formed. When the tensile stress reaches a certain value, almost no new transverse cracks are generated until failure. During this process transverse matrix crack opening, fiber debonding, breaking and sliding at the fiber/matrix interface is believed to dominate the failure process. This typical failure feature is best described by a periodic H-crack configuration as shown in Figure 2.13. Two models, one using singular integral equation technique, and the other using finite element method, are adopted to either explain the failure mechanism or simulate the observed tensile behavior of ceramic matrix composites.

The problem of concern is basically a three dimensional problem because of the discrete distribution of the fibers in the matrix. However, if one assumes that the fibers are made of composite strips of width $2H_1$, the problem can be treated in two dimensions.

3.1 SINGULAR INTEGRAL EQUATIONS FORMULATION.

The singular integral equation technique has been proven very powerful in dealing with crack problems. Figure 3.1 is a sketch of the proposed mathematical model. It is assumed that fibers are equally spaced in the ceramic matrix, and that the thermomechanical and fracture properties of the fiber and the matrix are known. The model contains cracks perpendicular to as well as on the interface and they are assumed to be periodic. By choosing different geometric parameters, one can generate different cracked geometries. For example: If one sets $a_1=0$, $a_2=H_2$ and $b_1=0$ in Figure 3.1, then the model reduces to a geometry with periodic intersecting H-shaped cracks as shown in Figure 3.2. This configuration closely resembles the actual cracked geometry observed in testing.

3.1.1 Formulation of The Problem

3.1.1.1 Equilibrium Equations

In the formulation, each strip is assumed to be orthotropic. The equilibrium equations for orthotropic materials expressed in terms of displacements are as follow [22]:

$$\beta_1\frac{\partial^2 u}{\partial x^2}+\frac{\partial^2 u}{\partial y^2}+\beta_3\frac{\partial^2 v}{\partial x\partial y}=0 \tag{3.1a}$$

$$\frac{\partial^2 v}{\partial x^2}+\beta_2\frac{\partial^2 v}{\partial y^2}+\beta_3\frac{\partial^2 u}{\partial x\partial y}=0 \tag{3.1b}$$

where β_1, β_2 and β_3 are materials constants for orthotropic material.

Assume that the solutions are of the following form:

$$u(x,y) = u^{(1)}(x,y) + u^{(2)}(x,y) \tag{3.2a}$$

$$v(x,y) = v^{(1)}(x,y) + v^{(2)}(x,y) \tag{3.2b}$$

where

$$u^{(1)}(x,y) = \frac{2}{\pi}\int_0^\infty f(\alpha,x)\cos\alpha y\,d\alpha \tag{3.3a}$$

$$v^{(1)}(x,y) = \frac{2}{\pi}\int_0^\infty g(\alpha,x)\sin\alpha y\,d\alpha \tag{3.3b}$$

and

$$u^{(2)}(x,y) = \frac{2}{\pi}\int_0^\infty h(\alpha,y)\sin\alpha x\,d\alpha \tag{3.4a}$$

$$v^{(2)}(x,y) = \frac{2}{\pi}\int_0^\infty l(\alpha,y)\cos\alpha x\,d\alpha \tag{3.4b}$$

Here $f(\alpha,x)$, $g(\alpha,x)$, $h(\alpha,y)$ and $l(\alpha,y)$ are shape functions which will be determined later.

Substituting (3.3ab) and (3.4ab) into (3.1ab) respectively, one gets the following characteristic equation:

$$r^4 + \beta_4 r^2 + \beta_5^2 = 0 \tag{3.5}$$

where $\beta_4 = \dfrac{\beta_3^2 - \beta_1\beta_2 - 1}{\beta_1}$ and $\beta_5 = \sqrt{\beta_2/\beta_1}$

The roots of eqn(3.5) are:

$$r_1 = - r_3 = w_1 + iw_2 = \sqrt{(-\beta_4 + \beta_6)/2}$$

$$r_2 = - r_4 = w_3 + iw_4 = \sqrt{(-\beta_4 - \beta_6)/2}$$

where $$\beta_6 = \sqrt{\beta_4^2 - 4\beta_5^2}$$

Then we have:

$$f(\alpha,x) = A(\alpha)e^{r_1\alpha x} + B(\alpha)e^{-r_1\alpha x} + C(\alpha)e^{r_2\alpha x} + D(\alpha)e^{-r_2\alpha x} \quad (3.6a)$$

$$g(\alpha,x) = \beta_7[A(\alpha)e^{r_1\alpha x} - B(\alpha)e^{-r_1\alpha x}] + \beta_8[C(\alpha)e^{r_2\alpha x} - D(\alpha)e^{-r_2\alpha x}] \quad (3.6b)$$

$$h(\alpha,y) = E(\alpha)e^{r_1\alpha y/\beta_5} + F(\alpha)e^{-r_1\alpha y/\beta_5} + G(\alpha)e^{r_2\alpha y/\beta_5} + H(\alpha)e^{-r_2\alpha y/\beta_5} \quad (3.6c)$$

$$l(\alpha,y) = \beta_9[E(\alpha)e^{r_1\alpha y/\beta_5} - F(\alpha)e^{-r_1\alpha y/\beta_5}] + \beta_{10}[G(\alpha)\, e^{r_2\alpha y/\beta_5} - H(\alpha)e^{-r_2\alpha y/\beta_5}] \quad (3.6d)$$

Here two types of orthotropic materials will be distinguished according to whether the roots of the characteristic equation are real or complex.

Material type I: where both r_1 and r_2 are real numbers(w_2=w_4=0).

Material type II: where r_1 and r_2 are all complex numbers.

Applying the symmetry conditions:

$$u(x,y) = -u(-x,y) \quad (3.7a)$$

$$v(x,y) = -v(x,-y) \quad (3.7b)$$

one gets:

$$B(a) = -A(a) \quad D(a) = -C(a) \quad (3.8ab)$$

$$F(a) = -E(a) \quad H(a) = -G(a) \quad (3.8cd)$$

Material type I will be considered because most materials fall into this category. Based on the fact that both u and v vanish when y goes to infinity and that the problem is symmetric about x axis, we obtain:

$$u(x,y) = \frac{4}{\pi}\int_0^\infty [A(\alpha)\sinh(w_1\alpha x) + C(\alpha)\sinh(w_3\alpha x)]\cos\alpha y d\alpha$$

$$+\frac{2}{\pi}\int_0^\infty [E(\alpha)e^{-|w_1|\alpha y/\beta_5} + G(\alpha)e^{-|w_3|\alpha y/\beta_5}]\sin\alpha x d\alpha \qquad (3.9a)$$

$$v(x,y) = \frac{4}{\pi}\int_0^\infty [\beta_7 A(\alpha)\cosh(w_1\alpha x) + \beta_8 C(\alpha)\cosh(w_3\alpha x)]\sin\alpha y d\alpha$$

$$-\frac{2}{\pi}\int_0^\infty [\beta_9 \text{sign}(w_1)E(\alpha)e^{-|w_1|\alpha y/\beta_5} + \beta_{10}\text{sign}(w_3)G(\alpha)e^{-|w_3|\alpha y/\beta_5}]\cos\alpha x d\alpha \qquad (3.9b)$$

3.1.1.2 Stress-Strain Relations

Let $\Delta = \frac{(1-\nu_{xy}\nu_{yx})}{E_x E_y}$, then we have:

$$\sigma_x(x,y) = \frac{1}{E_y\Delta}\varepsilon_x + \frac{\nu_{yx}}{E_y\Delta}\varepsilon_y \qquad (3.10a)$$

$$\sigma_y(x,y) = \frac{\nu_{xy}}{E_x\Delta}\varepsilon_x + \frac{1}{E_x\Delta}\varepsilon_y \qquad (3.10b)$$

$$\tau_{xy}(x,y) = G_{xy}\gamma_{xy} \qquad (3.10c)$$

3.1.1.3 Strain-Displacement Relations

$$\varepsilon_x = \frac{\partial u}{\partial x},\ \varepsilon_y = \frac{\partial v}{\partial y} \text{ and } \gamma_{xy} = \left(\frac{\partial u}{\partial y} + \frac{\partial v}{\partial x}\right) \qquad (3.11abc)$$

Utilizing eqns (3.9ab) and (3.11abc), eqns (3.10abc) can be reduced to:

$$\frac{\pi(1-\nu_{xy}\nu_{yx})}{2E_x}\sigma_x(x,y) = \int_0^\infty [\gamma_1 E(\alpha)e^{-|w_1|\alpha y/\beta_5} + \gamma_2 G(\alpha)e^{-|w_3|\alpha y/\beta_5}]\alpha\cos\alpha x d\alpha$$

$$+\int_0^\infty [2\gamma_3 A(\alpha)\cosh(w_1\alpha x) + 2\gamma_4 C(\alpha)\cosh(w_3\alpha x)]\alpha\cos\alpha y d\alpha \qquad (3.12a)$$

$$\frac{\pi(1-\nu_{xy}\nu_{yx})}{2E_y}\sigma_y(x,y) = \int_0^\infty [\gamma_5 E(\alpha)e^{-|w_1|\alpha y/\beta_5} + \gamma_6 G(\alpha)e^{-|w_3|\alpha y/\beta_5}]\alpha\cos\alpha x d\alpha$$

$$+\int_0^\infty [2\gamma_7 A(\alpha)\cosh(w_1\alpha x) + 2\gamma_8 C(\alpha)\cosh(w_3\alpha x)]\alpha\cos\alpha y d\alpha \qquad (3.12b)$$

$$\frac{\pi}{2G_{xy}}\tau_{xy}(x,y) = \int_0^\infty [\gamma_{11} E(\alpha)e^{-|w_1|\alpha y/\beta_5} + \gamma_{12} G(\alpha)e^{-|w_3|\alpha y/\beta_5}]\alpha\sin\alpha x d\alpha$$

$$+\int_0^\infty [2\gamma_9 A(\alpha)\sinh(w_1\alpha x) + 2\gamma_{10} C(\alpha)\sinh(w_3\alpha x)]\alpha\sin\alpha y d\alpha \qquad (3.12c)$$

The above expressions are for plane stress problems. They can also be used for plane strain problems with the following substitutions:

$$\nu_{yx} = -\frac{E_x}{E_y}\nu_{yx}, \qquad \nu_{xy} = -\frac{E_y}{E_x}\nu_{xy},$$

$$E_y\Delta = E_x \quad \text{and} \quad E_x\Delta = E_y.$$

3.1.2 Boundary and Continuity Conditions

At the interface($x_1=H_1$, $x_2=-H_2$)

$$\sigma_{1xx}(H_1,y)=\sigma_{2xx}(-H_2,y) \qquad 0<y<\infty \qquad (3.13a)$$

$$\tau_{1xy}(H_1,y)=\tau_{2xy}(-H_2,y) \qquad 0<y<\infty \qquad (3.13b)$$

$$u_1(H_1,y)=u_2(-H_2,y) \qquad 0<y<b_1 \text{ or } b_2<y<\infty \qquad (3.14a)$$

$$v_1(H_1,y)=v_2(-H_2,y) \qquad 0<y<b_1 \text{ or } b_2<y<\infty \qquad (3.14b)$$

$$\sigma_{1xx}(H_1,y)=p_3(y) \qquad b_1<y<b_2 \qquad (3.15a)$$

$$\tau_{1xy}(H_1,y)=p_4(y) \qquad b_1<y<b_2 \qquad (3.15b)$$

At y = 0 (cracks normal to the interface)

$$v_1(x_1,0)=0 \qquad -H_1<x_1<-a_1 \text{ and } a_1<x_1<H_1 \qquad (3.16a)$$

$$v_2(x_2,0)=0 \qquad -H_2<x_2<-a_2 \text{ and } a_2<x_2<H_2 \qquad (3.16b)$$

$$\sigma_{1yy}(x_1,0)=-p_1(x_1) \qquad -a_1<x_1<a_1 \qquad (3.17a)$$

$$\sigma_{2yy}(x_2,0)=-p_2(x_2) \qquad -a_2<x_2<a_2 \qquad (3.17b)$$

$$\tau_{1xy}(x_1,0)=0 \qquad -H_1<x_1<H_1 \qquad (3.18a)$$

$$\tau_{2xy}(x_2,0)=0 \qquad -H_2<x_2<H_2 \qquad (3.18b)$$

At $x_1 = 0$ or $x_2 = 0$

$$u_1(0,y)=0 \qquad 0\le y\le\infty \qquad (3.19a)$$

$$u_2(0,y)=0 \qquad 0\le y\le\infty \qquad (3.19b)$$

$$\tau_{1xy}(0,y)=0 \qquad 0\le y\le\infty \qquad (3.20a)$$

$$\tau_{2xy}(0,y)=0 \qquad 0\le y\le\infty \qquad (3.20b)$$

where $p_1(x_1)$ is the normal traction on fiber crack surfaces perpendicular to the interface ($-a_1<x_1<a_1$ and $y=0$), $p_2(x_2)$ is the normal traction on matrix crack surfaces perpendicular to the interface ($a_2<x_2<a_2$ and $y=0$), $p_3(y)$ is the normal traction on crack surfaces along the interface($x_1=H_1$, $b_1<y<b_2$) and $p_4(y)$ is the shear traction on crack surfaces along the interface ($x_1=H_1$, $b_1<y<b_2$).

Define: $\phi_1(x_1) = \frac{\partial v_1(x_1,0)}{\partial x_1}$, $\phi_2(x_2) = \frac{\partial v_2(x_2,0)}{\partial x_2}$

$$\phi_3(y) = \frac{\partial}{\partial y}[v_1(+H_1,y) - v_2(-H_2,y)], \quad \phi_4(y) = \frac{\partial}{\partial y}[u_1(+H_1,y) - u_2(-H_2,y)] \quad (3.21abcd)$$

From (3.14ab) and (3.16ab), we get:

$$\phi_1(x_1) = 0 \qquad a_1<|x_1|<H_1 \qquad (3.22a)$$

$$\phi_2(x_2) = 0 \qquad a_2<|x_2|<H_2 \qquad (3.22b)$$

$$\phi_3(y) = 0 \qquad 0<y<b_1 \quad \text{and} \quad b_2<y<\infty \qquad (3.22c)$$

$$\phi_4(y) = 0 \qquad 0<y<b_1 \& \quad \text{and} \quad b_2<y<\infty \qquad (3.22d)$$

The above 16 boundary and continuity conditions are yet to be satisfied.

Eqns(3.19ab) and (3.20ab) are satisfied identically from eqn(3.9a) and (3.12c)

Substituting eqns(3.18ab) into (3.12c) we have:

$$E(\alpha) = -\frac{\gamma_{12}}{\gamma_{11}}G(\alpha), \qquad E^*(\alpha) = -\frac{\gamma_{12}^*}{\gamma_{11}}G^*(\alpha)$$

Then eqns(3.9ab) and (3.12abc) become:

$$u(x,y) = \frac{4}{\pi}\int_0^\infty [A(\alpha)\sinh(w_1\alpha x) + C(\alpha)\sinh(w_3\alpha x)]\cos\alpha y d\alpha$$

$$+\frac{2}{\pi}\int_0^\infty E(\alpha)[e^{-|w_1|\alpha y/\beta_5} - \frac{\gamma_{11}}{\gamma_{12}}e^{-|w_3|\alpha y/\beta_5}]\sin\alpha x d\alpha \qquad (3.9a^*)$$

$$v(x,y) = \frac{4}{\pi}\int_0^\infty [\beta_7 A(\alpha)\cosh(w_1\alpha x) + \beta_8 C(\alpha)\cosh(w_3\alpha x)]\sin\alpha y d\alpha$$

$$-\frac{2}{\pi}\int_0^\infty E(\alpha)[\beta_9 \text{sign}(w_1)e^{-|w_1|\alpha y/\beta_5} - \frac{\gamma_{11}}{\gamma_{12}}\beta_{10}\text{sign}(w_3)e^{-|w_3|\alpha y/\beta_5}]\cos\alpha x d\alpha \quad (3.9b^*)$$

and

$$\frac{\pi(1-\nu_{xy}\nu_{yx})}{2E_x}\sigma_x(x,y) = \int_0^\infty E(\alpha)[\gamma_1 e^{-|w_1|\alpha y/\beta_5} - \gamma_2\frac{\gamma_{11}}{\gamma_{12}}e^{-|w_3|\alpha y/\beta_5}]\alpha\cos\alpha x d\alpha$$

$$+ \int_0^\infty [2\gamma_3 A(\alpha)\cosh(w_1\alpha x) + 2\gamma_4 C(\alpha)\cosh(w_3\alpha x)]\alpha\cos\alpha y d\alpha \qquad (3.12a^*)$$

$$\frac{\pi(1-\nu_{xy}\nu_{yx})}{2E_y}\sigma_y(x,y) = \int_0^\infty E(\alpha)[\gamma_5 e^{-|w_1|\alpha y/\beta_5} - \gamma_6\frac{\gamma_{11}}{\gamma_{12}}e^{-|w_3|\alpha y/\beta_5}]\alpha\cos\alpha x d\alpha$$

$$+ \int_0^\infty [2\gamma_7 A(\alpha)\cosh(w_1\alpha x) + 2\gamma_8 C(\alpha)\cosh(w_3\alpha x)]\alpha\cos\alpha y d\alpha \qquad (3.12b^*)$$

$$\frac{\pi}{2G_{xy}}\tau_{xy}(x,y) = \int_0^\infty E(\alpha)\gamma_{11}[e^{-|w_1|\alpha y/\beta_5} - e^{-|w_3|\alpha y/\beta_5}]\alpha\sin\alpha x d\alpha$$

$$+ \int_0^\infty [2\gamma_9 A(\alpha)\sinh(w_1\alpha x) + 2\gamma_{10} C(\alpha)\sinh(w_3\alpha x)]\alpha\sin\alpha y d\alpha \qquad (3.12c^*)$$

At y = 0, eqns(3.16ab) give:

$$v_1(x_1,0) = -\frac{2}{\pi}\int_0^\infty E(\alpha)[\beta_9\,\mathrm{sign}(w_1) - \frac{\gamma_{11}}{\gamma_{12}}\beta_{10}\,\mathrm{sign}(w_3)]\cos\alpha x_1 d\alpha \qquad a_1<x_1<H_1 \qquad (3.23a)$$

$$v_2(x_2,0) = -\frac{2}{\pi}\int_0^\infty E^*(\alpha)[\beta_9^*\,\mathrm{sign}(w_1^*) - \frac{\gamma_{11}^*}{\gamma_{12}^*}\beta_{10}^*\,\mathrm{sign}(w_3^*)]\cos\alpha x_2 d\alpha \quad a_2<x_2<H_2 \qquad (3.23b)$$

Then from eqns (3.21ab), we have:

$$\phi_1(x_1) = \frac{\partial v_1(x_1,0)}{\partial x_1} = \frac{2}{\pi}\int_0^\infty \gamma_{13}E(\alpha)\alpha\sin\alpha x_1 d\alpha,$$

$$\phi_2(x_2) = \frac{\partial v_2(x_2,0)}{\partial x_2} = \frac{2}{\pi}\int_0^\infty \gamma_{13}^*E^*(\alpha)\alpha\sin\alpha x_2 d\alpha$$

Taking the inverse Fourier transform of above expressions:

$$E(\alpha) = \frac{1}{\gamma_{13}\alpha}\int_0^{a_1} \phi_1(x_1)\sin\alpha x_1 dx_1 \qquad (3.24a)$$

$$E^*(\alpha) = \frac{1}{\gamma_{13}^*\alpha}\int_0^{a_2} \phi_2(x_2)\sin\alpha x_2 dx_2 \qquad (3.24b)$$

and substituting eqns(3.24ab) into eqn(3.9b) respectively and applying eqns(3.17ab), we get:

$$\gamma_{14}\int_{-a_1}^{a_1}\frac{\phi_1(t)}{t-x_1}dt + \int_0^\infty [2\gamma_7 A(\alpha)\cosh(w_1\alpha x_1) + 2\gamma_8 C(\alpha)\cosh(w_3\alpha x_1)]\alpha d\alpha$$

$$= -\frac{\pi(1-\nu_{xy}\nu_{yx})}{2E_y} p_1(x_1) \qquad (3.25a)$$

$$\gamma_{14}^* \int_{-a_2}^{a_2} \frac{\phi_2(t)}{t-x_2} dt + \int_0^\infty [2\gamma_7^* A^*(\alpha)\cosh(w_1^*\alpha x_2) + 2\gamma_8^* C^*(\alpha)\cosh(w_3^*\alpha x_2)]\alpha d\alpha$$

$$= -\frac{\pi(1-\nu_{xy}\nu_{yx})}{2E_y^*} p_2(x_2) \qquad (3.25b)$$

where γ_i and γ_i^* are given in Appendix B.

Substituting eqns (3.24ab) into eqns(3.15ab), we obtain:

$$\frac{\pi(1-\nu_{xy}\nu_{yx})}{2E_x} p_3(y) = \lim_{x_1 \to H_1} \int_0^\infty \int_0^{a_1} \frac{\phi_1(t)}{\gamma_{13}} \sin\alpha t dt [\gamma_1 e^{-|w_1|\alpha y/\beta_5} - \gamma_2 \frac{\gamma_{11}}{\gamma_{12}} e^{-|w_3|\alpha y/\beta_5}] \cos\alpha x_1 d\alpha$$

$$+ \lim_{x_1 \to H_1} \int_0^\infty [2\gamma_3 A(\alpha)\cosh(w_1\alpha x_1) + 2\gamma_4 C(\alpha)\cosh(w_3\alpha x_1)]\alpha\cos\alpha y d\alpha \quad b_1<y<b_2 \qquad (3.26a)$$

$$\frac{\pi}{2G_{xy}} p_4(y) = \lim_{x_1 \to H_1} \int_0^\infty \int_0^{a_1} \frac{\phi_1(t)}{\gamma_{13}} \sin\alpha t dt \gamma_{11} [e^{-|w_1|\alpha y/\beta_5} - e^{-|w_3|\alpha y/\beta_5}] \sin\alpha x_1 d\alpha$$

$$+ \lim_{x_1 \to H_1} \int_0^\infty [2\gamma_9 A(\alpha)\sinh(w_1\alpha x_1) + 2\gamma_{10} C(\alpha)\sinh(w_3\alpha x_1)]\alpha\sin\alpha y d\alpha \quad b_1<y<b_2 \qquad (3.26b)$$

Applying eqns(A.5ab), eqns(3.26ab) can be further reduced to:

$$\int_{-a_1}^{a_1} \frac{\phi_1(t)}{2\gamma_{13}} [-\gamma_1 \frac{H_1-t}{\frac{(|w_1|y)^2}{\beta_5^2}+(H_1-t)^2} + \gamma_2 (\frac{\gamma_{11}}{\gamma_{12}}) \frac{H_1-t}{\frac{(|w_3|y)^2}{\beta_5^2}+(H_1-t)^2}] dt$$

$$+ \lim_{x_1 \to H_1} \int_0^\infty [2\gamma_3 A(\alpha)\cosh(w_1\alpha x_1) + 2\gamma_4 C(\alpha)\cosh(w_3\alpha x_1)]\alpha\cos\alpha y d\alpha$$

$$= \frac{\pi(1-\nu_{xy}\nu_{yx})}{2E_x} p_3(y) \qquad b_1<y<b_2 \qquad (3.26a^*)$$

and

$$\int_{-a_1}^{a_1} \frac{\gamma_{11}\phi_1(t)}{2\gamma_{13}} [\frac{\frac{|w_1|y}{\beta_5}}{\frac{(|w_1|y)^2}{\beta_5^2}+(H_1-t)^2} - \frac{\frac{|w_3|y}{\beta_5}}{\frac{(|w_3|y)^2}{\beta_5^2}+(H_1-t)^2}] dt$$

$$+ \lim_{x_1 \to H_1} \int_0^\infty [2\gamma_9 A(\alpha)\sinh(w_1\alpha x_1) + 2\gamma_{10} C(\alpha)\sinh(w_3\alpha x_1)]\alpha\sin\alpha y d\alpha$$

$$= \frac{\pi}{2G_{xy}} p_4(y) \qquad b_1<y<b_2 \qquad (3.26b^*)$$

Applying eqns(3.14ab), (3.13ab) and (3.21abcd), one sets:

$$A(\alpha)\sinh(w_1\alpha H_1) + C(\alpha)\sinh(w_3\alpha H_1)$$

$$+ A^*(\alpha)\sinh(w_1{}^*\alpha H_2) + C^*(\alpha)\sinh(w_3{}^*\alpha H_2) = R_1(\alpha) \qquad (3.27a)$$

$$\beta_7 A(\alpha)\cosh(w_1\alpha H_1) + \beta_8 C(\alpha)\cosh(w_3\alpha H_1)$$

$$- \beta_7{}^* A^*(\alpha)\cosh(w_1{}^*\alpha H_2) - \beta_8{}^* C^*(\alpha)\cosh(w_3{}^*\alpha H_2) = R_2(\alpha) \qquad (3.27b)$$

$$[\gamma_3 A(\alpha)\cosh(w_1\alpha H_1) + \gamma_4 C(\alpha)\cosh(w_3\alpha H_1)$$

$$- \lambda_1\gamma_3{}^* A^*(\alpha)\cosh(w_1{}^*\alpha H_2) - \lambda_1\gamma_4{}^* C^*(\alpha)\cosh(w_3{}^*\alpha H_2)]\alpha = R_3(\alpha) \qquad (3.27c)$$

$$[\gamma_9 A(\alpha)\sinh(w_1\alpha H_1) + \gamma_{10} C(\alpha)\sinh(w_3\alpha H_1)$$

$$+ \lambda_2\gamma_9{}^* A^*(\alpha)\sinh(w_1{}^*\alpha H_2) + \lambda_2\gamma_{10}{}^* C^*(\alpha)\sinh(w_3{}^*\alpha H_2)]\alpha = R_4(\alpha) \qquad (3.27d)$$

where $R_1(\alpha)$, $R_2(\alpha)$, $R_3(\alpha)$ and $R_4(\alpha)$ are given in Appendix A.

Solving eqns(3.27abcd) for $A(\alpha)$,$C(\alpha)$, $A^*(\alpha)$ and $C^*(\alpha)$, we have:

$$A(\alpha) = \frac{1}{\cosh(\omega_1\alpha H_1)}\left[\frac{R_1(\alpha)}{f(\alpha)}g_1(\alpha) + \frac{R_2(\alpha)}{f(\alpha)}h_1(\alpha) + \frac{R_3(\alpha)}{f(\alpha)}m_1(\alpha) + \frac{R_4(\alpha)}{f(\alpha)}n_1(\alpha)\right] \qquad (3.28a)$$

$$C(\alpha) = \frac{1}{\cosh(\omega_3\alpha H_1)}\left[\frac{R_1(\alpha)}{f(\alpha)}g_2(\alpha) + \frac{R_2(\alpha)}{f(\alpha)}h_2(\alpha) + \frac{R_3(\alpha)}{f(\alpha)}m_2(\alpha) + \frac{R_4(\alpha)}{f(\alpha)}n_2(\alpha)\right] \qquad (3.28b)$$

$$A^*(\alpha) = \frac{1}{\cosh(\omega_1{}^*\alpha H_2)}\left[\frac{R_1(\alpha)}{f(\alpha)}g_3(\alpha) + \frac{R_2(\alpha)}{f(\alpha)}h_3(\alpha) + \frac{R_3(\alpha)}{f(\alpha)}m_3(\alpha) + \frac{R_4(\alpha)}{f(\alpha)}n_3(\alpha)\right] \qquad (3.28c)$$

$$C^*(\alpha) = \frac{1}{\cosh(\omega_3{}^*\alpha H_2)}\left[\frac{R_1(\alpha)}{f(\alpha)}g_4(\alpha) + \frac{R_2(\alpha)}{f(\alpha)}h_4(\alpha) + \frac{R_3(\alpha)}{f(\alpha)}m_4(\alpha) + \frac{R_4(\alpha)}{f(\alpha)}n_4(\alpha)\right] \qquad (3.28d)$$

where $f(\alpha)$, $g_i(\alpha)$, $h_i(\alpha)$, $m_i(\alpha)$ and $n_i(\alpha)$ (i=1,2,3,4) are given in Appendix C.

Finally, substituting (3.28abcd) into (3.25ab) and (3.26a*b*), we get:

$$\frac{1}{\pi}\int_{-a_1}^{a_1}\left[\frac{1}{t-x_1} + \pi K_{11}(x_1,t)\right]\phi_1(t)dt + \int_{-a_2}^{a_2} K_{12}(x_1,t)\phi_2(t)dt + \int_{b_1}^{b_2} K_{13}(x_1,t)\phi_3(t)dt$$

$$+ \int_{b_1}^{b_2} K_{14}(x_1,t)\phi_4(t)dt = -\frac{(1-\nu_{xy}\nu_{yx})}{2\gamma_{14}E_y}p_1(x_1) \qquad -a_1<x_1<a_1 \qquad (3.29a)$$

$$\int_{-a_1}^{a_1} K_{21}(x_2,t)\phi_1(t)dt + \frac{1}{\pi}\int_{-a_2}^{a_2}\left[\frac{1}{t-x_2} + \pi K_{22}(x_2,t)\right]\phi_2(t)dt + \int_{b_1}^{b_2} K_{23}(x_2,t)\phi_3(t)dt$$

$$+\int_{b_1}^{b_2} K_{24}(x_2,t)\phi_4(t)dt = -\frac{(1-\nu^*_{xy}\nu^*_{yx})}{2\gamma_{14}{}^*E_y{}^*}p_2(x_2) \qquad -a_2<x_2<a_2 \qquad (3.29b)$$

$$\int_{-a_1}^{a_1} K_{31}(y,t)\phi_1(t)dt + \int_{-a_2}^{a_2} K_{32}(y,t)\phi_2(t)dt + \int_{b_1}^{b_2} K_{33}'(y,t)\phi_3(t)dt$$

$$+\int_{b_1}^{b_2} K_{34}'(y,t)\phi_4(t)dt = \frac{(1-\nu_{xy}\nu_{yx})}{2E_x}p_3(y) \qquad b_1<y<b_2 \qquad (3.29c)$$

$$\int_{-a_1}^{a_1} K_{41}(y,t)\phi_1(t)dt + \int_{-a_2}^{a_2} K_{42}(y,t)\phi_2(t)dt + \int_{b_1}^{b_2} K_{43}'(y,t)\phi_3(t)dt$$

$$+\int_{b_1}^{b_2} K_{44}'(y,t)\phi_4(t)dt = \frac{1}{2G_{xy}}p_4(y) \qquad b_1<y<b_2 \qquad (3.29d)$$

where

$$K_{11}(x_1,t) = \frac{1}{\gamma_{14}\pi}\int_0^\infty [k_1(x_1,\alpha)e^{-\alpha(H_1-t)\beta_5/|w_1|} + k_2(x_1,\alpha)e^{-\alpha(H_1-t)\beta_5/|w_3|}]d\alpha$$

$$K_{12}(x_1,t) = \frac{1}{\gamma_{14}\pi}\int_0^\infty [k_3(x_1,\alpha)e^{-\alpha(H_2-t)\beta_5{}^*/|w_1{}^*|} + k_4(x_1,\alpha)e^{-\alpha(H_2-t)\beta_5{}^*/|w_3{}^*|}]d\alpha$$

$$K_{13}(x_1,t) = \frac{1}{\gamma_{14}\pi}\int_0^\infty [J_1(x_1,\alpha) + J_2(x_1,\alpha)]\cos\alpha t d\alpha$$

$$K_{14}(x_1,t) = \frac{1}{\gamma_{14}\pi}\int_0^\infty [J_3(x_1,\alpha) + J_4(x_1,\alpha)]\sin\alpha t d\alpha \qquad (3.30abcd)$$

$$K_{21}(x_2,t) = \frac{1}{\gamma_{14}{}^*\pi}\int_0^\infty [k_5(x_2,\alpha)e^{-\alpha(H_1-t)\beta_5/|w_1|} + k_6(x_2,\alpha)e^{-\alpha(H_1-t)\beta_5/|w_3|}]d\alpha$$

$$K_{22}(x_2,t) = \frac{1}{\gamma_{14}{}^*\pi}\int_0^\infty [k_7(x_2,\alpha)e^{-\alpha(H_2-t)\beta_5{}^*/|w_1{}^*|} + k_8(x_2,\alpha)e^{-\alpha(H_2-t)\beta_5{}^*/|w_3{}^*|}]d\alpha$$

$$K_{23}(x_2,t) = \frac{1}{\gamma_{14}{}^*\pi}\int_0^\infty [J_5(x_2,\alpha) + J_6(x_2,\alpha)]\cos\alpha t d\alpha$$

$$K_{24}(x_1,t) = \frac{1}{\gamma_{14}{}^*\pi}\int_0^\infty [J_7(x_2,\alpha) + J_8(x_2,\alpha)]\sin\alpha t d\alpha \qquad (3.31abcd)$$

$$K_{31}(y,t) = \frac{1}{2\gamma_{13}\pi}\left[-\gamma_1 \frac{H_1-t}{\frac{(|w_1|y)^2}{\beta_5^2}+(H_1-t)^2} + \gamma_2\left(\frac{\gamma_{11}}{\gamma_{12}}\right)\frac{H_1-t}{\frac{(|w_3|y)^2}{\beta_5^2}+(H_1-t)^2}\right]$$

$$+ \lim_{x_1\to H_1} \frac{1}{\pi}\int_0^\infty \left[k_9(y,x_1,\alpha)e^{-\alpha(H_1-t)\beta_5/|w_1|} + k_{10}(y,x_1,\alpha)e^{-\alpha(H_1-t)\beta_5/|w_3|}\right]d\alpha$$

$$K_{32}(y,t) = \lim_{x_1\to H_1} \frac{1}{\pi}\int_0^\infty \left[k_{11}(y,x_1,\alpha)e^{-\alpha(H_2-t)\beta_5^*/|w_1^*|} + k_{12}(y,x_1,\alpha)e^{-\alpha(H_2-t)\beta_5^*/|w_3^*|}\right]d\alpha$$

$$K_{33}'(y,t) = \lim_{x_1\to H_1} \frac{1}{\pi}\int_0^\infty \left[\frac{ch(w_1\alpha x_1)}{ch(w_1\alpha H_1)}J_9(y,\alpha) + \frac{ch(w_3\alpha x_1)}{ch(w_3\alpha H_1)}J_{10}(y,\alpha)\right]\cos\alpha t d\alpha$$

$$K_{34}'(y,t) = \lim_{x_1\to H_1} \frac{1}{\pi}\int_0^\infty \left[\frac{ch(w_1\alpha x_1)}{ch(w_1\alpha H_1)}J_{11}(y,\alpha) + \frac{ch(w_3\alpha x_1)}{ch(w_3\alpha H_1)}J_{12}(y,\alpha)\right]\sin\alpha t d\alpha \qquad (3.32abcd)$$

$$K_{41}(y,t) = \frac{\gamma_{11}}{2\gamma_{13}\pi}\left[\frac{\frac{|w_1|y}{\beta_5}}{\frac{(|w_1|y)^2}{\beta_5^2}+(H_1-t)^2} - \frac{\frac{|w_3|y}{\beta_5}}{\frac{(|w_3|y)^2}{\beta_5^2}+(H_1-t)^2}\right]$$

$$+ \lim_{x_1\to H_1} \frac{1}{\pi}\int_0^\infty \left[k_{13}(y,x_1,\alpha)e^{-\alpha(H_1-t)\beta_5/|w_1|} + k_{14}(y,x_1,\alpha)e^{-\alpha(H_1-t)\beta_5/|w_3|}\right]d\alpha$$

$$K_{42}(y,t) = \lim_{x_1\to H_1} \frac{1}{\pi}\int_0^\infty \left[k_{15}(y,x_1,\alpha)e^{-\alpha(H_2-t)\beta_5^*/|w_1^*|} + k_{16}(y,x_1,\alpha)e^{-\alpha(H_2-t)\beta_5^*/|w_3^*|}\right]d\alpha$$

$$K_{43}'(y,t) = \lim_{x_1\to H_1} \frac{1}{\pi}\int_0^\infty \left[\frac{sh(w_1\alpha x_1)}{ch(w_1\alpha H_1)}J_{13}(y,\alpha) + \frac{sh(w_3\alpha x_1)}{ch(w_3\alpha H_1)}J_{14}(y,\alpha)\right]\cos\alpha t d\alpha$$

$$K_{44}'(y,t) = \lim_{x_1\to H_1} \frac{1}{\pi}\int_0^\infty \left[\frac{sh(w_1\alpha x_1)}{ch(w_1\alpha H_1)}J_{15}(y,\alpha) + \frac{sh(w_3\alpha x_1)}{ch(w_3\alpha H_1)}J_{16}(y,\alpha)\right]\sin\alpha t d\alpha \qquad (3.33abcd)$$

The derivation of the terms k_i and J_i (i=1 to 16) are given in Appendix C.

Note that for t = y the integrals (3.32cd) and (3.33cd) are divergent. These divergent parts must be studied and separated by analyzing the asymptotic behavior of the integrands. After the asymptotic analysis of the divergent parts in (3.32cd) and (3.33cd), eqns(3.29cd) are finally reduced to:

$$\int_{-a_1}^{a_1} K_{31}(y,t)\phi_1(t)dt + \int_{-a_2}^{a_2} K_{32}(y,t)\phi_2(t)dt + \frac{\rho_1}{2}\phi_3(y) + \int_{b_1}^{b_2} K_{33}(y,t)\phi_3(t)dt$$

$$-\frac{\rho_2}{2\pi}\int_{b_1}^{b_2}\left(\frac{1}{t-y}+\frac{1}{t+y}\right)\phi_4(t)dt+\int_{b_1}^{b_2}K_{34}(y,t)\phi_4(t)dt=\frac{(1-\nu_{xy}\nu_{yx})}{2E_x}p_3(y)\qquad b_1<y<b_2\qquad (3.29c^*)$$

$$\int_{-a_1}^{a_1}K_{41}(y,t)\phi_1(t)dt+\int_{-a_2}^{a_2}K_{42}(y,t)\phi_2(t)dt-\frac{\rho_4}{2}\phi_4(y)+\int_{b_1}^{b_2}K_{43}(y,t)\phi_3(t)dt$$

$$+\frac{\rho_3}{2\pi}\int_{b_1}^{b_2}\left(\frac{-1}{t-y}+\frac{1}{t+y}\right)\phi_3(t)dt+\int_{b_1}^{b_2}K_{44}(y,t)\phi_4(t)dt=\frac{1}{2G_{xy}}p_4(y)\qquad b_1<y<b_2\qquad (3.29d^*)$$

where ρ_1, ρ_2, ρ_3 and ρ_4 and $K_{33}(y,t)$, $K_{34}(y,t)$, $K_{43}(y,t)$ and $K_{44}(y,t)$ are defined in Appendix D.

3.1.3 Normalization of The Singular Integral Equations

Using the following variable replacement formulae:

for x_1 and x_2: $x_1=a_1r$, $t=a_1s$; and $x_2=a_2r$, $t=a_2s$; $\quad -1\le r\le 1,\quad -1\le s\le 1$

for y: $y=\frac{1}{2}(b_2-b_1)r+\frac{1}{2}(b_2+b_1)$, $\quad t=\frac{1}{2}(b_2-b_1)s+\frac{1}{2}(b_2+b_1)$.

then $t+y=\frac{1}{2}(b_2-b_1)[s+r+b_0]$, $b_0=\frac{2(b_2+b_1)}{(b_2-b_1)}\qquad -1\le r\le 1,\quad -1\le s\le 1$

Substituting the above into the four singular integral equations, we obtain:

$$\frac{1}{\pi}\int_{-1}^{1}\left[\frac{1}{s-r}+\pi a_1k_{11}^{\circ}(r,s)\right]\phi_1^{\circ}(s)ds+\int_{-1}^{1}a_2k_{12}^{\circ}(r,s)\phi_2^{\circ}(s)ds$$

$$+\frac{b_2-b_1}{2}\int_{-1}^{1}k_{13}^{\circ}(r,s)\phi_3^{\circ}(s)ds+\frac{b_2-b_1}{2}\int_{-1}^{1}k_{14}^{\circ}(r,s)\phi_4^{\circ}(s)ds=-\frac{(1-\nu_{xy}\nu_{yx})}{2\gamma_{14}E_y}p_1^{\circ}(r)\qquad (3.34a)$$

$$\int_{-1}^{1}a_1k_{21}^{\circ}(r,s)\phi_1^{\circ}(s)ds+\frac{1}{\pi}\int_{-1}^{1}\left[\frac{1}{s-r}+\pi a_2k_{22}^{\circ}(r,s)\right]\phi_1^{\circ}(s)ds$$

$$+\frac{b_2-b_1}{2}\int_{-1}^{1}k_{23}^{\circ}(r,s)\phi_3^{\circ}(s)ds+\frac{b_2-b_1}{2}\int_{-1}^{1}k_{24}^{\circ}(r,s)\phi_4^{\circ}(s)ds=-\frac{(1-\nu_{xy}^{*}\nu_{yx}^{*})}{2\gamma_{14}^{*}E_y^{*}}p_2^{\circ}(r)\qquad (3.34b)$$

$$\int_{-1}^{1}a_1k_{31}^{\circ}(r,s)]\phi_1^{\circ}(s)ds+\int_{-1}^{1}a_2k_{32}^{\circ}(r,s)]\phi_2^{\circ}(s)ds+\frac{\rho_1}{2}\phi_3^{\circ}(r)+\frac{b_2-b_1}{2}\int_{-1}^{1}k_{33}^{\circ}(r,s)\phi_3^{\circ}(s)ds$$

$$-\frac{\rho_2}{2\pi}\int_{-1}^{1}\left(\frac{1}{s-r}+\frac{1}{s+r+b_o}\right)\phi_4^{\circ}(s)ds+\frac{b_2-b_1}{2}\int_{-1}^{1}k_{34}^{\circ}(r,s)\phi_4^{\circ}(s)ds=\frac{1-\nu_{xy}\nu_{yx}}{2E_x}p_3^{\circ}(r)\qquad (3.34c)$$

$$\int_{-1}^{1} a_1 k_{41}^{o}(r,s)]\phi_1^{o}(s)ds + \int_{-1}^{1} a_2 k_{42}^{o}(r,s)]\phi_2^{o}(s)ds + \frac{\rho_3}{2\pi}\int_{-1}^{1}\left(\frac{-1}{s-r} + \frac{1}{s+r+b_o}\right)\phi_3^{o}(s)ds$$

$$\frac{b_2-b_1}{2}\int_{-1}^{1} k_{34}^{o}(r,s)\phi_3^{0}(s)ds - \frac{\rho_4}{2}\phi_4^{o}(r) + \frac{b_2-b_1}{2}\int_{-1}^{1} k_{44}^{o}(r,s)\phi_4^{o}(s)ds = \frac{1}{2G_{xy}}p_4^{o}(r) \qquad (3.34d)$$

here superscript "o" is used to denote the normalized quantities.

For orthotropic materials, the dominant parts of eqns (3.34c) and (3.34d) are coupled. It is necessary to decouple these dominant parts before any numerical method is applied. Using the technique described in [23], we first let:

$$\phi = \begin{Bmatrix} \phi_3^{o} \\ \phi_4^{o} \end{Bmatrix},\ \theta = \begin{Bmatrix} \phi_1^{o} \\ \phi_2^{o} \end{Bmatrix},\ A = \begin{bmatrix} \frac{\rho_1}{2} & 0 \\ 0 & -\frac{\rho_4}{2} \end{bmatrix},\ B = \begin{bmatrix} 0 & -\frac{\rho_2}{2}i \\ -\frac{\rho_3}{2}i & 0 \end{bmatrix},\ B' = \begin{bmatrix} 0 & -\frac{\rho_2}{2}i \\ \frac{\rho_3}{2}i & 0 \end{bmatrix}$$

$$'C = \begin{bmatrix} a_1 k_{31}^{o} & a_2 k_{32}^{o} \\ a_1 k_{41}^{o} & a_2 k_{42}^{o} \end{bmatrix},\ K = \frac{b_2-b_1}{2}\begin{bmatrix} k_{33}^{o} & k_{34}^{o} \\ k_{43}^{o} & k_{44}^{o} \end{bmatrix},\ \text{and}\ P = \begin{bmatrix} \frac{1-\nu_{xy}\nu_{yx}}{2E_x}p_3^{o} \\ \frac{1}{2G_{xy}}p_4^{o} \end{bmatrix}.$$

then eqns (3.34c) and (3.34d) are combined to yield:

$$A\phi + \frac{B}{\pi i}\int_{-1}^{1}\frac{\phi ds}{s-r} + \frac{B'}{\pi i}\int_{-1}^{1}\frac{\phi ds}{s+r+b_0} + \int_{-1}^{1} C\theta ds + \int_{-1}^{1} K\phi ds = P \qquad (3.35)$$

Multiplying both sides of eqn (3.35) by A^{-1} gives:

$$\phi + \frac{1}{\pi i}\int_{-1}^{1}\frac{A^{-1}B\phi ds}{s-r} + \frac{1}{\pi i}\int_{-1}^{1}\frac{A^{-1}B'\phi ds}{s+r+b_0} + \int_{-1}^{1} A^{-1}C\theta ds + \int_{-1}^{1} A^{-1}K\phi ds = A^{-1}P \qquad (3.36)$$

Let $D = A^{-1}B = \begin{bmatrix} 0 & -i\frac{\rho_2}{\rho_1} \\ i\frac{\rho_3}{\rho_4} & 0 \end{bmatrix}$, $D' = A^{-1}B' = \begin{bmatrix} 0 & -i\frac{\rho_2}{\rho_1} \\ -i\frac{\rho_3}{\rho_4} & 0 \end{bmatrix}$

then the eigenvalues $\mu_{1,2}$ of D can be determined from:

$$D - \mu I = 0 \qquad (3.37)$$

which gives: $\mu^2 - \frac{\rho_2\rho_3}{\rho_1\rho_4} = 0 \rightarrow \mu_{1,2} = \pm\sqrt{\frac{\rho_2\rho_3}{\rho_1\rho_4}} = \pm\frac{1}{\zeta}$

Now let R be a square matrix such that:

$$DR = R\Lambda \tag{3.38}$$

where: $\Lambda = \begin{bmatrix} \zeta^{-1} & 0 \\ 0 & -\zeta^{-1} \end{bmatrix}$, then $R = \begin{bmatrix} 1 & i\sqrt{\frac{\eta_1}{\eta_2}} \\ i\sqrt{\frac{\eta_2}{\eta_1}} & 1 \end{bmatrix}$ with $\eta_1 = \frac{\rho_2}{\rho_1}$, and $\eta_2 = \frac{\rho_3}{\rho_4}$

Introducing : $\phi = R\psi$, where $\psi = \begin{bmatrix} \psi_3^o \\ \psi_4^o \end{bmatrix}$, then eqn (3.36) is reduced to:

$$\psi + \frac{1}{\pi i}\int_{-1}^{1} \frac{\Lambda\psi ds}{s-r} + \frac{1}{\pi i}\int_{-1}^{1} \frac{R^{-1}A^{-1}B' R\psi ds}{s+r+b_0} + \int_{-1}^{1} R^{-1}A^{-1}C\theta ds$$

$$+\int_{-1}^{1} R^{-1}A^{-1}K\phi ds = R^{-1}A^{-1}P \tag{3.39}$$

where

$$R^{-1}A^{-1}C = \begin{bmatrix} a_1c_1(r,s) & a_2c_2(r,s) \\ a_1c_3(r,s) & a_2c_4(r,s) \end{bmatrix} = \begin{bmatrix} a_1(\frac{k_{31}^o}{\rho_1} + \frac{ik_{41}^o}{\rho_4}\sqrt{\frac{\eta_1}{\eta_2}}) & a_2(\frac{k_{32}^o}{\rho_1} + \frac{ik_{42}^o}{\rho_4}\sqrt{\frac{\eta_1}{\eta_2}}) \\ a_1(-\frac{k_{41}^o}{\rho_4} - \frac{ik_{31}^o}{\rho_1}\sqrt{\frac{\eta_2}{\eta_1}}) & a_2(-\frac{k_{42}^o}{\rho_4} - \frac{ik_{32}^o}{\rho_1}\sqrt{\frac{\eta_2}{\eta_1}}) \end{bmatrix} \tag{3.40}$$

$$R^{-1}A^{-1}KR = \frac{b_2 - b_1}{2}\begin{bmatrix} k_1^o(r,s) & k_2^o(r,s) \\ k_3^o(r,s) & k_4^o(r,s) \end{bmatrix} = \frac{b_2 - b_1}{2} \times$$

$$\begin{bmatrix} (\frac{k_{33}^o}{\rho_1} - \frac{k_{44}^o}{\rho_4}) + i(\sqrt{\frac{\eta_2}{\eta_1}}\frac{k_{34}^o}{\rho_1} + \sqrt{\frac{\eta_1}{\eta_2}}\frac{k_{43}^o}{\rho_4}) & (\frac{k_{34}^o}{\rho_1} - \frac{\eta_1}{\eta_2}\frac{k_{43}^o}{\rho_4}) + i\sqrt{\frac{\eta_1}{\eta_2}}(\frac{k_{33}^o}{\rho_1} + \frac{k_{44}^o}{\rho_4}) \\ (\frac{\eta_2}{\eta_1}\frac{k_{34}^o}{\rho_1} - \frac{k_{43}^o}{\rho_4}) - i\sqrt{\frac{\eta_2}{\eta_1}}(\frac{k_{33}^o}{\rho_1} + \frac{k_{44}^o}{\rho_4}) & (\frac{k_{33}^o}{\rho_1} - \frac{k_{44}^o}{\rho_4}) - i(\sqrt{\frac{\eta_2}{\eta_1}}\frac{k_{34}^o}{\rho_1} + \sqrt{\frac{\eta_1}{\eta_2}}\frac{k_{43}^o}{\rho_4}) \end{bmatrix} \tag{3.41}$$

and $$R^{-1}A^{-1} = \begin{bmatrix} m_1 & im_2 \\ -m_3 & -m_4 \end{bmatrix} = \begin{bmatrix} \frac{1}{\rho_1} & i\sqrt{\frac{\rho_2}{\rho_1\rho_3\rho_4}} \\ -i\sqrt{\frac{\rho_3}{\rho_1\rho_2\rho_4}} & -\frac{1}{\rho_4} \end{bmatrix} \tag{3.42}$$

Finally eqns (3.34c) and (3.34d) reduces to:

$$\psi_3^o(r) + \frac{\zeta^{-1}}{\pi i}\int_{-1}^{1} \psi_3^o(s)\frac{ds}{s-r} - \frac{\zeta^{-1}}{\pi}\int_{-1}^{1} \psi_4^o(s)\frac{ds}{s+r+b_o} + \int_{-1}^{1} a_1c_1(r,s)\phi_1^o(s)ds + \int_{-1}^{1} a_2c_2(r,s)\phi_2^o(s)ds$$

$$+\frac{b_2-b_1}{2}\int_{-1}^{1}k_1^{\circ}(r,s)\psi_3^{\circ}(s)ds+\frac{b_2-b_1}{2}\int_{-1}^{1}k_2^{\circ}(r,s)\psi_4^{\circ}(s)ds$$

$$=m_1\frac{1-\nu_{xy}\nu_{yx}}{2E_x}p_3(r)+im_2\frac{1}{2G_{xy}}p_4(r) \qquad (3.43a)$$

$$\psi_4^{\circ}(r)-\frac{\zeta^{-1}}{\pi i}\int_{-1}^{1}\psi_4^{\circ}(s)\frac{ds}{s-r}-\frac{\zeta^{-1}}{\pi}\int_{-1}^{1}\psi_3^{\circ}(s)\frac{ds}{s+r+b_o}+\int_{-1}^{1}a_1c_3(r,s)\phi_1^{\circ}(s)ds+\int_{-1}^{1}a_2c_4(r,s)\phi_2^{\circ}(s)ds$$

$$+\frac{b_2-b_1}{2}\int_{-1}^{1}k_3^{\circ}(r,s)\psi_3^{\circ}(s)ds+\frac{b_2-b_1}{2}\int_{-1}^{1}k_4^{\circ}(r,s)\psi_4^{\circ}(s)ds$$

$$=-im_3\frac{1-\nu_{xy}\nu_{yx}}{2E_x}p_3(r)-m_4\frac{1}{2G_{xy}}p_4(r) \qquad (3.43b)$$

Note that the functions $\psi_3^{\circ}(r)$ and $\psi_4^{\circ}(r)$ are related through the following relations:

$$\psi_3^{\circ}(r)=\frac{1}{2}[\phi_3^{\circ}(r)-i\sqrt{\frac{\eta_1}{\eta_2}}\phi_4^{\circ}(r)] \;\&\; \psi_4^{\circ}(r)=\frac{1}{2}[-i\sqrt{\frac{\eta_2}{\eta_1}}\phi_3^{\circ}(r)+\phi_4^{\circ}(r)]=-i\sqrt{\frac{\eta_2}{\eta_1}}\overline{\psi}_3^{\circ}(r) \quad (3.44ab)$$

If both materials are isotropic, it is found that $\sqrt{\frac{\eta_2}{\eta_1}}=1$, and the above equations reduce to:

$$\psi_3^{\circ}(r)=\frac{1}{2}[\phi_3^{\circ}(r)-i\phi_4^{\circ}(r)] \;\&\; \psi_4^{\circ}(r)=\frac{1}{2}[-i\phi_3^{\circ}(r)+\phi_4^{\circ}(r)]=-i\overline{\psi}_3^{\circ}(r) \qquad (3.44a^*,b^*)$$

Now expressing eqns (3.34ab) also in terms of $\psi_3^{\circ}(r)$ and $\psi_4^{\circ}(r)$, we have:

$$\frac{1}{\pi}\int_{-1}^{1}[\frac{1}{s-r}+\pi a_1k_{11}^{\circ}(r,s)]\phi_1^{\circ}(s)ds+\int_{-1}^{1}a_2k_{12}^{\circ}(r,s)\phi_2^{\circ}(s)ds$$

$$+\frac{b_2-b_1}{2}\int_{-1}^{1}[T_1\psi_3^{\circ}(s)ds+\overline{T}_1\overline{\psi}_3^{\circ}(s)]ds=\frac{1-\nu_{xy}\nu_{yx}}{2\gamma_{14}E_y}p_1^0(r) \qquad (3.34a^*)$$

$$\int_{-1}^{1}a_1k_{21}^{\circ}(r,s)\phi_1^{\circ}(s)ds+\frac{1}{\pi}\int_{-1}^{1}[\frac{1}{s-r}+\pi a_2k_{22}^{\circ}(r,s)]\phi_2^{\circ}(s)ds$$

$$+\frac{b_2-b_1}{2}\int_{-1}^{1}[T_2\psi_3^{\circ}(s)ds+\overline{T}_2\overline{\psi}_3^{\circ}(s)]ds=\frac{1-\nu_{xy}^*\nu_{yx}^*}{2\gamma_{14}^*E_y^*}p_2^0(r) \qquad (3.34b^*)$$

where $\quad T_1=k_{13}^{\circ}+i\sqrt{\frac{\eta_2}{\eta_1}}k_{14}^{\circ} \qquad \overline{T}_1=k_{13}^{\circ}-i\sqrt{\frac{\eta_2}{\eta_1}}k_{14}^{\circ}$

$$T_2 = k_{23}^{o} + i\sqrt{\frac{\eta_2}{\eta_1}}k_{24}^{o} \quad \text{and} \quad \overline{T}_2 = k_{23}^{o} - i\sqrt{\frac{\eta_2}{\eta_1}}k_{24}^{o} \qquad (3.45abcd)$$

3.1.4 Numerical Solutions

In this section, numerical procedures are outlined for solving the singular integral equations for different crack configurations as discussed in the previous section. The goal is to determine the stress intensity factor and or the strain energy release rate at the crack tip for each crack configuration. Three H-shaped crack configurations are used. These are: (a) embedded H-shaped cracks, (b) broken matrix H-shaped cracks and (c) the intersecting H-shaped cracks.

3.1.4.1 Embedded H-shaped Cracks

Figure 3.1 shows the embedded H-shaped crack geometry. In this case, the normalized singular integral equations take the following form as derived above:

$$\frac{1}{\pi}\int_{-1}^{1}\left[\frac{1}{s-r}+\pi a_1 k_{11}^{o}(r,s)\right]\phi_1^{o}(s)ds+\int_{-1}^{1}a_2 k_{12}^{o}(r,s)\phi_2^{o}(s)ds$$
$$+\frac{b_2-b_1}{2}\int_{-1}^{1}\left[T_1\psi_3^{o}(s)ds+\overline{T}_1\overline{\psi}_3^{o}(s)\right]ds=\frac{1-\nu_{xy}\nu_{yx}}{2\gamma_{14}E_y}p_1^{0}(r) \qquad (3.46a)$$

$$\int_{-1}^{1}a_1 k_{21}^{o}(r,s)\phi_1^{o}(s)ds+\frac{1}{\pi}\int_{-1}^{1}\left[\frac{1}{s-r}+\pi a_2 k_{22}^{o}(r,s)\right]\phi_2^{o}(s)ds$$
$$+\frac{b_2-b_1}{2}\int_{-1}^{1}\left[T_2\psi_3^{o}(s)ds+\overline{T}_2\overline{\psi}_3^{o}(s)\right]ds=\frac{1-\nu_{xy}^{*}\nu_{yx}^{*}}{2\gamma_{14}^{*}E_y^{*}}p_2^{0}(r) \qquad (3.46b)$$

$$\psi_3^{o}(r)+\frac{\zeta^{-1}}{\pi i}\int_{-1}^{1}\psi_3^{o}(s)\frac{ds}{s-r}-\frac{\zeta^{-1}}{\pi}\int_{-1}^{1}\psi_4^{o}(s)\frac{ds}{s+r+b_o}+\int_{-1}^{1}a_1 c_1(r,s)\phi_1^{o}(s)ds+\int_{-1}^{1}a_2 c_2(r,s)\phi_2^{o}(s)ds$$
$$+\frac{b_2-b_1}{2}\int_{-1}^{1}k_1^{o}(r,s)\psi_3^{o}(s)ds+\frac{b_2-b_1}{2}\int_{-1}^{1}k_2^{o}(r,s)\psi_4^{o}(s)ds$$
$$=m_1\frac{1-\nu_{xy}\nu_{yx}}{2E_x}p_3(r)+im_2\frac{1}{2G_{xy}}p_4(r) \qquad (3.46c)$$

$$\psi_4^{o}(r)-\frac{\zeta^{-1}}{\pi i}\int_{-1}^{1}\psi_4^{o}(s)\frac{ds}{s-r}-\frac{\zeta^{-1}}{\pi}\int_{-1}^{1}\psi_3^{o}(s)\frac{ds}{s+r+b_o}+\int_{-1}^{1}a_1 c_3(r,s)\phi_1^{o}(s)ds+\int_{-1}^{1}a_2 c_4(r,s)\phi_2^{o}(s)ds$$

$$+\frac{b_2-b_1}{2}\int_{-1}^{1} k_3^o(r,s)\psi_3^o(s)ds+\frac{b_2-b_1}{2}\int_{-1}^{1} k_4^o(r,s)\psi_4^o(s)ds$$

$$=-im_3\frac{1-\nu_{xy}\nu_{yx}}{2E_x}p_3(r)-m_4\frac{1}{2G_{xy}}p_4(r) \qquad (3.46d)$$

Of the four equations above, only three are independent since $\psi_3^o(r)$ and $\psi_4^o(r)$ are related through eqn (3.44b). Thus only the first three will be used.

Equations (3.46a) and (3.46b) are Fredholm equations of first kind. For the solution the Lobatto-Chebyshev integration formula is used. Equation (3.46c) is Fredholm equation of second kind and thus a Lobatto-Jacobi quadrature rule is used.

Let $\phi_1^0(s)=\frac{F_1^o(s)}{\sqrt{1-s^2}}$, $\phi_2^o(s)=\frac{F_2^o(s)}{\sqrt{1-s^2}}$ and $\psi_3^o(s)=\frac{F_3(s)}{(1+s)^{\alpha_3}(1-s)^{\beta_3}}$

here $\alpha = -\beta_3$, $\beta = -\alpha_3$,

Using the methods described in [24-31], we obtain:

$$\sum_{k=1}^{n}\{\frac{W_k}{\pi}[\frac{1}{s_k-r_i}+\pi a_1 K_{11}^o(r_i,s_k)]F_1^o(s_k)+a_2W_kK_{12}^o(r_i,s_k)F_2^o(s_k)\}$$

$$+\frac{b_2-b_1}{2}\sum_{j=1}^{N+1}[T_1(r_i,s_{yj})W_{yj}F_3^o(s_{yj})+\overline{T}_1(r_i,s_{yj})\overline{W}_{yj}\overline{F}_3^o(s_{yj})]=\frac{1-\nu_{xy}\nu_{yx}}{2\gamma_{14}E_y}p_1^0(r_i) \qquad (3.47a)$$

$$\sum_{k=1}^{n}\{a_1W_kK_{21}^o(r_i,s_k)F_1^o(s_k)+\frac{W_k}{\pi}[\frac{1}{s_k-r_i}+\pi a_2K_{22}^o(r_i,s_k)]F_2^o(s_k)\}$$

$$+\frac{b_2-b_1}{2}\sum_{j=1}^{N+1}[T_2(r_i,s_{yj})W_{yj}F_3^o(s_{yj})+\overline{T}_2(r_i,s_{yj})\overline{W}_{yj}\overline{F}_3^o(s_{yj})]=\frac{1-\nu_{xy}^*\nu_{yx}^*}{2\gamma_{14}^*E_y^*}p_2^0(r_i) \qquad (3.47b)$$

$$\frac{\zeta^{-1}}{\pi i}\sum_{j=1}^{N+1}\frac{W_{yj}F_3^o(s_{yj})}{s_{yj}-r_{yi}}-\frac{\zeta^{-1}}{\pi}\sum_{j=1}^{N+1}\frac{\overline{W}_{yj}\overline{F}_3^o(s_{yj})}{s_{yj}+r_{yi}+b_o}+\sum_{k=1}^{n}[a_1c_1(r_i,s_k)F_1^o(s_k)+a_2c_2(r_i,s_k)F_2^o(s_k)]W_k$$

$$+\frac{b_2-b_1}{2}\sum_{j=1}^{N+1}[T_3(r_{yi},s_{yj})W_{yj}F_3^o(s_{yj})+T_4(r_{yi},s_{yj})\overline{W}_{yj}\overline{F}_3^o(s_{yj})]$$

$$=m_1\frac{1-\nu_{xy}\nu_{yx}}{2E_x}p_3(r_{yi})+im_2\frac{1}{2G_{xy}}p_4(r_{yi}) \qquad (3.47c)$$

where $T_3 = k_1^o(r_{yi}, s_{yj})$, $T_4 = -i\sqrt{\frac{\eta_2}{\eta_1}}\, k_2^o(r_{yi}, s_{yj})$ and

$$W_k = \frac{1}{2}\frac{\pi}{n-1} \qquad (k = 1, n)$$

$$W_k = \frac{\pi}{n-1} \qquad (k = 2,..n-1)$$

$$s_k = \cos[\frac{\pi(k-1)}{(n-1)}] \qquad (k = 1,...n)$$

$$r_i = \cos[\frac{\pi(2i-1)}{2(n-1)}] \qquad (i = 1,...n-1)$$

$$W_{yj} = \frac{2^{\alpha+\beta+1} N![\Gamma(\beta+1)]^2 \Gamma(\alpha+N+2)}{\Gamma(\beta+N+2)\Gamma(\alpha+\beta+N+3)}(1+\beta) \qquad (yj = 0)$$

$$W_{yj} = \frac{2^{\alpha+\beta+1} N![\Gamma(\alpha+1)]^2 \Gamma(\beta+N+2)}{\Gamma(\alpha+N+2)\Gamma(\alpha+\beta+N+3)}(1+\alpha) \qquad (yj = N+1)$$

$$W_{yj} = \frac{2^{\alpha+\beta+1}\Gamma(\alpha+N+2)\Gamma(\beta+N+2)}{(N+1)(N+1)!\Gamma(\alpha+\beta+N+3)}\frac{1}{[P_N^{(\alpha,\beta)}(s_{yj})]^2} \qquad (yj = 1,..N)$$

The abscissas s_{yj} are the roots of the following equation:

$$(1- s_{yj}^2)P_{N-1}^{(\alpha+1,\beta+1)}(s_{yj}) = 0$$

and the collocation points r_{yi} satisfy the N-th order Jacobi polynomial:

$$P_N^{(-\alpha-1,-\beta-1)}(r_{yi}) = 0$$

$\overline{W}_{yj}$ and $\overline{F}_3^o(s_{yj})$ are the complex conjugates of W_{yj} and $F_3^o(s_{yj})$ respectively.

At the interface, since α and β are complex numbers, the weights W_{yj}, the abscissas s_{yj} and the collocation points r_{yi} will also be complex. The technique of using the complex weights, abscissas and collocation points is not new. One can refer to [31-34] for more detail.

Note that generally $F_3^o(s_{yj})$ (yj = 1,...N+1) are complex numbers, equation (3.47c) actually provides two sets of equations (for real and imaginary parts). Together, equations

(3.47abc) provide 2(n-1)+2(N) equations. Since there are 2(n)+2(N+1) unknowns in eqns (3.47abc), the following additional single valuedness conditions are needed:

$$\int_{-1}^{1} \phi_1^{\circ}(s)ds = 0, \qquad \int_{-1}^{1} \phi_2^{\circ}(s)ds = 0 \qquad \text{and} \qquad \int_{-1}^{1} \psi_3^{\circ}(s)ds = 0$$

These in turn provide four additional linear equations:

$$\sum_{k=1}^{n} W_k F_1^{\circ}(t_k) = 0$$

$$\sum_{k=1}^{n} W_k F_2^{\circ}(t_k) = 0$$

$$\sum_{j=1}^{N+1} W_j F_3^{\circ}(s_{yj}) = 0 \qquad (3.48abcd)$$

Note also that here the last expression provides two sets of equations.

Once the values of $F_1^{\circ}(t_k)$, $F_2^{\circ}(t_k)$ (k=1,...n) and $F_3^{\circ}(s_{yj})$=Re[$F_3^{\circ}(s_{yj})$] + iIm[$F_3^{\circ}(s_{yj})$] (y_j = 1,...N+1) are determined, the stress intensity factors can be found as: (see Appendix E for the details of derivation):

$$k(a_1) = -\frac{2\gamma_{14}E_y\sqrt{a_1}}{(1-\nu_{xy}\nu_{yx})}F_1^{\circ}(1), \quad k(a_2) = -\frac{2\gamma_{14}^{*}E_y^{*}\sqrt{a_2}}{(1-\nu_{xy}^{*}\nu_{yx}^{*})}F_2^{\circ}(1) \qquad (3.49ab)$$

$$\frac{1}{\rho_3}\frac{1}{2G_{xy}}k_2(b_1) - i\sqrt{\frac{\rho_4}{\rho_1\rho_2\rho_3}}\frac{1-\nu_{xy}\nu_{yx}}{2E_x}k_1(b_1) = L\sqrt{1-\zeta^2}\,F_3^{\circ}(-1) \qquad (3.49c)$$

$$\frac{1}{\rho_3}\frac{1}{2G_{xy}}k_2(b_2) - i\sqrt{\frac{\rho_4}{\rho_1\rho_2\rho_3}}\frac{1-\nu_{xy}\nu_{yx}}{2E_x}k_1(b_2) = -L\sqrt{1-\zeta^2}\,F_3^{\circ}(1) \qquad (3.49d)$$

It should be noted that in eqns (3.49cd), k_1 and k_2 have the unit of $\sigma\sqrt{b}$ instead of the conventional $\sigma\sqrt{b}$ and $L = \frac{b_2 - b_1}{2}$.

If the materials of both layers are isotropic, it can be shown numerically that the coefficients of k_1 and k_2 in eqns (3.49cd) are equal, i.e.:

$$\frac{1}{\rho_3}\frac{1}{2G_{xy}} = \sqrt{\frac{\rho_4}{\rho_1\rho_2\rho_3}}\frac{1-\nu_{xy}\nu_{yx}}{2E_x}$$

and eqns (3.49c,d) reduce to

$$k_2(b_1) - ik_1(b_1) = 2G_{xy}\rho_3\sqrt{1-\zeta^2}\,LF_3^{\circ}(-1) \qquad (3.49c^*)$$

$$k_2(b_2) - ik_1(b_2) = -2G_{xy}\rho_3\sqrt{1-\zeta^2}\,LF_3^{\circ}(1) \qquad (3.49d^*)$$

The strain energy release rate at the interface crack tip can be derived as follows:

$$\frac{\Delta E}{\Delta y} = \frac{\pi}{\sqrt{1-\zeta^2}}\left[\frac{1-\nu_{xy}\nu_{yx}}{2E_x}\frac{1}{\rho_2}k_1^2 + \frac{1}{2G_{xy}}\frac{1}{\rho_3}k_2^2\right] \qquad (3.50)$$

Again if both layers are made of isotropic materials, the above equation reduces to

$$\frac{\Delta E}{\Delta y} = \frac{\pi}{\sqrt{1-\zeta^2}}\frac{1}{2G_{xy}}\frac{1}{\rho_3}(k_1^2 + k_2^2) \qquad (3.50^*)$$

It should be noted that when upper and lower interface cracks meet (that is when $b_1 = 0$), eqns (3.46a-d) should be modified before proceeding to the numerical solution. First the integral limits for interface cracks should be extended from $(0, b_2)$ to $(-b_2, b_2)$. Then, using the following relations:

$$\phi_3^{\circ}(t) = \phi_3^{\circ}(-t) \qquad \phi_4^{\circ}(t) = -\phi_4^{\circ}(-t)$$

$$K_{j3}(x_i, t) = K_{j3}(x_i, -t) \qquad K_{i4}(x_i, t) = -K_{i4}(x_i, -t) \quad (i = 1,2)$$

$$K_{j3}(y, t) = K_{j3}(y, -t) \quad \text{and} \quad K_{j4}(y, t) = -K_{j4}(y, -t) \quad (j = 3,4)$$

eqns (3.46abcd) can be reduced to:

$$\frac{1}{\pi}\int_{-1}^{1}\left[\frac{1}{s-r} + \pi a_1 k_{11}^{\circ}(r,s)\right]\phi_1^{\circ}(s)ds + \int_{-1}^{1} a_2 k_{12}^{\circ}(r,s)\phi_2^{\circ}(s)ds$$
$$+ \frac{b_2}{2}\int_{-1}^{1}\left[T_1\psi_3^{\circ}(s)ds + \overline{T}_1\overline{\psi}_3^{\circ}(s)\right]ds = \frac{1-\nu_{xy}\nu_{yx}}{2\gamma_{14}E_y}p_1^0(r) \qquad (3.51a)$$

$$\int_{-1}^{1} a_1 k_{21}^{\circ}(r,s)\phi_1^{\circ}(s)ds + \frac{1}{\pi}\int_{-1}^{1}\left[\frac{1}{s-r} + \pi a_2 k_{22}^{\circ}(r,s)\right]\phi_2^{\circ}(s)ds$$
$$+ \frac{b_2}{2}\int_{-1}^{1}\left[T_2\psi_3^{\circ}(s)ds + \overline{T}_2\overline{\psi}_3^{\circ}(s)\right]ds = \frac{1-\nu_{xy}^{*}\nu_{yx}^{*}}{2\gamma_{14}^{*}E_y^{*}}p_2^0(r) \qquad (3.51b)$$

$$\psi_3^{\circ}(r) + \frac{\zeta^{-1}}{\pi i}\int_{-1}^{1}\psi_3^{\circ}(s)\frac{ds}{s-r} + \int_{-1}^{1} a_1 c_1(r,s)\phi_1^{\circ}(s)ds + \int_{-1}^{1} a_2 c_2(r,s)\phi_2^{\circ}(s)ds$$

$$+\frac{b_2}{2}\int_{-1}^{1}[k_1^{\circ}(r,s)\psi_3^{\circ}(s)+k_2^{\circ}(r,s)\psi_4^{\circ}(s)]ds$$

$$=m_1\frac{1-\nu_{xy}\nu_{yx}}{2E_x}p_3(r)+im_2\frac{1}{2G_{xy}}p_4(r) \qquad (3.51c)$$

$$\psi_4^{\circ}(r)-\frac{\zeta^{-1}}{\pi i}\int_{-1}^{1}\psi_4^{\circ}(s)\frac{ds}{s-r}+\int_{-1}^{1}a_1c_3(r,s)\phi_1^{\circ}(s)ds+\int_{-1}^{1}a_2c_4(r,s)\phi_2^{\circ}(s)ds$$

$$+\frac{b_2}{2}\int_{-1}^{1}[k_3^{\circ}(r,s)\psi_3^{\circ}(s)+k_4^{\circ}(r,s)\psi_4^{\circ}(s)]ds$$

$$=-im_3\frac{1-\nu_{xy}\nu_{yx}}{2E_x}p_3(r)-m_4\frac{1}{2G_{xy}}p_4(r) \qquad (3.51d)$$

The numerical procedure and the single valuedness conditions mentioned above should also be applied to solve eqns (3.51abc). In this case (i.e. when $b_1 = 0$), $L = b_2$ should be used in eqns (3.49cd) and (3.49cd*)

3.1.4.2 Broken Matrix H-shaped Cracks ($a_2=H_2$, $b_1>0$)

When matrix cracks touch the interface, the kernel $F_{11}^{\circ}(x_1,t)$ becomes unbounded. And the singular behavior at the crack tip changes. Now, redefining $\phi_1^0(s)$ as:

$$\phi_1^0(s)=\frac{F_1^{\circ}(s)}{(1-s^2)^{\gamma}}$$

The determination of the power of singularity γ is shown in Appendix F.

Since γ is generally different than 0.5, in the numerical procedures described for eqns (3.47a-c), Lobatto-Jacobi quadrature was used for integrals containing $\phi_1^{\circ}(s)$. The rest of the definitions and numerical calculations in eqns (3.47abc) remain the same. The modified version takes the following form:

$$\sum_{k=1}^{n}\{\frac{W_k'}{\pi}[\frac{1}{s_k'-r_i'}+\pi a_1K_{11S}^{\circ}(r_i',s_k')]F_1^{\circ}(s_k')+W_k'a_1K_{11f}^{\circ}(r_i',s_k')F_1^{\circ}(s_k')+a_2W_kK_{12}^{\circ}(r_i',s_k)F_2^{\circ}(s_k)\}$$

$$+\frac{b_2-b_1}{2}\sum_{j=1}^{N+1}[T_1(r_i',s_{yj})W_{yj}\,F_3^{\circ}(s_{yj})+\overline{T}_1(r_i',s_{yj})\overline{W}_{yj}\,\overline{F}_3^{\circ}(s_{yj})]=\frac{1-\nu_{xy}\nu_{yx}}{2\gamma_{14}E_y}p_1^0(r_i') \qquad (3.52a)$$

$$\sum_{k=1}^{n} \{a_1 W_k' K_{21}^{\circ}(r_i,s_k')F_1^{\circ}(s_k') + \frac{W_k}{\pi}[\frac{1}{s_k - r_i} + \pi a_2 K_{22}^{\circ}(r_i,s_k)]F_2^{\circ}(s_k)\}$$

$$+ \frac{b_2 - b_1}{2}\sum_{j=1}^{N+1} [T_2(r_i,s_{yj})W_{yj}F_3^{\circ}(s_{yj}) + \overline{T}_2(r_i,s_{yj})\overline{W}_{yj}\,\overline{F}_3^{\circ}(s_{yj})] = \frac{1-\nu_{xy}^{*}\nu_{yx}^{*}}{2\gamma_{14}^{*}E_y^{*}} p_2^{0}(r_i) \qquad (3.52b)$$

$$\frac{\zeta^{-1}}{\pi i}\sum_{j=1}^{N+1} \frac{W_{yj}F_3^{\circ}(s_{yj})}{s_{yj} - r_{yi}} - \frac{\zeta^{-1}}{\pi}\sum_{j=1}^{N+1} \frac{\overline{W}_{yj}\overline{F}_3^{\circ}(s_{yj})}{s_{yj} + r_{yi} + b_o} + \sum_{k=1}^{n} [a_1 c_1(r_{yi},s_k')F_1^{\circ}(s_k')W_k' + a_2 c_2(r_{yi},s_k)F_2^{\circ}(s_k)W_k]$$

$$+ \frac{b_2 - b_1}{2}\sum_{j=1}^{N+1} [T_3(r_{yi},s_{yj})W_{yj}F_3^{\circ}(s_{yj}) + T_4(r_{yi},s_{yj})\overline{W}_{yj}\,\overline{F}_3^{\circ}(s_{yj})]$$

$$= m_1 \frac{1-\nu_{xy}\nu_{yx}}{2E_x} p_3(r_{yi}) + im_2 \frac{1}{2G_{xy}} p_4(r_{yi}) \qquad (3.52c)$$

Where: $K_{11S}^{\circ}(r_i',s_k')$ and $K_{11f}^{\circ}(r_i',s_k')$ are the singular and finite part of the kernel $K_{11}^{\circ}(r_i',s_k')$ respectively (a detailed analysis of the singular behaviors of the kernels is given in Appendix D), and

$$W_k' = \frac{2^{1-\gamma-\gamma}(n-1)![\Gamma(1-\gamma)]^2}{\Gamma(n+2-2\gamma)}(1-\gamma) \qquad (k=1,n)$$

$$W_k' = \frac{2^{1-\gamma-\gamma}(n-1)![\Gamma(1-\gamma)]^2}{\Gamma(n+2-2\gamma)} \frac{1}{[P_{n-1}^{(-\gamma,-\gamma)}(s_k')]^2} \qquad (k=2,..n-1)$$

The abscissa s_k' are the roots of the following equation:

$$(1-s_k'^2)P_{n-2}^{(1-\gamma,1-\gamma)}(s_k') = 0$$

and the collocation points r_i' may be obtained from:

$$P_{n-1}^{(\gamma-1,\gamma-1)}(r_i') = 0$$

The methods of evaluating the weights, abscissa W_k, t_k for Lobatto-Chebyshev integration rule, W_j, s_{yj} for Lobatto-Jacobi integration rule and the collocation points r_i and r_{yi} will be the same as those described in section 3.1.4.1.

Also the single valuedness conditions become:

$$\sum_{k=1}^{n} W_k' F_1^{\circ}(t_k) = 0$$

$$\sum_{k=1}^{n} W_k F_2^{\circ}(t_k) = 0$$

$$\sum_{j=1}^{N+1} W_{yj} F_3^{\circ}(s_{yj}) = 0 \qquad (3.53abcd)$$

The expressions for stress intensity factors and strain energy release rates given in eqn (3.49ab) and (3.50) remain valid for interface crack. But for $k(a_1)$, the following expression should be used:

$$k(a_1) = \frac{(H_1)^{2\gamma}\gamma_{14}^{*}E_y^{*}F_1^{\circ}(1)}{(1-\nu_{xy}^{*}\nu_{yx}^{*})\sin(\pi\gamma)}\left[\lambda_{101}\frac{|w_1|/\beta_5}{\left[|w_1^{*}||w_1|/\beta_5\right]^{\gamma}} + \lambda_{102}\frac{|w_1|/\beta_5}{\left[|w_3^{*}||w_1|/\beta_5\right]^{\gamma}}\right.$$

$$\left. + \lambda_{103}\frac{|w_3|/\beta_5}{\left[|w_3||w_1^{*}|/\beta_5\right]^{\gamma}} + \lambda_{101}\frac{|w_3|/\beta_5}{\left[|w_3||w_3^{*}|/\beta_5\right]^{\gamma}}\right] \qquad (3.54)$$

For detailed derivation please see Appendix E.

3.1.4.3 Intersecting H-shaped Cracks ($a_2=H_2$, $b_1=0$)

When $a_1 = H_1$ and $b_1 = 0$, the transverse matrix cracks intersect with the interface crack to form H-shaped cracks as shown in Fig. 3.2. This configuration has been observed during the tensile test of the uniaxial ceramic matrix composites. Since the power of singularity at the point of intersection is zero, which has been confirmed numerically, $\phi_1^{\circ}(s)$ will no longer be singular at this crack tip. Also, the kernels K_{11}, K_{13}, K_{14}, K_{31} and K_{41} become unbounded. In this case, because $b_1 = 0$, the numerical calculations will be based on eqns (3.51abc) instead of eqns (3.46abc).

First, the singular parts of the kernels K_{11}, K_{13}, K_{14}, K_{31} and K_{41} in eqns (3.51abc) will be extracted and integrated in closed form. Consequently the modified equations take the following form:

$$\frac{1}{\pi}\int_{-1}^{1}\left[\frac{1}{s-r}+\pi a_1 k_{11s}^{\circ}(r,s)\right]\phi_1^{\circ}(s)ds + \int_{-1}^{1} a_1[k_{11}^{\circ}(r,s)-k_{11s}^{\circ}(r,s)]\phi_1^{\circ}(s)ds$$

$$+ \int_{-1}^{1} a_2 k_{12}^{\circ}(r,s)\phi_2^{\circ}(s)ds + \frac{b_2}{2}\int_{-1}^{1}\left[T_{1s}\psi_3^{\circ}(s)ds + \overline{T}_{1s}\overline{\psi}_3^{\circ}(s)\right]ds$$

$$+\frac{b_2}{2}\int_{-1}^{1}[(T_1-T_{1s})\psi_3^o(s)ds+(\overline{T}_1-\overline{T}_{1s})\overline{\psi}_3^o(s)]ds=\frac{1-\nu_{xy}\nu_{yx}}{2\gamma_{14}E_y}p_1^0(r) \tag{3.55a}$$

$$\int_{-1}^{1}a_1k_{21}^o(r,s)\phi_1^o(s)ds+\frac{1}{\pi}\int_{-1}^{1}[\frac{1}{s-r}+\pi a_2k_{22}^o(r,s)]\phi_2^o s)ds$$

$$+\frac{b_2}{2}\int_{-1}^{1}[T_2\psi_3^o(s)ds+\overline{T}_2\overline{\psi}_3^o(s)]ds=\frac{1-\nu_{xy}^*\nu_{yx}^*}{2\gamma_{14}^*E_y^*}p_2^0(r) \tag{3.55b}$$

$$\psi_3^o(r)+\frac{\zeta^{-1}}{\pi i}\int_{-1}^{1}\psi_3^o(s)\frac{ds}{s-r}+\int_{-1}^{1}a_1c_{1s}(r,s)\phi_1^o(s)ds+\int_{-1}^{1}a_1[c_1(r,s)-c_{1s}(r,s)]\phi_1^o(s)ds$$

$$+\int_{-1}^{1}a_2c_2(r,s)\phi_2^o(s)ds+\frac{b_2}{2}\int_{-1}^{1}[k_1^o(r,s)\psi_3^o(s)+k_2^o(r,s)\psi_4^o(s)]ds$$

$$=m_1\frac{1-\nu_{xy}\nu_{yx}}{2E_x}p_3(r)+im_2\frac{1}{2G_{xy}}p_4(r) \tag{3.55c}$$

where $T_{1s}=k_{13s}^o+i\sqrt{\frac{\eta_2}{\eta_1}}k_{14s}^o \qquad \overline{T}_{1s}=k_{13s}^o-i\sqrt{\frac{\eta_2}{\eta_1}}k_{14s}^o$

and $c_{1s}(r,s)=[\frac{k_{31s}^o}{\rho_1}+i\frac{k_{41s}^o}{\rho_4}\sqrt{\frac{\eta_1}{\eta_2}}]$

Now defining $\phi_1^o(s) = F_1^o(s)$, and the definitions for the rest of the displacement density functions remaining the same as in section 3.1.4.1, we have:

$$\sum_{k=1}^{n}\{\frac{W_k'}{\pi}[\frac{1}{s_k'-r_i'}+\pi a_1K_{11s}^o(r_i',s_k')]F_1^o(s_k')+a_1W_k'[K_{11}^o(r_i',s_k')-K_{11s}^o(r_i',s_k')]F_1^o(s_k')$$

$$a_2W_kK_{12}^o(r_i',s_k)F_2^o(s_k)\}+\frac{b_2}{2}\sum_{j=1}^{N+1}[T_{1s}(r_i',s_{yj})W_{yj}F_3^o(s_{yj})+\overline{T}_{1s}(r_i',s_{yj})\overline{W}_{yj}\overline{F}_3^o(s_{yj})]$$

$$\frac{b_2}{2}\sum_{j=1}^{N+1}\{[T_1(r_i',s_{yj})-T_{1s}(r_i',s_{yj})]W_{yj}F_3^o(s_{yj})+[\overline{T}_1(r_i',s_{yj})-\overline{T}_{1s}(r_i',s_{yj})]\overline{W}_{yj}\overline{F}_3^o(s_{yj})\}$$

$$=\frac{1-\nu_{xy}\nu_{yx}}{2\gamma_{14}E_y}p_i^o(r_i') \tag{3.56a}$$

$$\sum_{k=1}^{n}\{a_1W_k'K_{21}^o(r_i,s_k')F_1^o(s_k')+\frac{W_k}{\pi}[\frac{1}{s_k-r_i}+\pi a_2K_{22}^o(r_i,s_k)]F_2^o(s_k)\}$$

$$+\frac{b_2}{2}\sum_{j=1}^{N+1}[T_2(r_i,s_{yj})W_{yj}F_3^o(s_{yj})+\overline{T}_2(r_i,s_{yj})\overline{W}_{yj}\overline{F}_3^o(s_{yj})]=\frac{1-\nu_{xy}^*\nu_{yx}^*}{2\gamma_{14}^*E_y^*}p_2^0(r_i) \tag{3.56b}$$

$$\frac{\zeta^{-1}}{\pi i}\sum_{j=1}^{N+1}\frac{W_{yj}F_3^{\circ}(s_{yj})}{s_{yj}-r_{yi}}-\frac{\zeta^{-1}}{\pi}\sum_{j=1}^{N+1}\frac{\overline{W}_{yj}\overline{F}_3^{\circ}(s_{yj})}{s_{yj}+r_{yi}+b_o}+\sum_{k=1}^{n}W_k' a_1 c_{1s}(r_{yj},s_k')F_1^{\circ}(s_k')$$

$$+\sum_{k=1}^{n}W_k' a_1[\,c_1(r_{yj},s_k')-c_{1s}(r_{yj},s_k')F_1^{\circ}(s_k')+\sum_{k=1}^{n}W_k a_2 c_2(r_i,s_k)F_2^{\circ}(s_k)$$

$$+\frac{b_2}{2}\sum_{j=1}^{N+1}[T_3(r_{yi},s_{yj})W_{yj}F_3^{\circ}(s_{yj})+T_4(r_{yi},s_{yj})\overline{W}_{yj}\overline{F}_3^{\circ}(s_{yj})]$$

$$=m_1\frac{1-\nu_{xy}\nu_{yx}}{2E_x}p_3(r_{yi})+im_2\frac{1}{2G_{xy}}p_4(r_{yi}) \qquad (3.56c)$$

where

$$W_k' = \frac{2}{n(n-1)} \qquad (k=1,n)$$

$$W_k' = \frac{2}{n(n-1)}\frac{1}{[P_{n-1}(s_k')]^2} \qquad (k=2,..n-1)$$

and the abscissas s_k' are the roots of the following equation:

$$(1-s_k'^2)P_{n-2}^{(1,1)}(s_k')=0$$

W_k' and s_k' are the weights and abscissas of the Lobatto-Legendre integration rule.

The collocation points r_i' are given by:

$$P_{n-1}^{(-1,-1)}(r_i')=0$$

Again, the methods of evaluating the weights and abscissas W_k, t_k for Lobatto-Chebyshev integration rule; W_j, s_{yj} for Lobatto-Jacobi integration rule and the collocation points r_i and r_{yi} remain the same as those given in section 3.1.4.1.

The remaining four additional equations take the following form:

$$F_1^{\circ}(-1)=0 \qquad (3.57a)$$

$$F_1^{\circ}(1)=0 \qquad (3.57b)$$

$$\int_{-1}^{1}\phi_2^{\circ}(s)ds=0 \qquad (3.57c)$$

and

$$\int_{-H_1}^{H_1}\phi_1(s)ds=\int_0^{b_2}\phi_3(s)ds \qquad (3.57d)$$

The first two equations originate from the requirement that $\phi_i^{\circ}(s)$ remains finite at both crack tips. The third equation is deduced from the single valuedness condition for

embedded cracks in the fiber if a_2 is not zero. And the last equation states the condition of continuity of displacement at the point of intersection.

Eqns (3.57ab) can be directly used in the numerical calculations. Eqn (3.57c) can be written as:

$$\sum_{k=1}^{n} W_k F_2^{\circ}(t_k) = 0 \qquad (3.57c^*)$$

Using the fact that

$$\int_0^{b_2} \phi_3(s)ds = \frac{b_2}{2}\int_{-1}^{1} \phi_3^{\circ}(s)ds$$

$$= -i\frac{b_2}{2}\int_{-1}^{1} \psi_3^{\circ}(s)ds$$

the real part of above equation can be written as:

$$\sum_{k=1}^{n} W_k F_1^{\circ}(t_k) = \mathrm{Re}\left(-i\frac{b_2}{2}\sum_{j=1}^{N+1} W_j F_3^{\circ}(s_{yj})\right) \qquad (3.57d^*)$$

This gives the last equation that is needed for the numerical calculations.

The calculation of the stress intensity factors and the strain energy release rate at the interface crack remain the same as given in eqns(3.49cd) (with $L = b_2$) and eqns(3.50).

3.1.5 Results for Singular Integral Equation Formulation

It is well known that the interface bonding strength plays a significant role in the toughness of brittle ceramic matrix composites. A "weak" bonding strength generally improves the toughness of the composite. A direct indication of weak bonding between the matrix and the fiber interface is the existence of interface crack or defects due to debonding process during loading. From the experiment, it was observed that under tensile loading, matrix cracks developed first and then propagated to the interface. Once the matrix cracks reached the interface, they didn't penetrate through the fibers. This means the fracture energy of the fiber is larger than the fracture energy along the interface due to purposely made weak interface bonding strength during manufacture. Therefore the energy will be released along the interface to cause interface debonding or to generate

interface cracks. The actual role that the interface plays has drawn a lot of attention in both research and manufacturing areas. One can refer to [35,36] for detailed discussions. The goal here is to explain or simulate the damage mechanism of the brittle ceramic matrix composites by analyzing the interactions between matrix and interface cracks using different crack configurations.

Table 3.1 Comparison of stress intensity factors

Materials		$\frac{k_1(b)}{\sigma_0 b}$		$\frac{k_2(b)}{\sigma_0 b}$	
Layer 1	Layer 2	Results from [38]	Results from eqn (3.49d)	Results from [38]	Results from eqn (3.49d)
Aluminum	Epoxy	1.0000	1.0000	-0.1342	-0.13421
Steel	Epoxy	1.0000	1.0000	-0.1443	-0.14431
Steel	Aluminum	1.0000	1.0000	-0.09158	-0.091576
Nicalon	CAS II	1.0000	1.0000	-0.071076	-0.071074

To check the correctness of the numerical procedure, some simple crack configurations have been studied first. For periodic transverse cracks in the matrix and the fibers without interface cracks, the results for stress intensity factors match those found in [22,37]; For interface cracks without transverse cracks, if both H_1 and H_2 are set to be very large and the materials of both layers are isotropic, the problem is reduced to an interface crack in an infinite domain and the results from [38,39] for stress intensity factors at the interface are recovered. Table 3.1 gives the results of stress intensity factors at the interface for four different materials combinations. As can be seen from the table, the two results compare well with those found in the literature. Also, the strain energy release rates at the interface for the above four material combinations were calculated using eqn (3.50*). For isotropic materials, the exact expression for the specific strain energy release rate at the interface was first given in [40] as follows:

$$\frac{\Delta E}{\Delta y} = \frac{\pi}{2} \frac{(\mu_1 + \kappa_1\mu_2)(\mu_2 + \kappa_2\mu_1)}{\mu_1\mu_2[(1+\kappa_1)\mu_2 + (1+\kappa_2)\mu_1]} (k_1^2 + k_2^2) \tag{3.58}$$

where μ_1 and μ_2 are the shear moduli of layer one and layer two respectively, $\kappa_{1,2} = 3 - 4\nu_{1,2}$, and k_1 and k_2 are the mode I and Mode II stress intensity factors at the interface crack tip.

The specific strain energy release rates using both eqn (3.50*) and eqn (3.58) are compared in Table 3.2. The error is within 3 percent. Considering the fact that all the derivations are based on the orthotropic materials, and the isotropic behavior was approximated in the calculation, the results are quite good. Table 3.3 gives the Young's moduli and the Poisson's ratios for the materials used in the calculation.

Table 3.2 Comparison of strain energy release rates

Materials		Specific strain energy release rates	
Layer 1	Layer 2	Using eqn (3.58)	Using eqn (3.50*)
Aluminum	Epoxy	0.6246×10^{-5}	0.6320×10^{-5}
Steel	Epoxy	0.6035×10^{-5}	0.6125×10^{-5}
Steel	Aluminum	0.3765×10^{-6}	0.3766×10^{-6}
Nicalon	CAS II	0.3192×10^{-6}	0.3212×10^{-6}

Table 3.3 Material constants

Material	Young's modulus E (lb in. $^{-2}$)	Poisson's ratio
Aluminum	1×10^{7}	0.3
Steel	3×10^{7}	0.3
Epoxy	4.5×10^{5}	0.35
Nicalon	28.3×10^{7}	0.28
CAS II	13.2×10^{7}	0.28

If both transverse and interface cracks exist and both the widths of the periodic layers $2H_1$ and $2H_2$ are finite, this formulation can also be used to calculate the stress intensity factor at a transverse crack tip in an infinite strip of finite width under uniform far field tension. In Figure 3.3, two results for the stress intensity factor at a transverse crack tip in an infinite strip made of isotropic material are given. The first one is the classical finite element solution which gives the stress intensity factor at the crack tip in terms of a polynomial expression [41]:

$$\frac{k(a)}{\sigma\sqrt{a}} = [\sec(\frac{\pi a}{2W}]^{1/2}[1-0.025(\frac{a}{W})^2+0.06(\frac{a}{W})^4] \qquad (3.59)$$

The second one is this singular integral equation formulation based on the periodic infinite strips containing both collinear transverse cracks and interface cracks. The two results matched quite well. The influence of the interface crack length on the stress intensity factors at the transverse crack tip is shown in Figure 3.4. The asymptote was obtained from eqn (3.59) with a/W = 0.9 for an infinite strip.

Next, the effects of the transverse and interface cracks on the tensile damage behavior of the ceramic matrix composite are investigated.

(a) Embedded H-shaped Cracks ($a_2 < H_2$, $b_1 = 0$)

This configuration is used to simulate the early stages of tensile damage of brittle matrix composites in which both small transverse matrix cracks and interface cracks or defects exist. The effects of interface crack length on the stress intensity factors at the matrix crack tips are shown in Figure 3.5. If the interface crack length is small (b_2/H_2 = 0.001), the stress intensity factor will drop as the matrix crack approaches the interface. This is due to the fiber's constraining effect. However, if there exists a sufficiently large interface crack ($b_2/H_2 \geq 0.5$) in front of the matrix crack tip, the stress intensity factor at the matrix crack tips increases sharply as the matrix crack reaches the interface. The fiber constrain effect disappears. It is also noted that if the interface crack is small, as the matrix

crack approaches the interface, the strain energy release rates at the interface crack tips increase rapidly as can be seen from Figure 3.6. This suggests that small interface crack tend to extend along the interface as the matrix crack approaches the interface. As a result of the interactions between matrix cracks and interface cracks, one can conclude that if there is an interface crack whether it is small or large in front of the matrix crack tip, then the constraining effects of the fibers will eventually disappear.

To find the effect of interface crack length on the stress intensity factors at both matrix and interface crack tips, the matrix crack was fixed (a_2/H_2=0.9) and interface crack was allowed to extend. Figure 3.7 shows the stress intensity factors at the matrix crack tips. The strain energy release rates at the interface crack tip for different interface crack length are shown in Figure 3.8. A rising stress intensity factor at the matrix crack tip is seen as expected. The decrease in the strain energy release rates at the interface crack tip as the interface crack advances indicates that the interface crack will eventually stop opening.

(b) Broken Matrix H-shaped Cracks ($a_2 = H_2$, $b_1 > 0$)

In this case the matrix crack touches the interface. But a small interface crack with a crack length of $d = (b_2 - b_1)$ is assumed to be located some distance away from the tip of matrix crack. One possible damage to the interface would be that the inner interface crack tip propagate toward the matrix crack tip. The variations of the stress intensity factors and the strain energy release rates at both the matrix crack and the interface crack tips are calculated as the inner interface crack tip approaches the matrix crack tip (i.e. b_1 approaching zero while b_2 remains fixed). Figure 3.9 shows that an increase in stress intensity factors at the matrix crack tip occur only when the inner interface crack tip approaches the matrix crack tip. Sharp increase of strain energy release rates are also found at the inner interface crack tip when the inner interface crack reaches the matrix crack tip as can be seen from Figure 3.10. As a result of the sharp changes in stress

intensity factors at the matrix crack tips and strain energy release rates at the interface crack tips, either the interface crack advances first to intersect with the matrix crack and leave the fiber intact, or the matrix crack extends first into the fibers and causes fiber damage. This depends on the relative strength of the fiber fracture toughness and the interface bonding strength.

(c) Intersecting H-shaped Cracks ($a_2 = H_2$, $b_1 = 0$)

When the matrix crack intersects with the interface crack, then intersecting H-shaped cracks are formed. Since there is no stress singularity at the point of intersection therefore no driving force to allow matrix crack to extend to the fiber, one possible further damage to the composite would be along the interface. Figure 3.11 shows strain energy release rate at the interface for increasing interface crack length. The strain energy release rates drop significantly as the interface crack increase. The sharp decrease in strain energy release rate as the interface crack propagate indicates that the progression of interface crack will end as soon as the interface crack length reaches a certain value.

In the above numerical calculations, the normal stresses p_1 on the fiber, p_2 on the matrix and p_3 on the fiber/matrix interface are chosen in such a way so that the following two conditions are satisfied:

$$\frac{p_1}{E_y} - \nu_{yx}\frac{p_3}{E_x} = \frac{p_2}{E_y^*} - \nu_{yx}^*\frac{p_3}{E_x^*}$$

$$\left(\frac{p_3}{E_x} - \nu_{xy}\frac{p_1}{E_y}\right)H_1 + \left(\frac{p_3}{E_x^*} - \nu_{xy}^*\frac{p_2}{E_y^*}\right)H_2 = 0$$

The first one is to ensure that the far field strain in y direction is constant. And the second one makes sure that the strain in x direction is continuous across the interface.

3.2 FINITE ELEMENT ANALYSIS

The finite element model is used to simulate the nonlinear stress strain behavior of the brittle matrix composite. In the previous singular integral equation formulation, only single row intersecting H-shaped cracks was considered. In the finite element formulation, the multiple row intersecting H-shaped crack configuration as shown in Figure 3.12 is used which is closer to the actual damage pattern observed during the tests.

3.2.1 Description of the Multiple-row Intersecting H-shaped Cracks Model

From the experiments, it is observed that, after the appearance of initial transverse matrix cracks, the stress-strain behavior starts to become nonlinear. With increase of the tensile load (about 10 ksi as can be seen from Figures 2.4 and 2.5), a regularly spaced multiple transverse matrix crack pattern is formed. Once this stage is reached, further increase of load generates few new matrix cracks until final failure. Therefore, during the period from which saturated matrix crack formed to eventual failure, interface debonding, matrix crack opening and sequential fiber breaking dominate the failure process. To capture the effect of damage accumulation due to interface debonding, a crack configuration as shown in Figure 3.12 is used where the interface crack length is allowed to increase with increasing load. The popular ABAQUS finite element code is used with strain energy release rate as the criterion for the interface crack propagation. First, the strain energy was calculated for a certain interface crack length, then the interface crack length was allowed to increase by releasing the node at the crack tip and the strain energy was again calculated. Thus an estimation of the strain energy release rate G at the interface crack tip can be determined using the following expression:

$$G = \frac{U_n - U_{n+1}}{t\Delta D} \qquad (n=0,1,2, \cdots\cdots)$$

where U_n and U_{n+1} are the strain energies associated with the two subsequent crack lengths, ΔD is the interface crack increment and t is the thickness of the specimen. If this G value is greater than G_{cr} (critical strain energy release rate), then the crack is assumed to propagate. In practice, the G_{cr} value at the interface is extremely difficult to measure. Here we estimate G_{cr} by matching one point of the stress-strain curve with the calculated value. Table 3.4 shows the computed G_{cr} for both $V_f = 30\%$ and $V_f = 40\%$.

Table 3.4 Estimated critical strain energy release rate G_{cr}

Fiber volume fraction	$L/2H_2$	Estimated G_{cr}
30%	2.5	85.36 (lbs/in)
40%	3.0	62.70 (lbs/in)

3.2.2 Finite Element Results and Discussion

Before the finite element calculation is carried out, one has to determine the matrix crack spacing L and the fiber spacing $2H_2$ used in the model as shown in Figure 3.12. The ratio $L/2H_2$ affects the results significantly. Matrix crack spacing is determined by averaging the matrix crack length from the micrographs taken during the experiment. It is found that the matrix crack spacing decreases with increasing fiber volume fraction of the specimen. The average matrix crack spacing for $V_f = 30\%$ was found to be L = 166 μm. And for $V_f = 40\%$, the value is L = 111 μm. The fiber spacing varies with fiber volume fraction, the fiber diameter and how evenly the fibers are distributed in the matrix. The average fiber diameter for Nicalon fiber is about 16 μm as measured from the test results. Consider the ideal case where fibers are evenly distributed in the matrix media, then for $V_f = 30\%$, $2H_2 = (0.7)(16)/0.3 = 37.3$ μm and for $V_f = 40\%$, $2H_2 = (0.6)(16)/0.4 = 24$ μm. Therefore we have:

$$\frac{L}{2H_2} = 166/37 = 4.44 \qquad \text{for } V_f = 30\%$$

and $\frac{L}{2H_2} = 111/24 = 4.625$ for $V_f = 40\%$

A close observation of the damage surface of the specimens reveals that the actual ratio varies between 0.9 to 4.5. Therefore the ratios derived above for both V_f =30% and V_f = 40% can be considered as upper limits. An average value between 2 and 3 is used in the actual calculation. Figure 3.13 is a comparison of finite element results with the test results for V_f = 30%. Figure 3.14 shows the comparison for V_f = 40 %. It can be seen that finite element results match the test results quite well at the start of the non-linear stress-strain curve. Then the two results deviate somewhat as the load is further increased. This is because at higher loading the fibers start to break as can be seen from the micrographs taken during the tests. This contributes to the flattening of the actual stress-strain curve. It may also be noted that the finite element results for V_f = 30% match the stress-strain diagram better than those for V_f = 40%. This can be explained as follows: with more fibers in the 40% fiber volume fraction specimen, more sequential fiber breakings occurred during the final stage of the experiment after the saturated multiple matrix crack pattern was formed. This can not be simulated by considering interface cracks only.

4. CONCLUSIONS

The following conclusions can be drawn from the experimental data:

1. The damage to the ceramic matrix composite started with matrix cracking, followed by multiple matrix cracking, interface debonding, sequential fiber breaking and eventual fracture of specimens.
2. Matrix crack density can be used to characterize the damage behavior of brittle matrix composites. Matrix crack density increases with increasing fiber volume fraction.
3. Fiber volume fraction affects the matrix crack initiation stress, fiber pullout length, matrix crack density, and the ultimate tensile strength of the composites.
4. Temperature effect was not significant on the tensile damage behavior of the composite within the range tested ($T = 0^0$ to 700^0).
5. Specimen size effect was observed. Thin specimens tend to have a tail in the stress strain curve, while thick specimens always fail catastrophically without any tail in the stress stain curve.

Singular integral equation analysis on singular behavior at the matrix and interface crack tips and the finite element simulation of the tensile stress strain curves indicate:

6. For embedded H-shaped cracks, that is with interface crack in front of matrix crack tip, the matrix crack tends to propagate until it reaches the interface. The fiber constrain effect disappears because of the interface crack.
7. For broken matrix H-shaped cracks, when interface crack enters the interaction zone (i.e. when interface crack is very close to the matrix crack), both the stress intensity factors at the matrix crack tip and at the interface crack tip exhibit rapid increase. Depending on the relative strength of the fibers and the fiber/matrix interface, the interface crack might advance first to intersect with the matrix crack and to relieve the stress singularity at the matrix crack tip, or the matrix crack may extend into the fibers. Experimental results indicate that matrix cracks seldom collineate with the fiber cracks

therefore the possibility of interface crack extension or interface debonding is more likely to happen .

8. For the intersecting H-shaped cracks, a sharp decrease in the strain energy release rates at the interface crack tips as the interface crack propagates indicate that interface crack propagation or interface debonding will end as soon as the interface crack length reaches certain value.
9. The finite element results using the multiple rows of the intersecting H-shaped cracks configuration matched the first part of the experimentally obtained nonlinear stress stain curve quite well. This indicate that interface debonding might actually play a dominant role during that stage of the damage. Further loading after this stage would cause sequential fiber breaking, and fiber slipping along the interface. In that case the finite element model based on interface debonding has to be modified to account for those effects.

In the end, some comments and recommendations are also given here:

(a) The stress strain curves obtained from the experiments only serve to characterize the damage behavior of the ceramic matrix composite. More testing needs to be done if the test results are to be used for other purposes;

(b) It is recommended that the heater elements in the tensile/heating substage be modified, to reduce the influence of photons generated from the heater elements during high temperature testing on the surface image of the specimen captured by SEM.

(c) The in-situ testing technique can also be used for compression, three or four-point bending tests with some modifications or alterations to the tensile/heating substage;

(d) In the numerical calculations, both the matrix and the fibers are assumed to be isotropic. Due to the typical manufacturing process, in reality, fiber might exhibit anisotropic or orthotropic behavior. The singular behavior of cracks in orthotropic materials can also be treated by the singular integral equation formulation if the orthotropic material constants for the constituents of the composite can be determined.

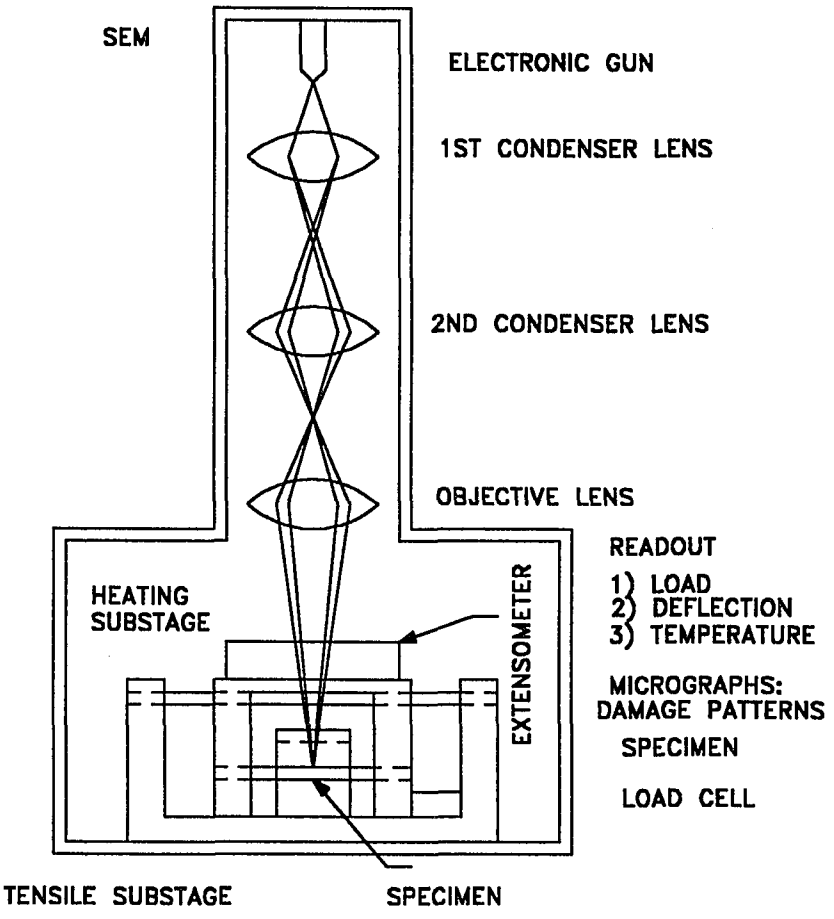

FIGURE 2.1 EXPERIMENTAL SETUP

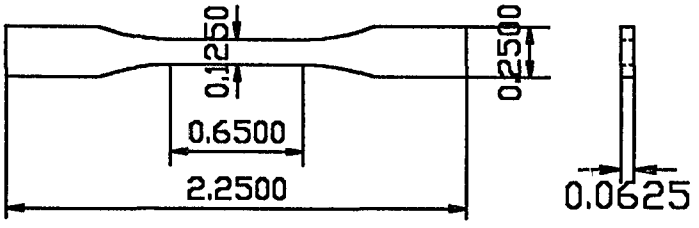

FIGURE 2.2 SPECIMEN GEOMETRY (UNITS IN INCHES)

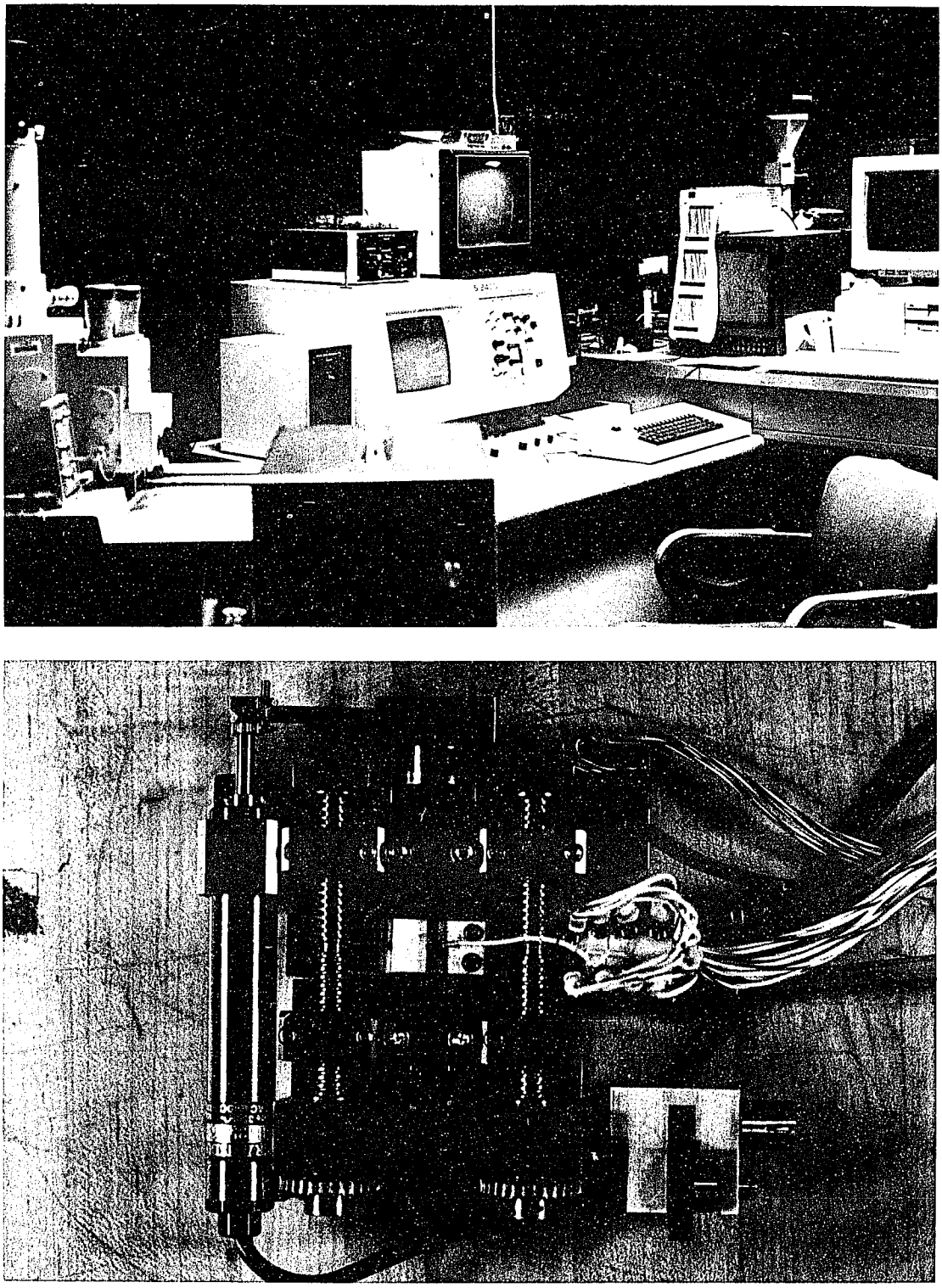

FIGURE 2.3 THE ACTUAL LAYOUT OF THE TEST EQUIPMENT AND ITS TENSILE/HEATING SUBSTAGE

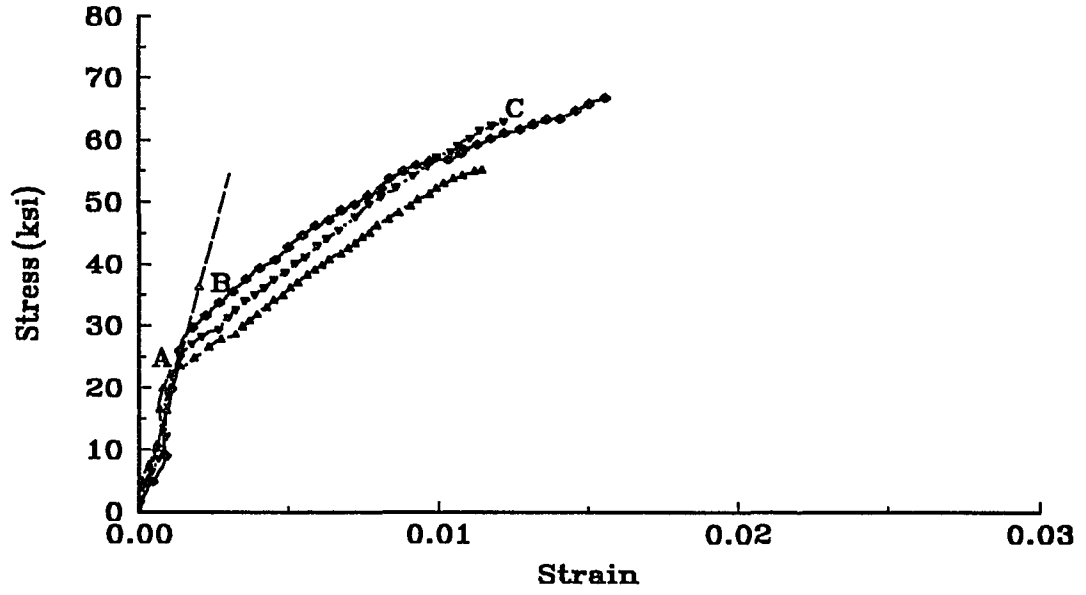

FIGURE 2.4 TENSILE TEST RESULTS FOR NICALON/CAS II WITH V_f=30% AT ROOM TEMPERATURE

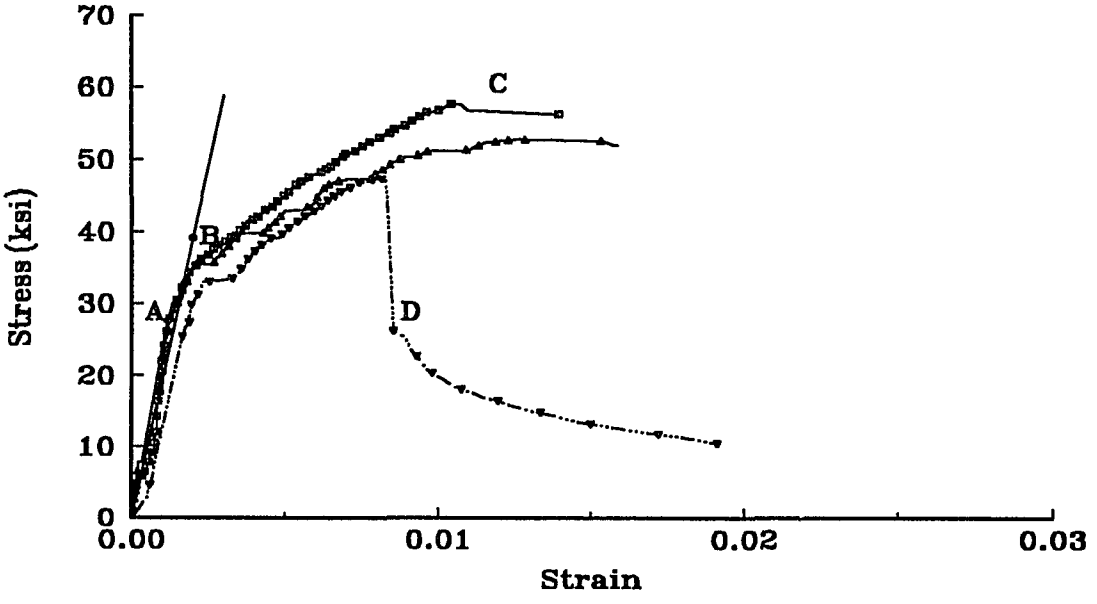

FIGURE 2.5 TENSILE TEST RESULTS FOR NICALON/CAS II WITH V_f=40% AT ROOM TEMPERATURE

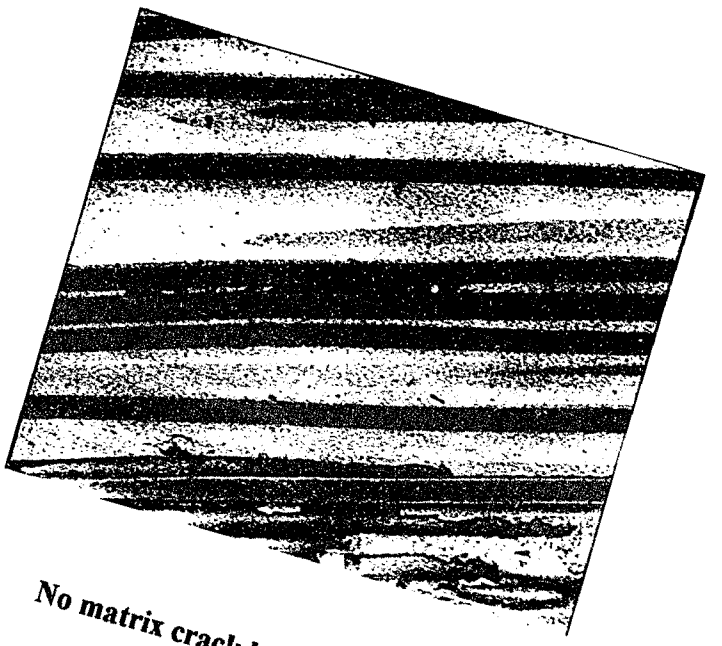

No matrix crack has been observed

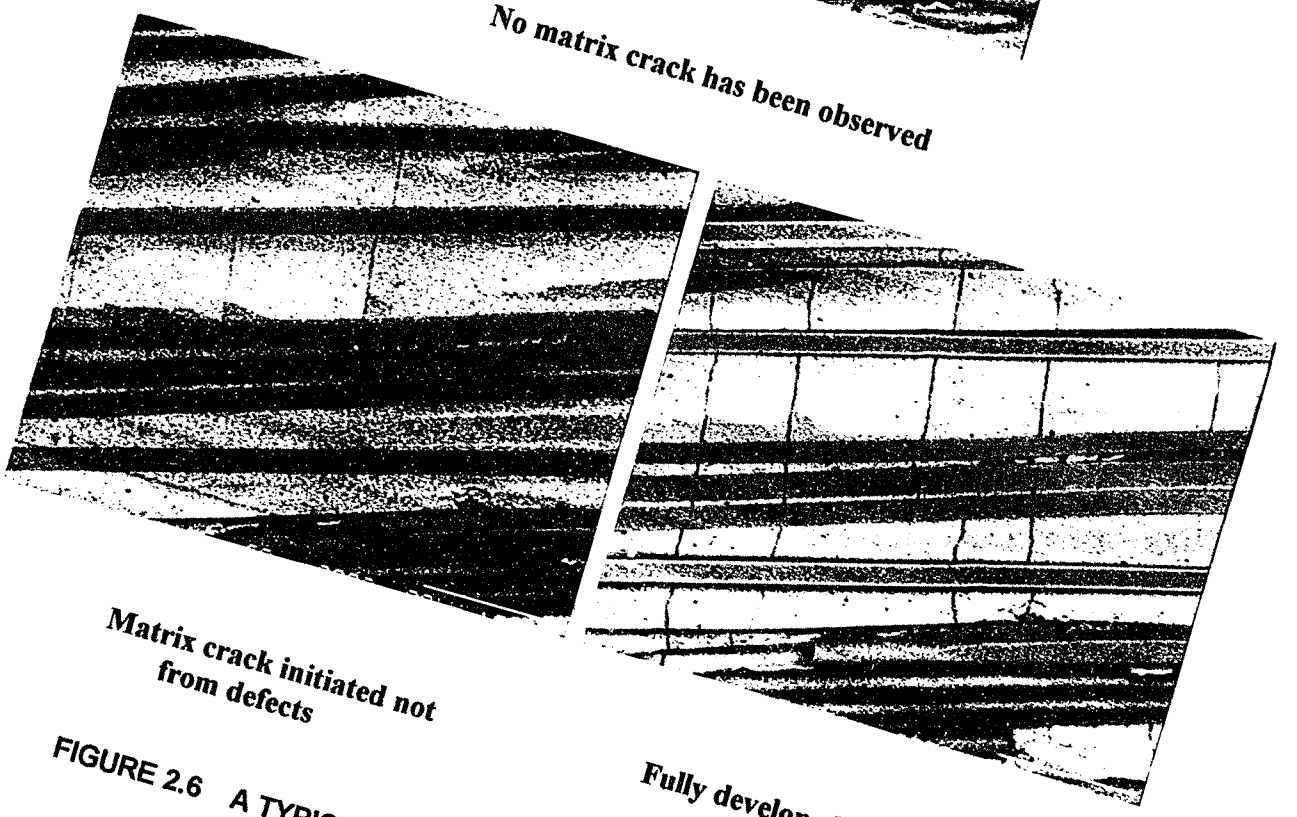

Matrix crack initiated not from defects

Fully developed matrix cracks

FIGURE 2.6 A TYPICAL PATTERN OF MATRIX CRACK INITIATION

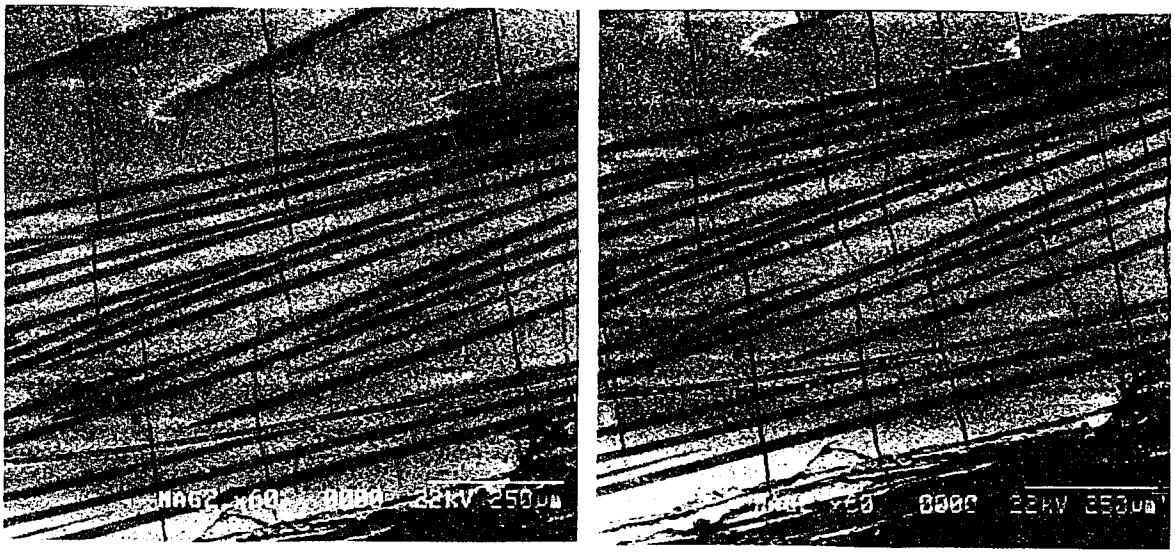

FIGURE 2.7 ANOTHER PATTERN OF MATRIX CRACK INITIATION AND ITS DEVELOPMENT

(A) at 30 ksi

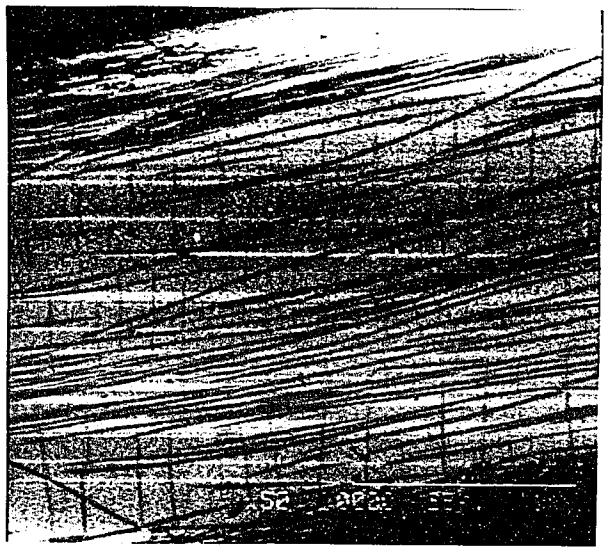

(B) at 40 ksi

(C) at 55 ksi

(D) at 20 ksi

FIGURE 2.8 TENSILE DAMAGE OF A NICALON/CAS II SPECIMEN WITH V_F = 40%

Load = 60 lb

Load = 49 lb

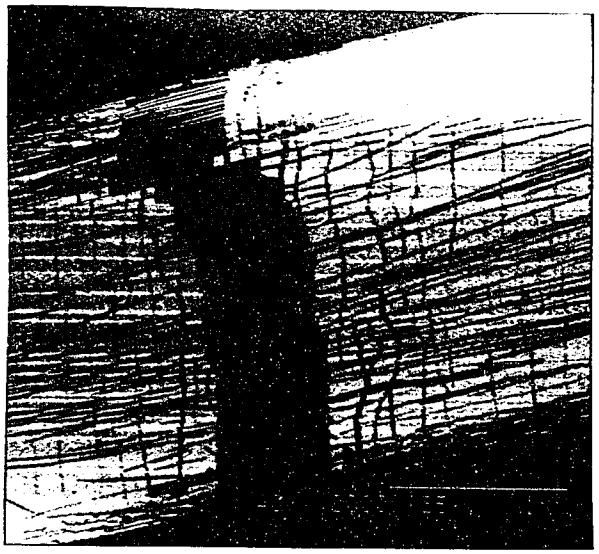

Load = 33 lb

FIGURE 2.9 FURTHER LOADING OF THE SPECIMEN IS POSSIBLE AFTER FAILURE FOR THIN SPECIMENS

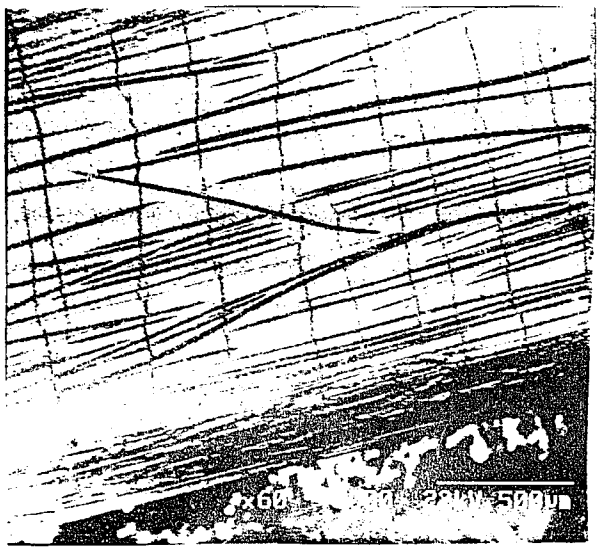

Site of the major fracture just before the specimen fractured

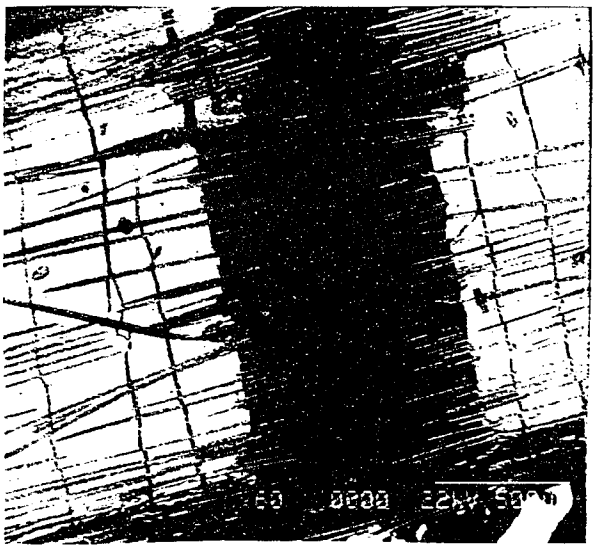

Major fracture of the specimen

FIGURE 2.10 BRITTLE BEHAVIOR OF THICK NICALON/CAS II SPECIMENS

FIGURE 2.11 LONG FIBER PULL-OUT LENGTH FOR A NICALON/CAS II SPECIMEN WITH V_F = 40%

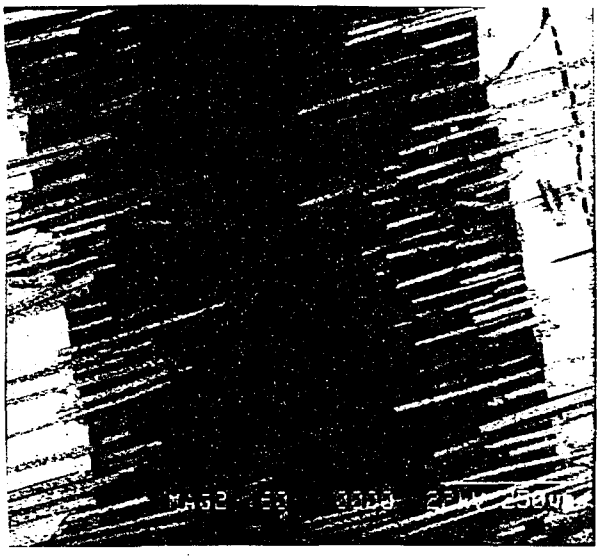

FIGURE 2.12 SHORT FIBER PULL-OUT LENGTH FOR A NICALON/CAS II SPECIMEN WITH V_F = 30%

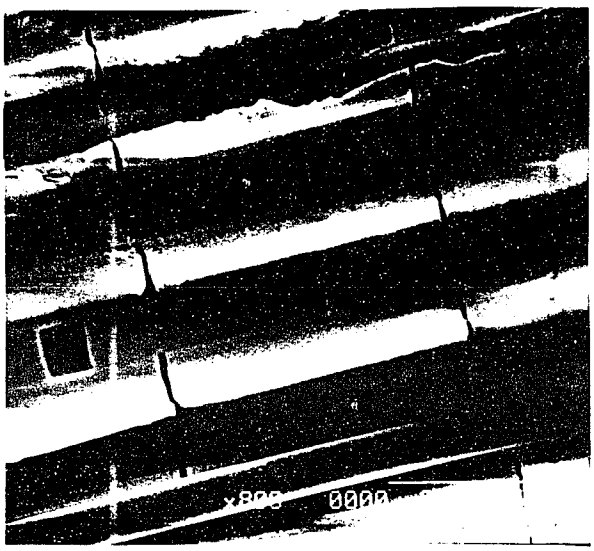

(a)

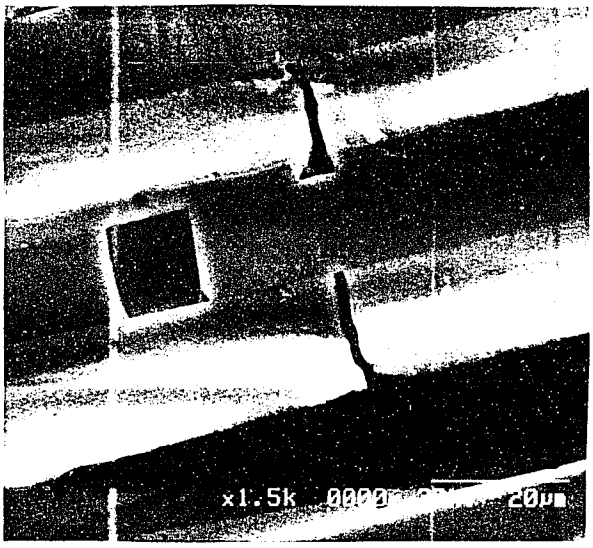

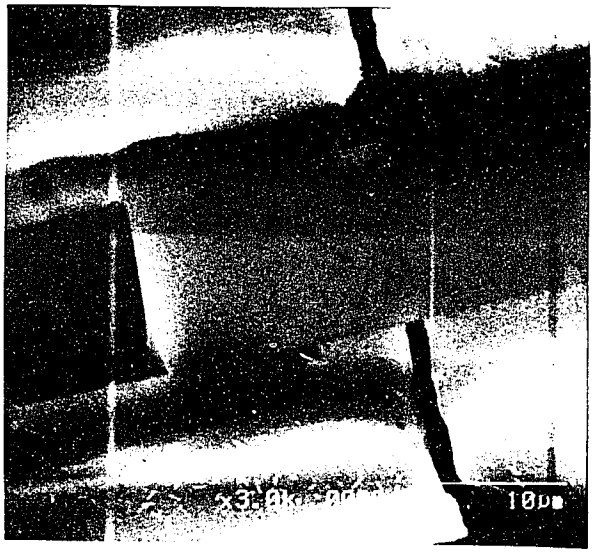

(b) (c)

FIGURE 2.13 TYPICAL DAMAGE PATTERN FOR NICALON/CAS II SPECIMEN (a) 800x; (b) 1500x AND (c) 3000x

200x

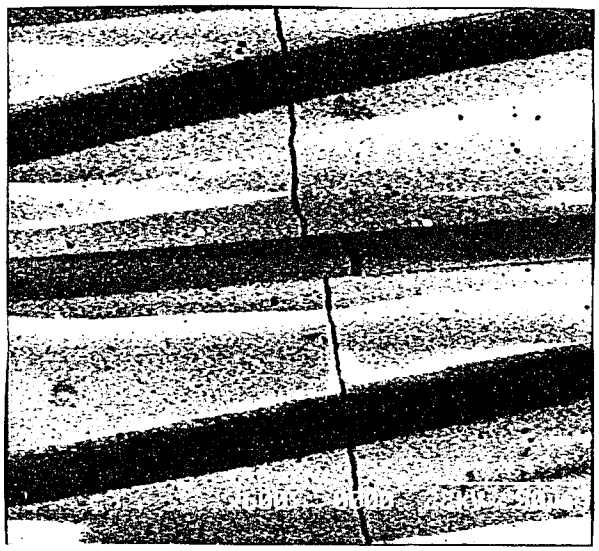

600x

FIGURE 2.14 TYPICAL FIBER BREAKING PATTERN FOR NICALON/CAS II SPECIMEN

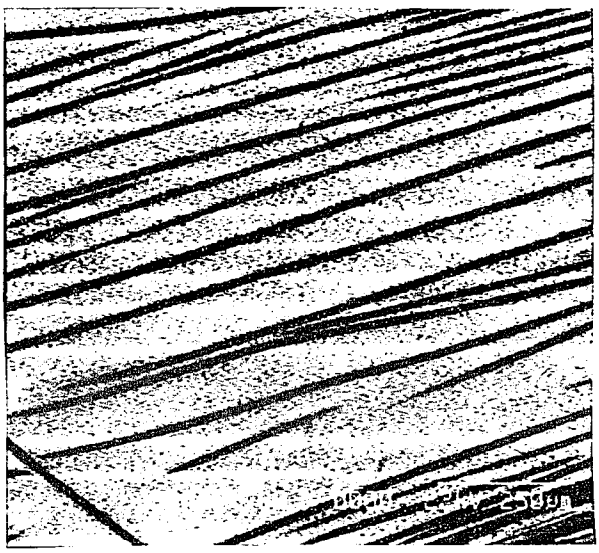

(a) at 19.5 ksi

(b) at 32.0 ksi

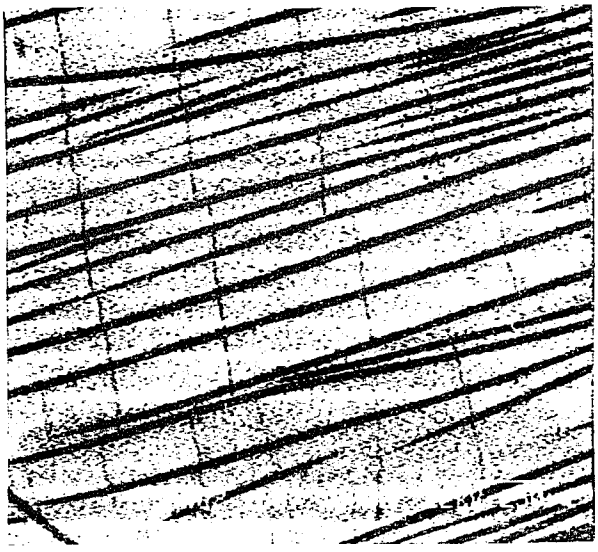

(c) at 36.5 ksi

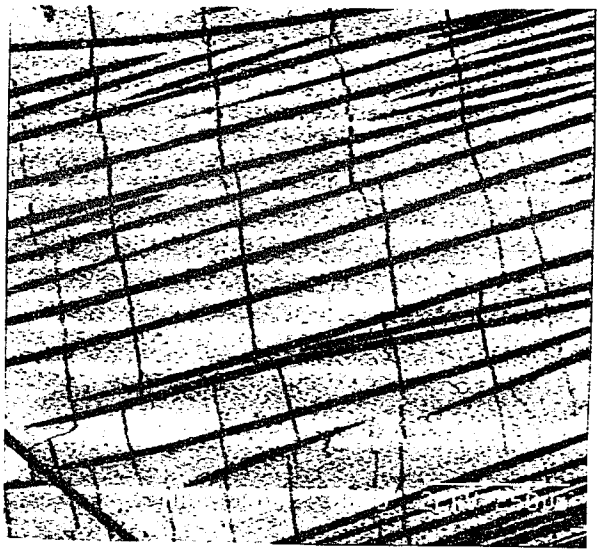

(d) at 51.5 ksi

FIGURE 2.15 MATRIX CRACK DENSITY VERSUS TENSILE STRESS FOR NICALON/CAS II SPECIMEN WITH V_F=30% AT ROOM TEMPERATURE

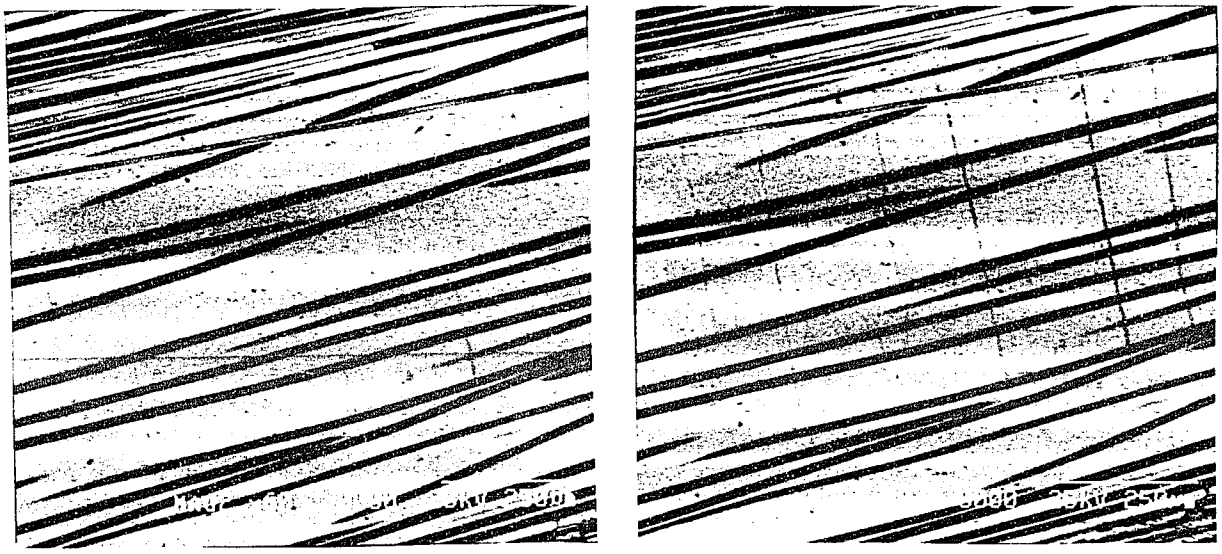

(a) at 28.3 ksi

(b) at 29.8 ksi

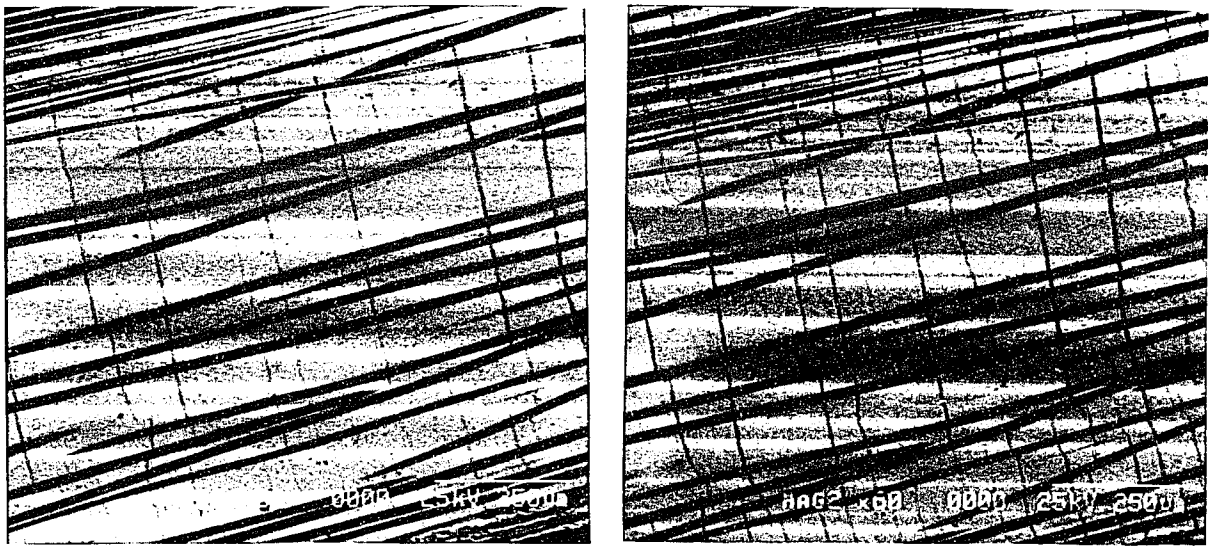

(c) at 30.8 ksi

(d) at 51.7 ksi

FIGURE 2.16 MATRIX CRACK DENSITY VERSUS TENSILE STRESS FOR NICALON/CAS II SPECIMEN WITH V_F=40% AT ROOM TEMPERATURE

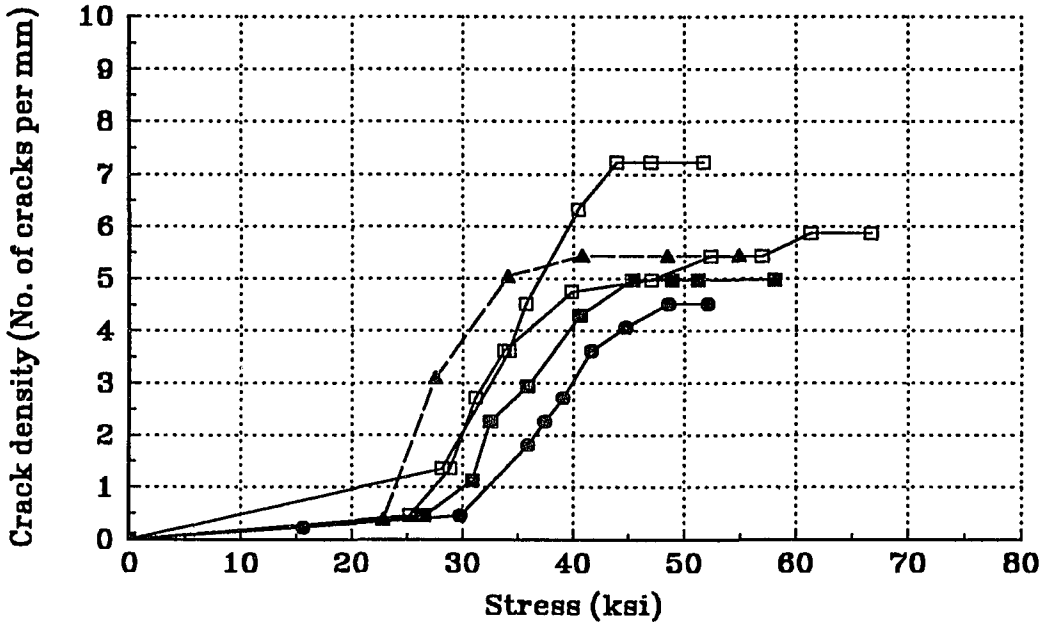

FIGURE 2.17 MATRIX CRACK DENSITY VS. TENSILE STRESS FOR NICALON/CAS II WITH V_f=30% AT ROOM TEMPERATURE

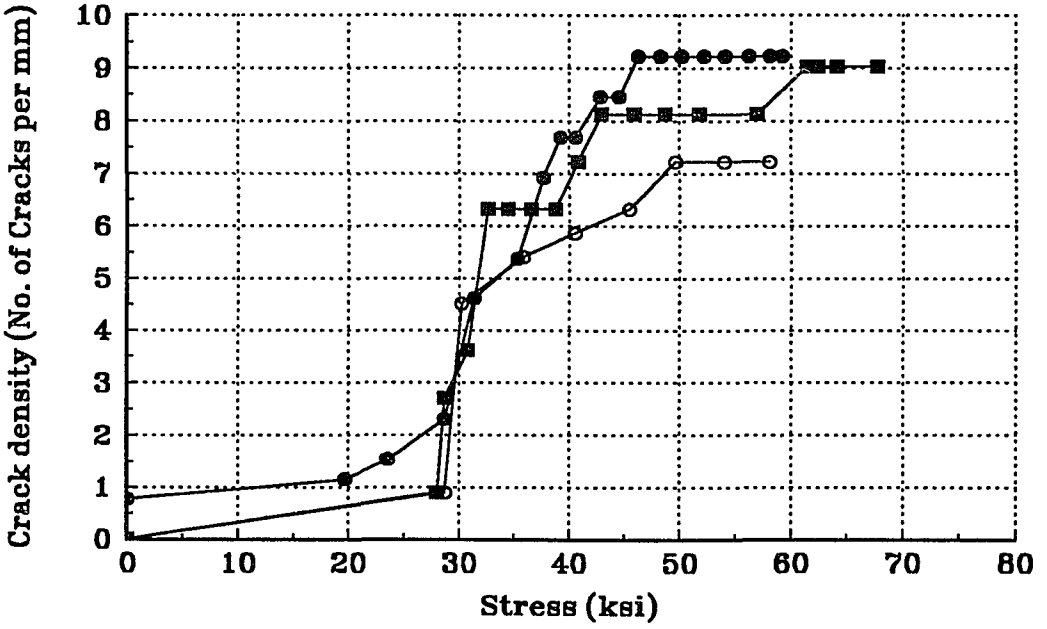

FIGURE 2.18 MATRIX CRACK DENSITY VS. TENSILE STRESS FOR NICALON/CAS II WITH V_f=40% AT ROOM TEMPERATURE

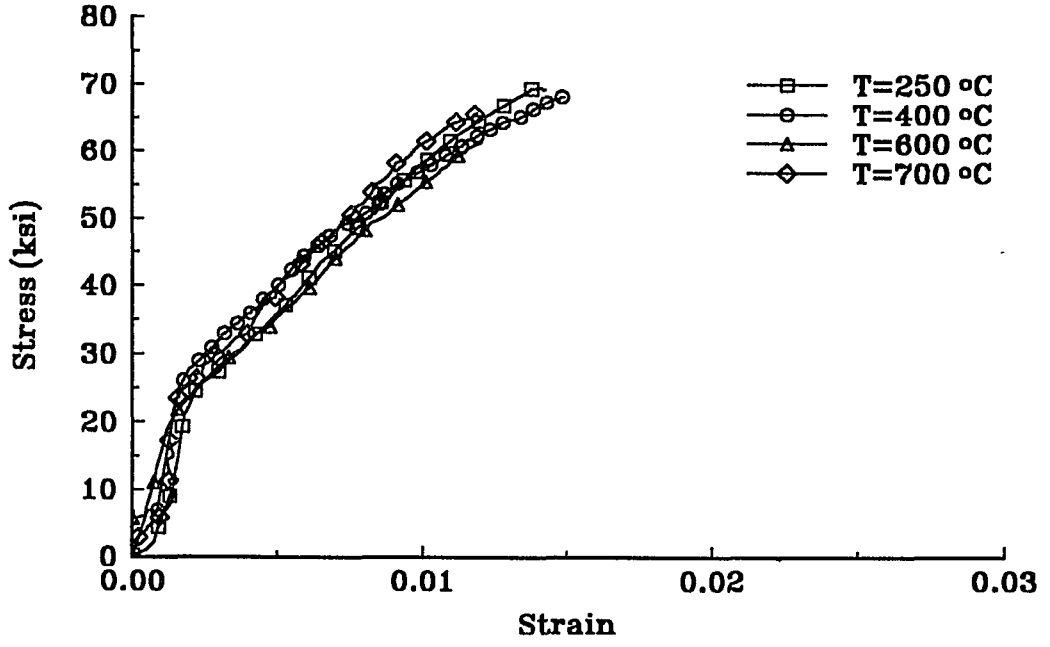

FIGURE 2.19 TENSILE TESTS ON NICALON/CAS II SPECIMENS WITH V_f=30% AT HIGH TEMPERATURES

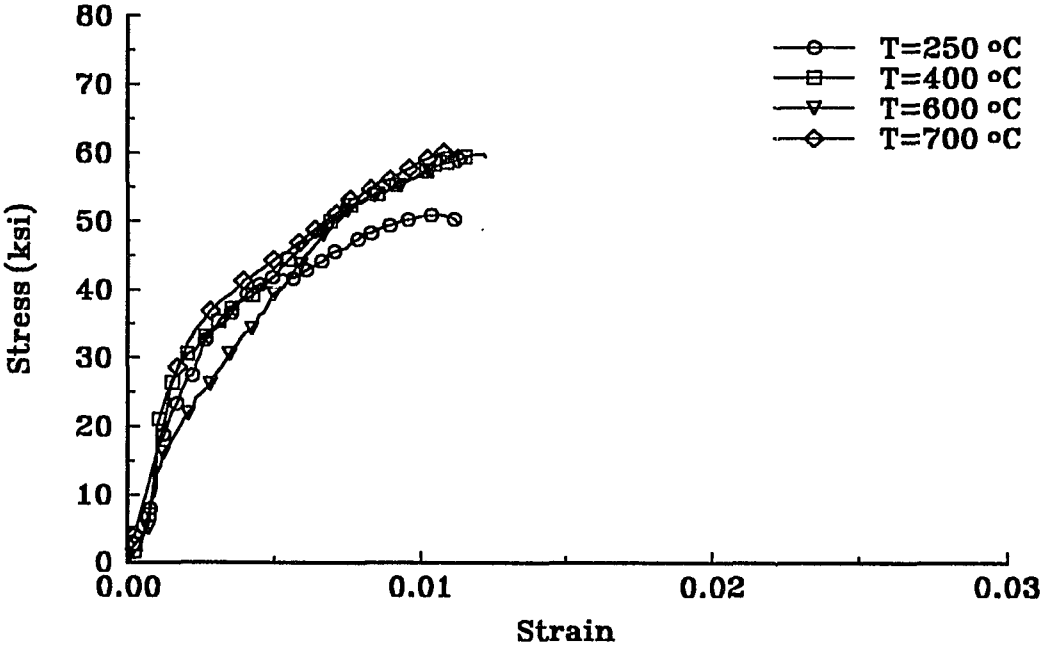

FIGURE 2.20 TENSILE TESTS ON NICALON/CAS II SPECIMENS WITH V_f=40% AT HIGH TEMPERATURES

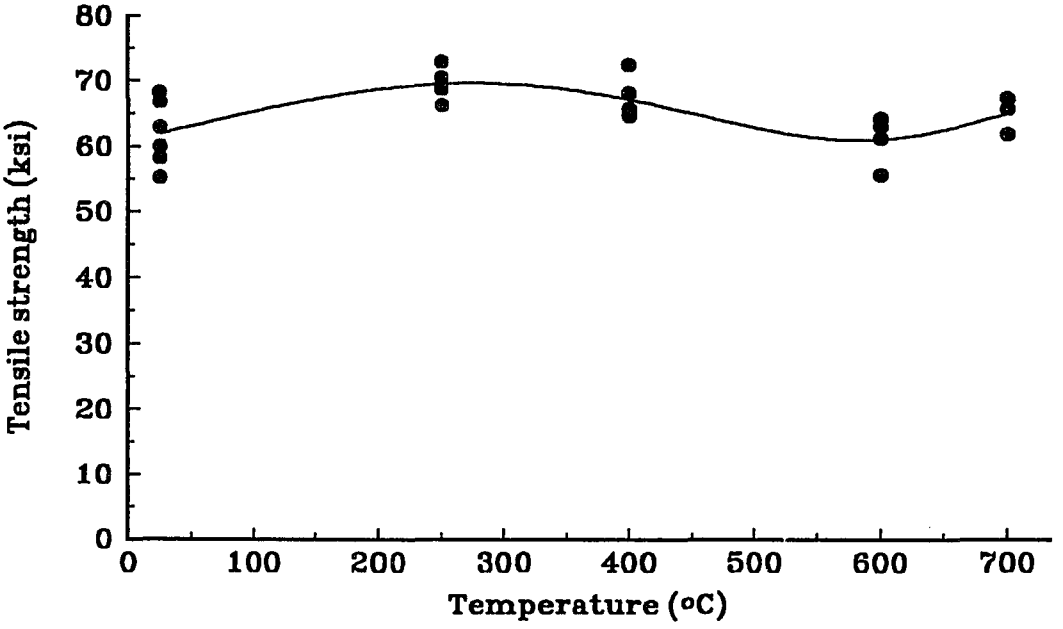

FIGURE 2.21 ULTIMATE TENSILE STRENGTH OF NICALON/CAS II WITH V_f=30% AT VARIOUS TEMPERATURES

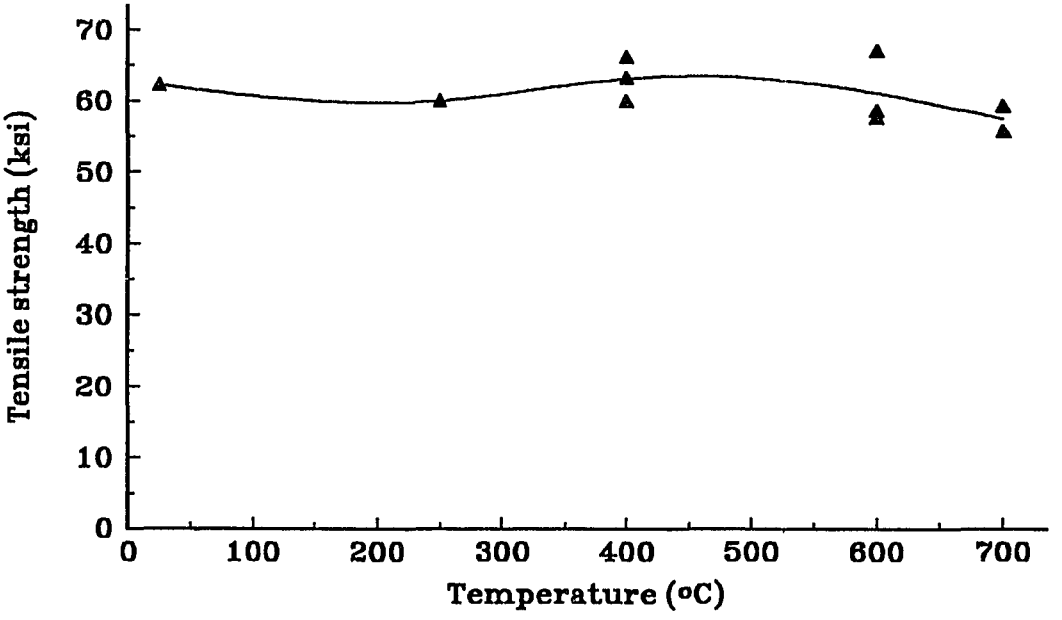

FIGURE 2.22 ULTIMATE TENSILE STRENGTH OF NICALON/CAS II WITH V_f=40% AT VARIOUS TEMPERATURES

(a) at 25.9 ksi

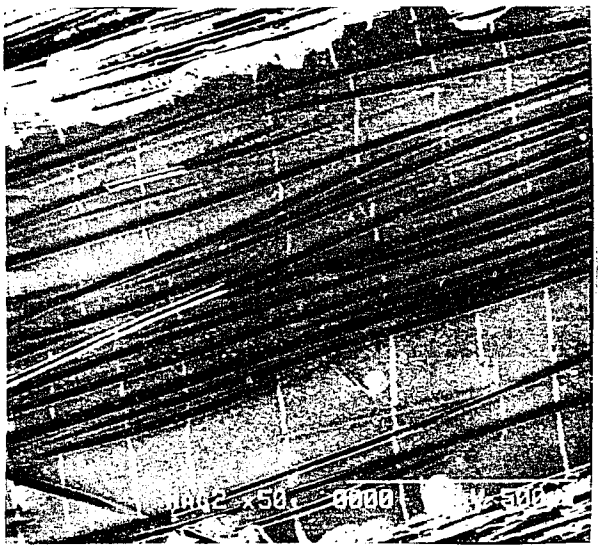

(c) at 30.3 ksi

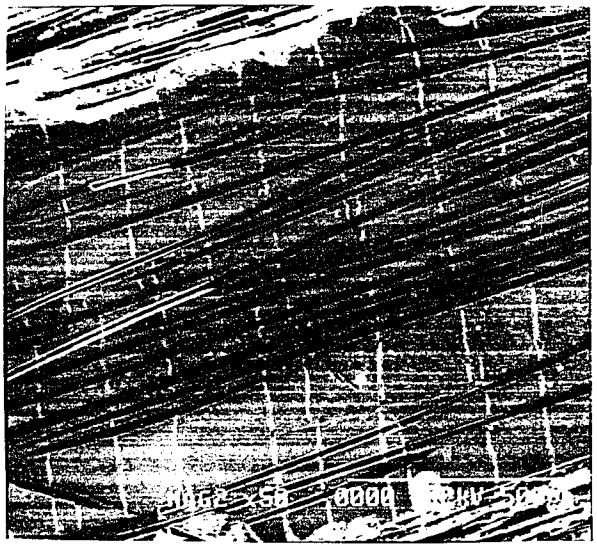

(c) at 52.0 ksi

FIGURE 2.23 DEVELOPMENT OF MATRIX CRACKS AT T= 600 ^{o}C
FOR A NICALON/CAS II SPECIMEN WITH V_F=30%

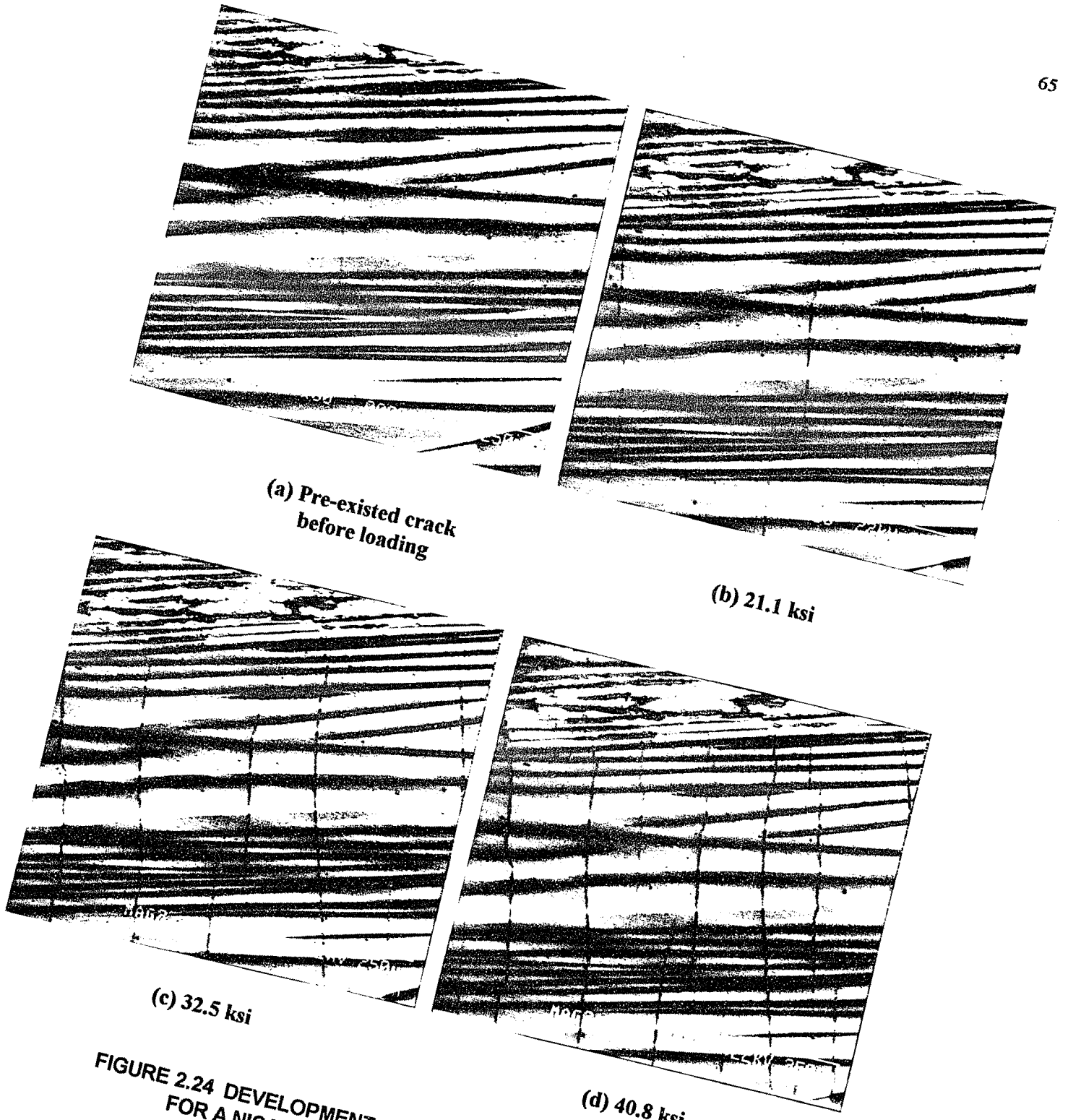

(a) Pre-existed crack before loading

(b) 21.1 ksi

(c) 32.5 ksi

(d) 40.8 ksi

FIGURE 2.24 DEVELOPMENT OF MATRIX CRACKS AT T= 400 °C FOR A NICALON/CAS II SPECIMEN WITH V_F=40%

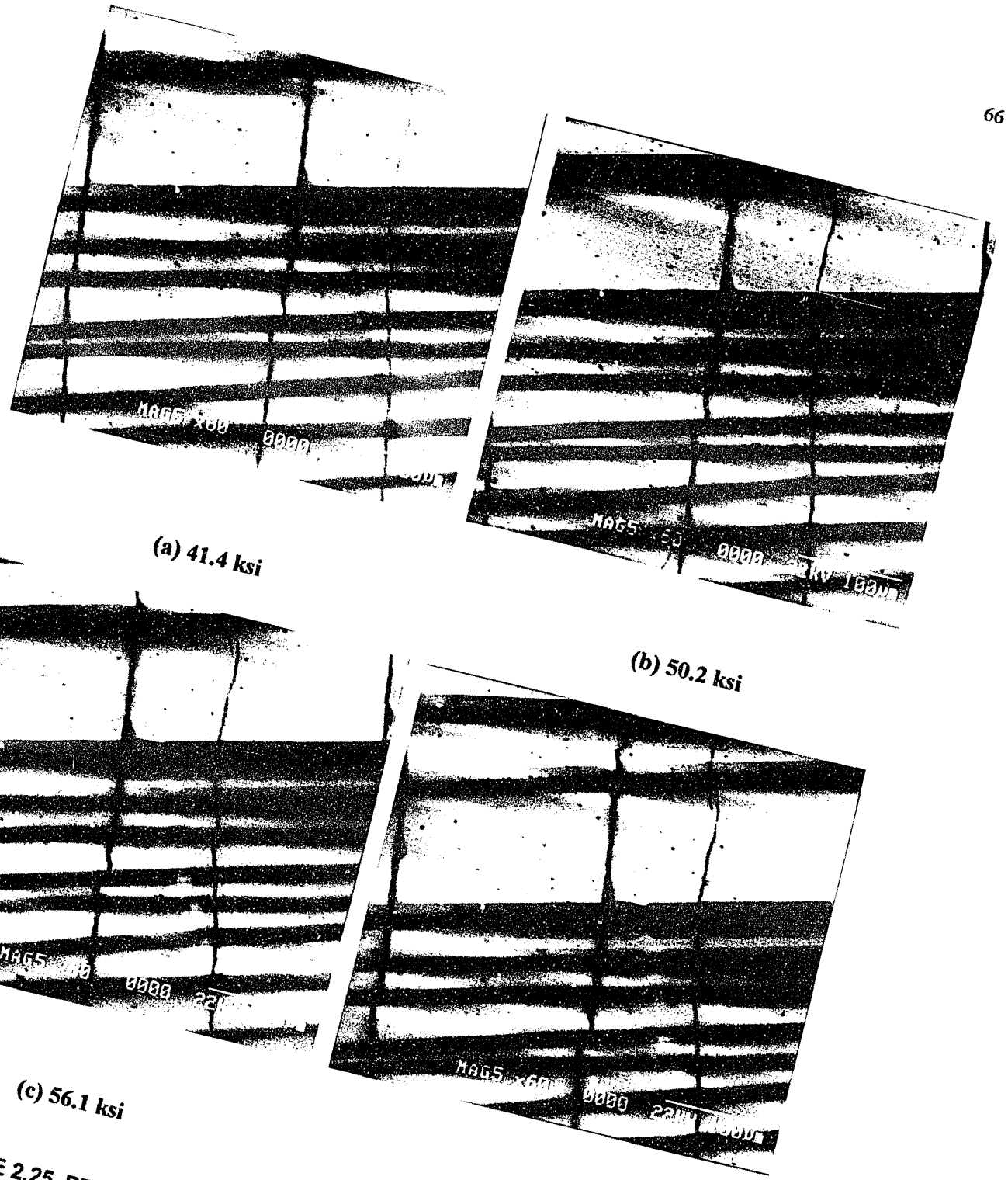

(a) 41.4 ksi

(b) 50.2 ksi

(c) 56.1 ksi

(d) 64.1 ksi

FIGURE 2.25 PROGRESSION OF FIBER CRACKS OPENING AT T= 400 °C FOR A NICALON/CAS II SPECIMEN WITH V_F=40%

(a) 47.4 ksi

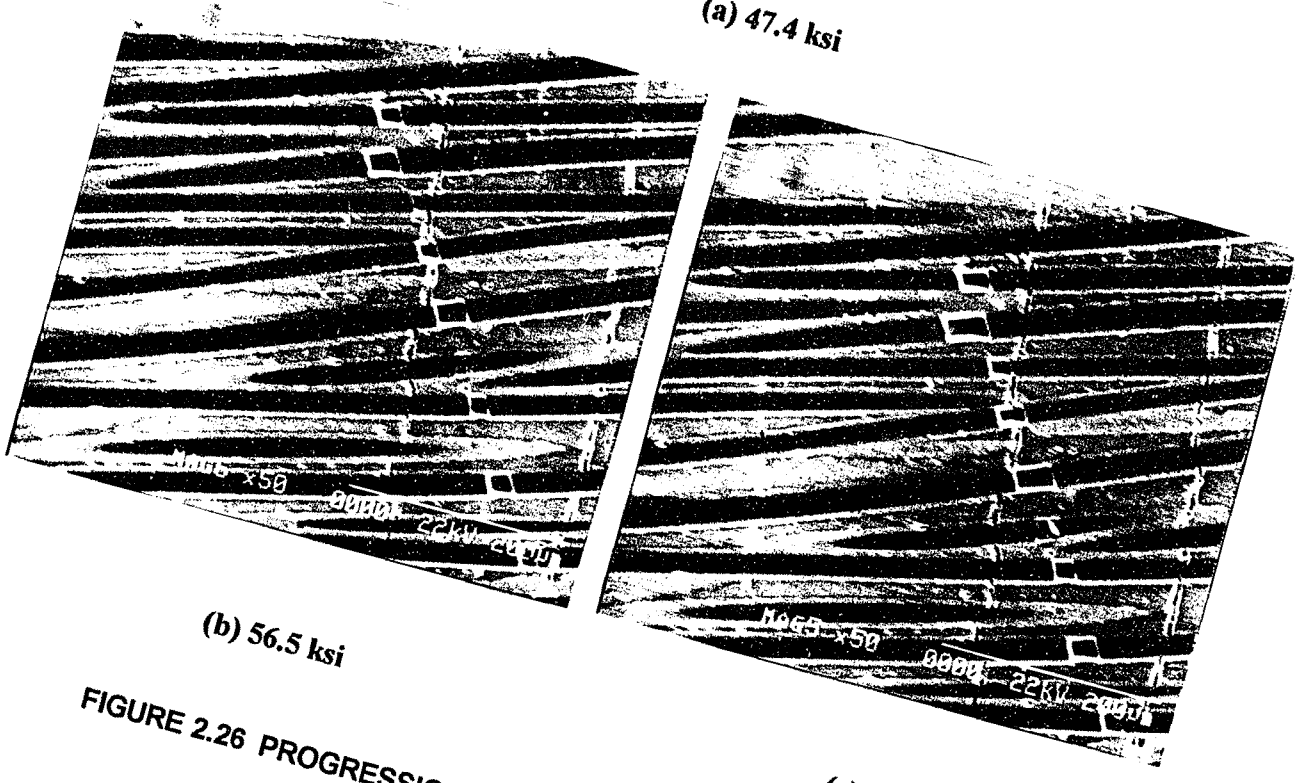

(b) 56.5 ksi

(c) 64.1 ksi

FIGURE 2.26 PROGRESSION OF FIBER CRACKS OPENING AT T= 600 °C FOR A NICALON/CAS II SPECIMEN WITH V_F=30%

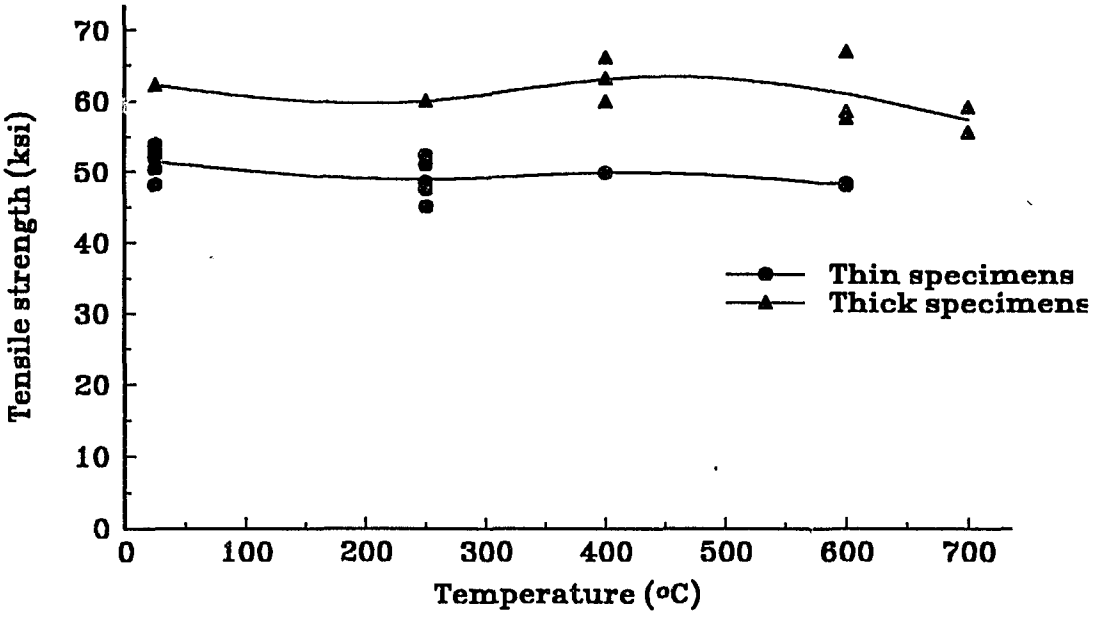

FIGURE 2.27 ULTIMATE TENSILE STRENGTH OF NICALON/CAS II WITH V_f =40% AT VARIOUS TEMPERATURES

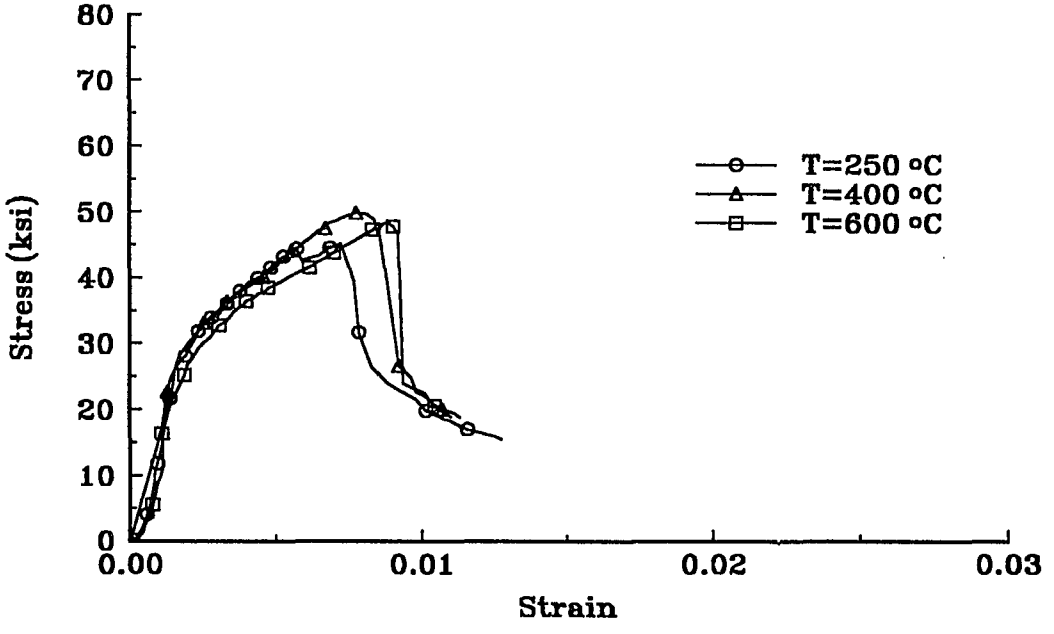

FIGURE 2.28 TENSILE STRESS ON NICALON/CAS II SPECIMENS WITH V_f =40% AT HIGH TEMPERATURES (THIN SPECIMENS)

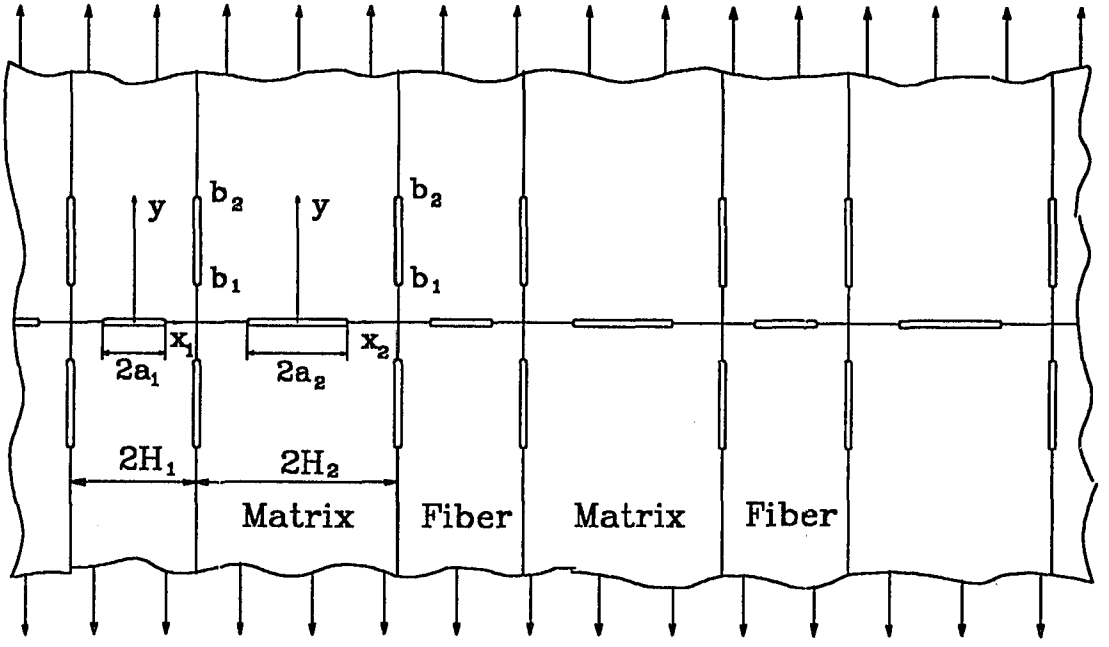

FIGURE 3.1 MATHEMATICAL MODEL

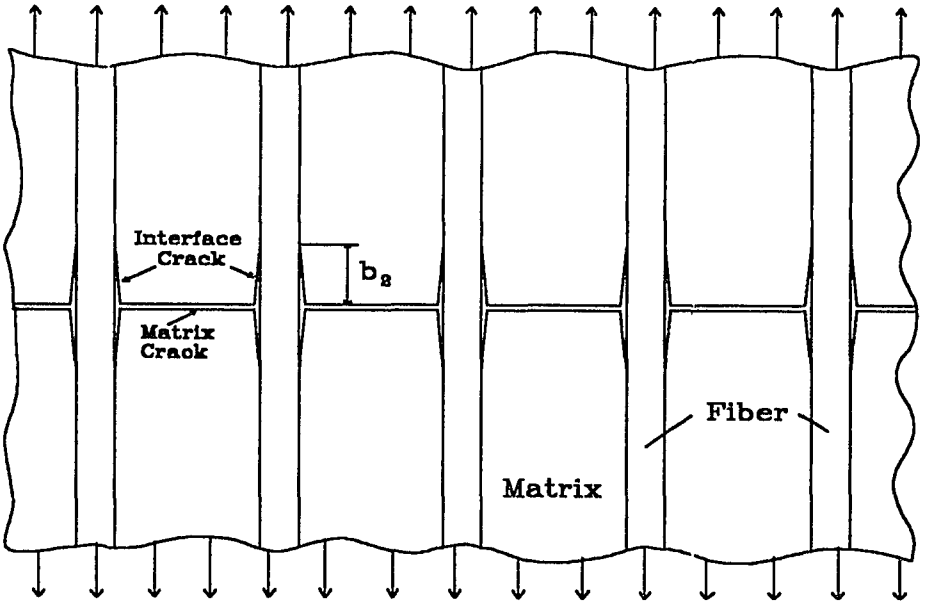

FIGURE 3.2 INTERSECTING H-SHAPED CRACKS

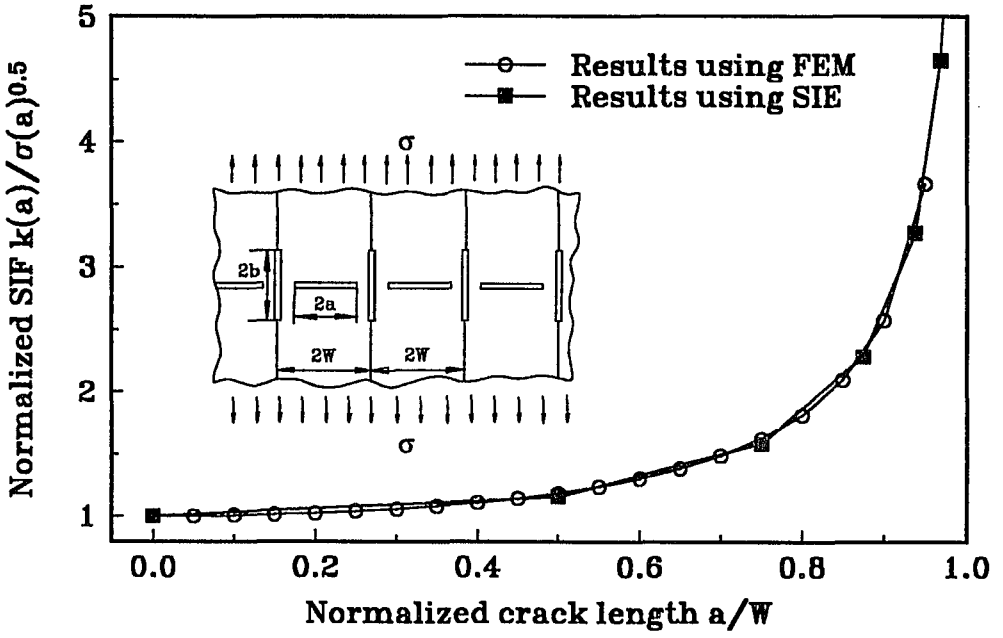

FIGURE 3.3 EFFECT OF FINITE WIDTH ON THE STRESS INTENSITY FACTORS AT A TRANSVERSE CRACK TIP UNDER TENSILE LOAD

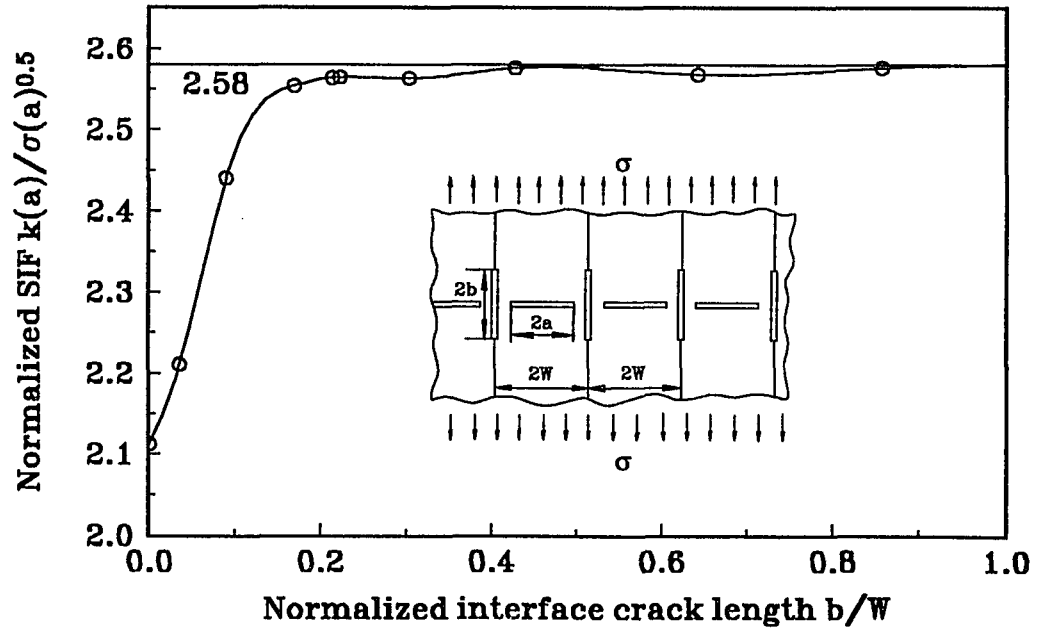

FIGURE 3.4 STRESS INTENSITY FACTORS AT THE TRANSVERSE CRACK TIP FOR DIFFERENT INTERFACE CRACK LENGTHS (a/W=0.9)

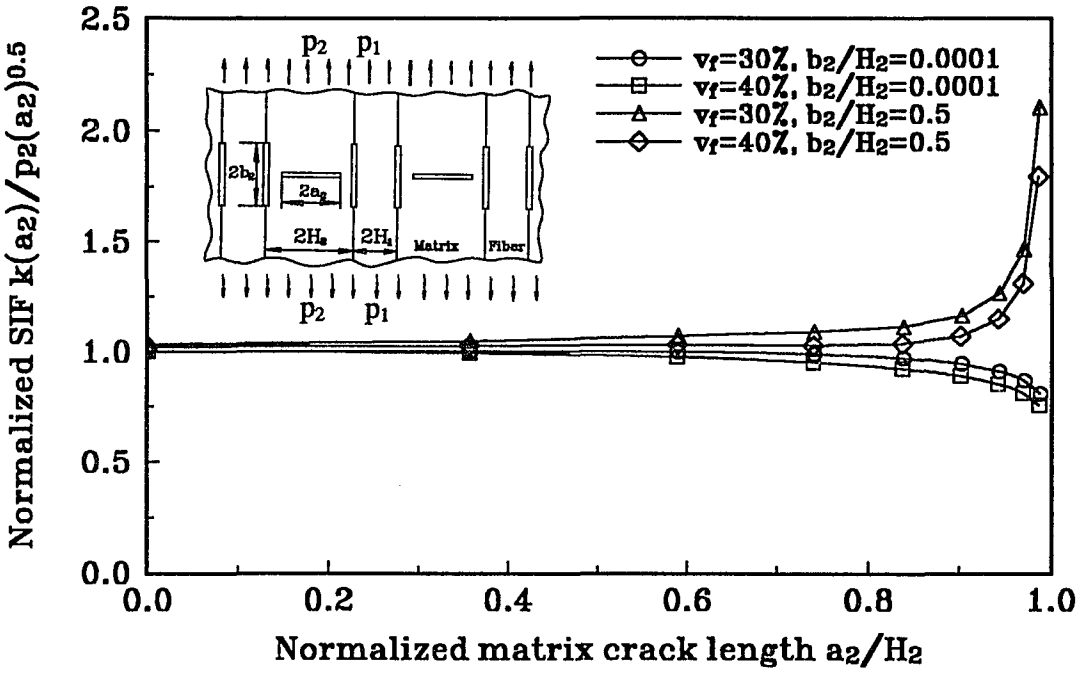

FIGURE 3.5 NORMALIZED STRESS INTENSITY FACTORS AT THE MATRIX CRACK TIPS FOR DIFF. INTERFACE CRACK LENGTH

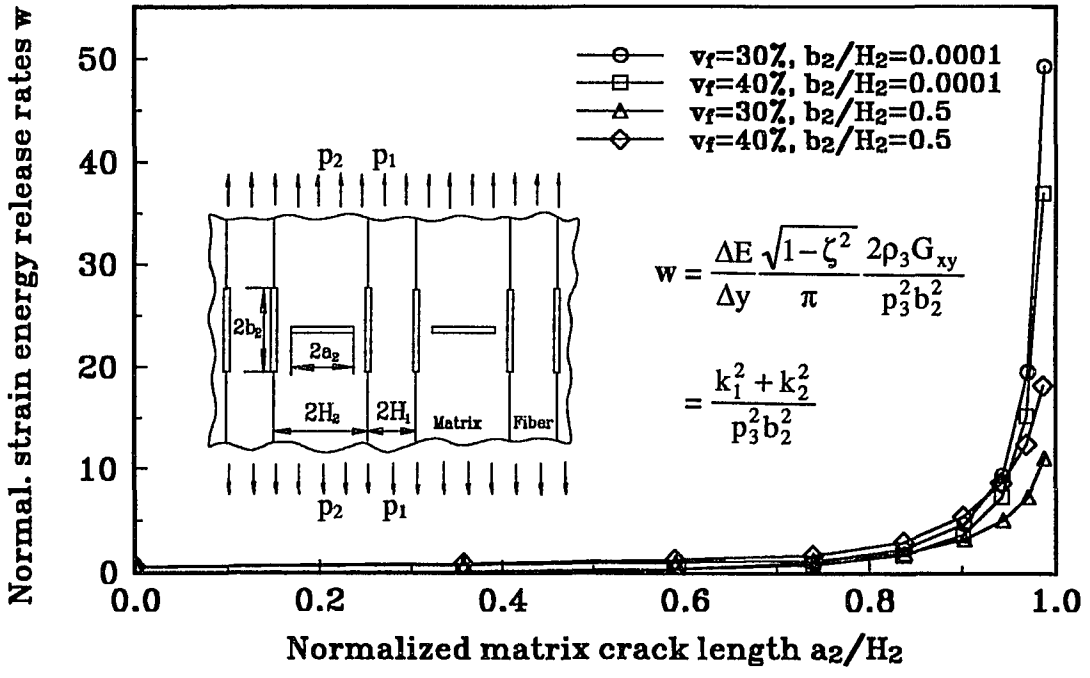

FIGURE 3.6 NORMALIZED STRAIN ENERGY RELEASE RATES AT THE INTERFACE CRACK TIPS FOR DIFF. INTERFACE CRACK LENGTHS

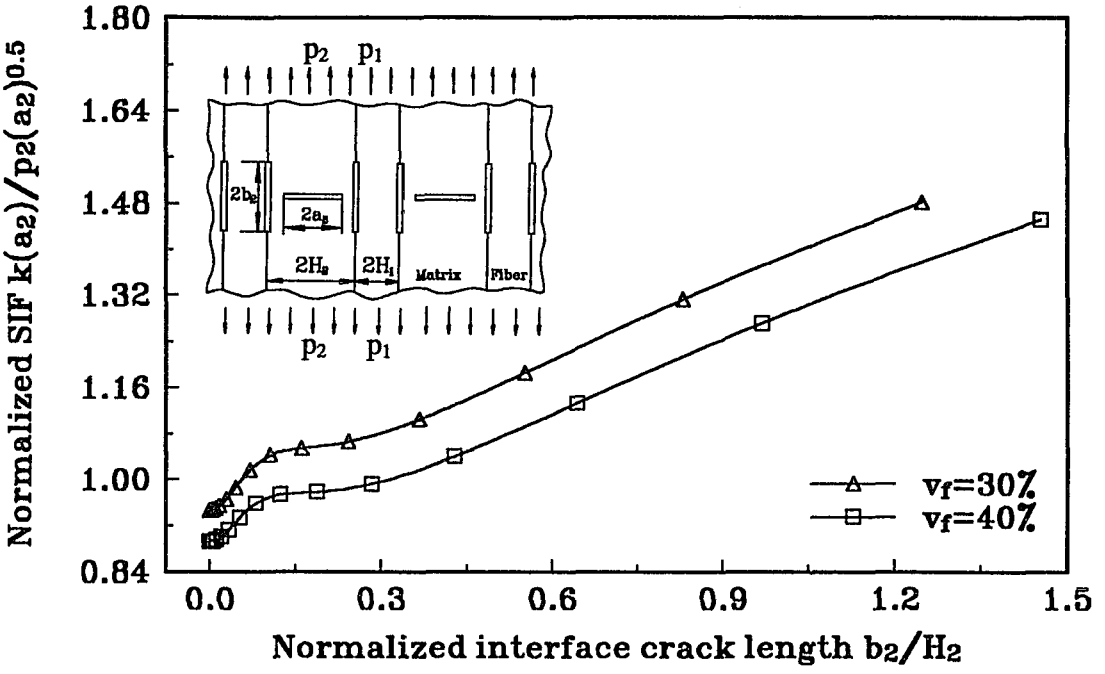

FIGURE 3.7 NORMALIZED SIF AT THE MATRIX CRACK TIPS FOR EMBEDDED H-SHAPED CRACKS ($a_1/H_1=0$, $a_2/H_2=0.9$)

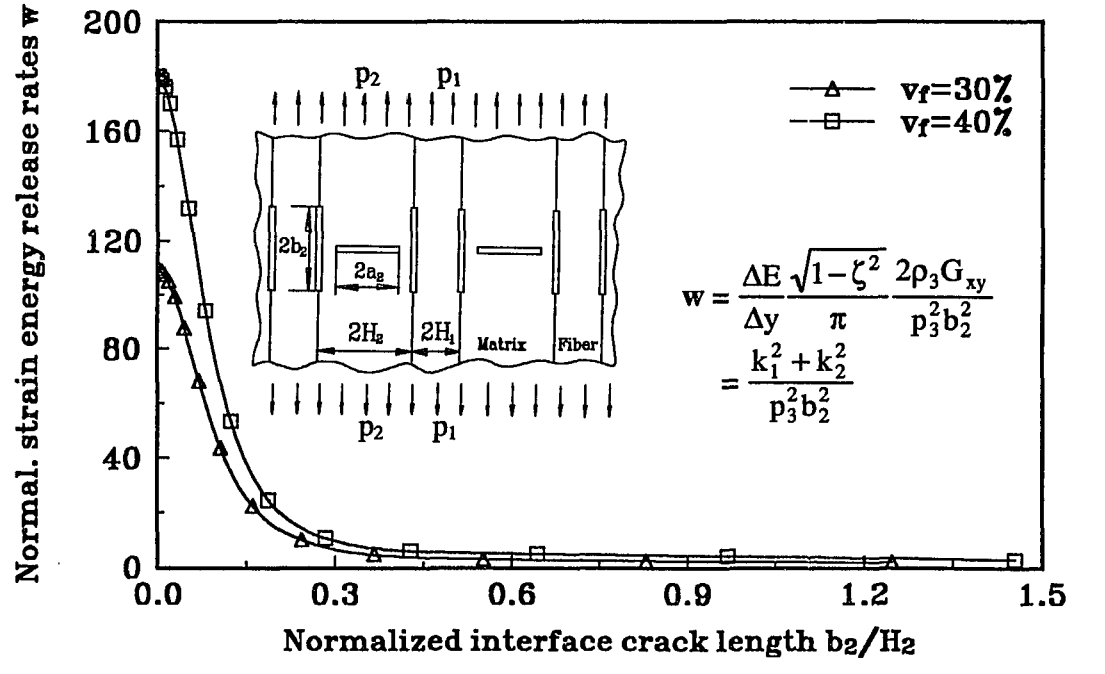

FIGURE 3.8 NORMAL. STRAIN ENER. RELEASE RATES AT THE INTERFACE CRACK TIPS FOR EMBEDDED H-SHAPED CRACKS ($a_1/H_1=0$, $a_2/H_2=0.9$)

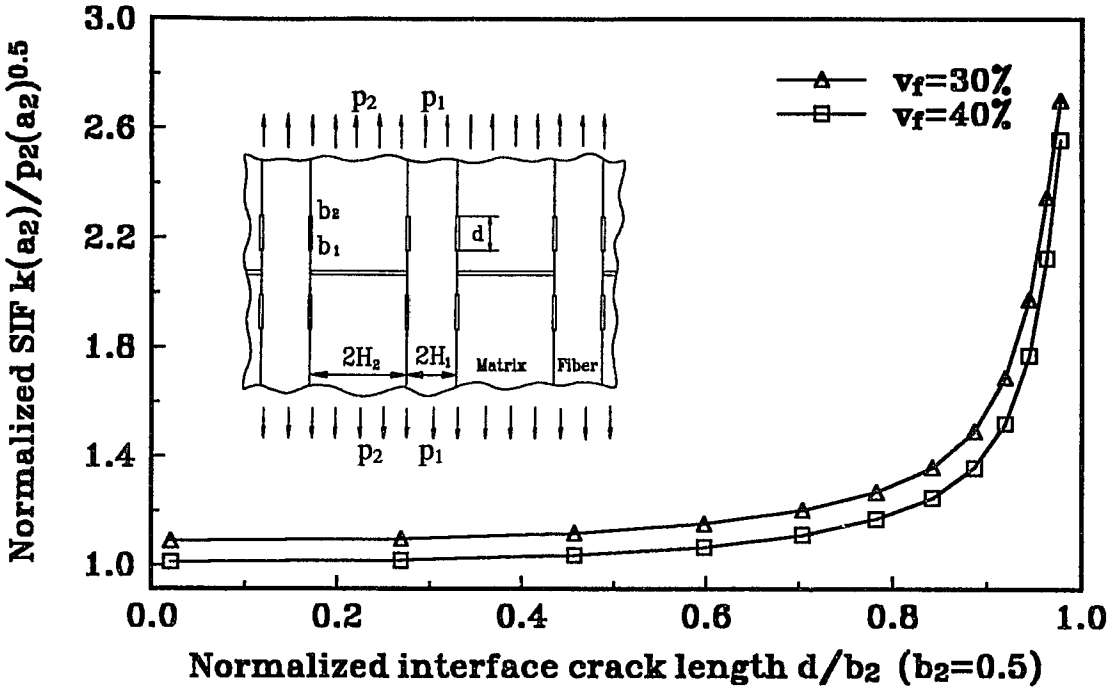

FIGURE 3.9 NORMALIZED STRESS INTENSITY FACTORS AT THE MATRIX CRACK TIPS FOR BROKEN MATRIX H-SHAPED CRACKS

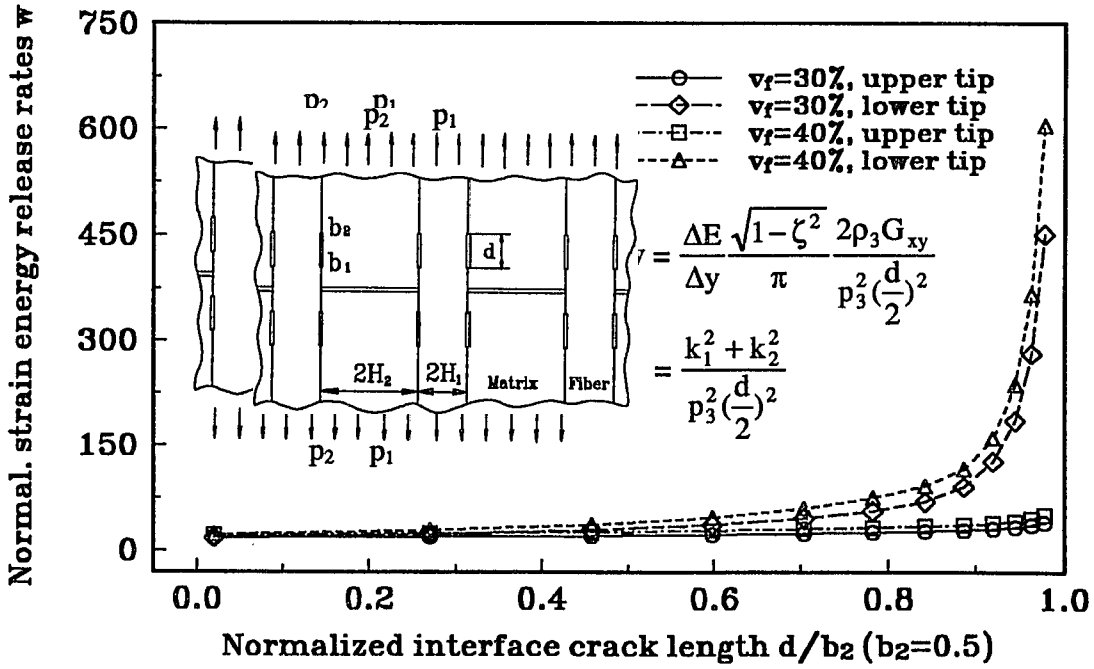

FIGURE 3.10 NORMAL. STRAIN ENER. RELEASE RATES AT THE UPPER AND LOWER INTERFACE CRACK TIPS FOR BROKEN MATRIX H-SHAPED CRACKS

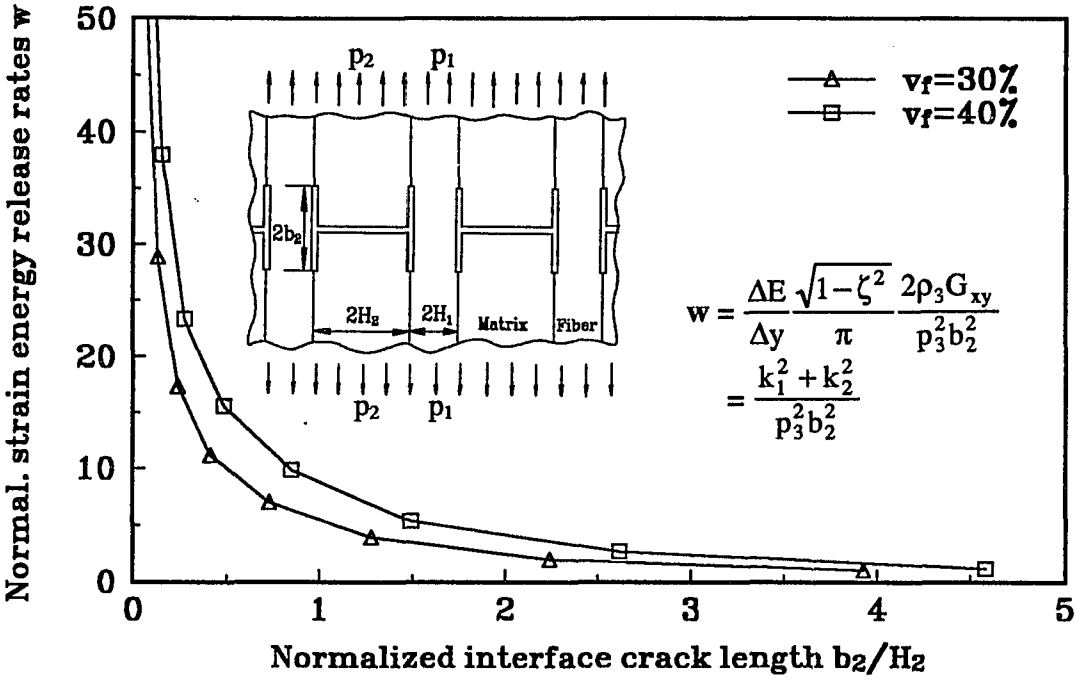

FIGURE 3.11 NORMALIZED STRAIN ENERGY RELEASE RATES AT THE INTERFACE CRACK TIPS FOR INTERSECTING H-SHAPED CRACKS

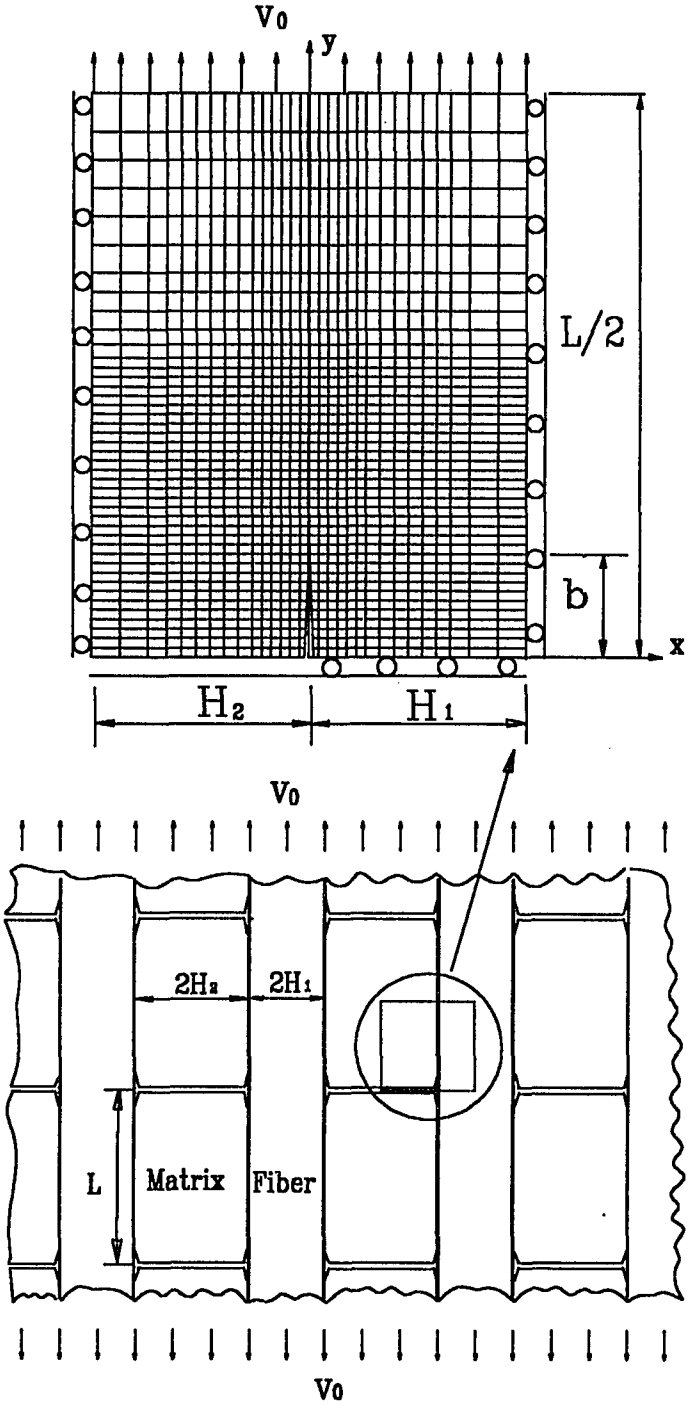

FIGURE 3.12 FINITE ELEMENT MODEL

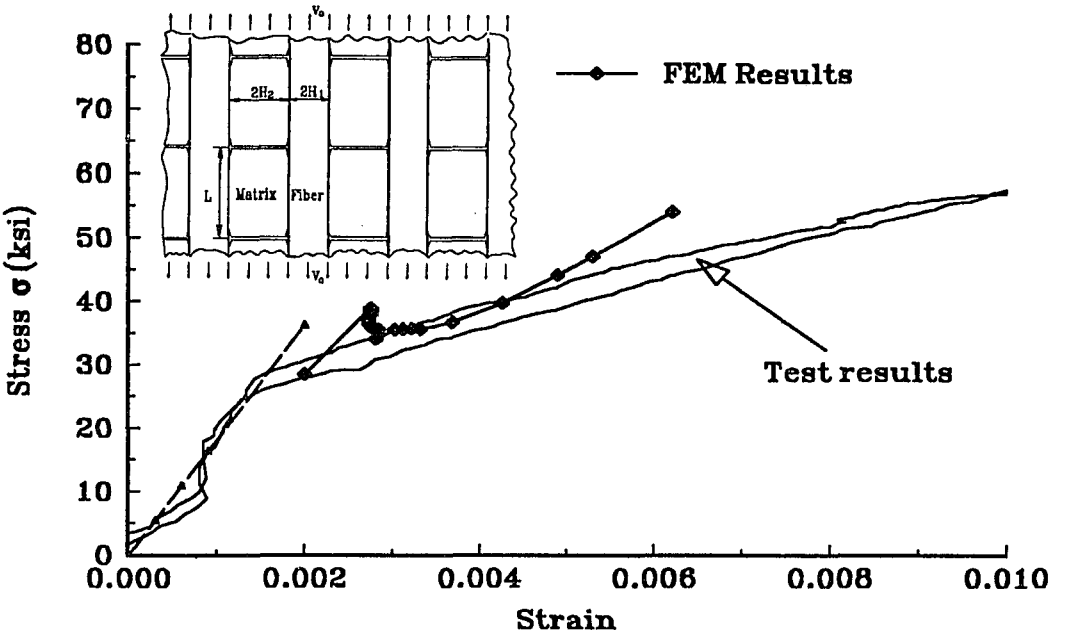

FIGURE 3.13 COMPARISON OF TENSILE TEST AND FEA RESULTS FOR SPECIMENS WITH V_f=30% AT ROOM TEMPERATURE ($L/2H_2$=2.5)

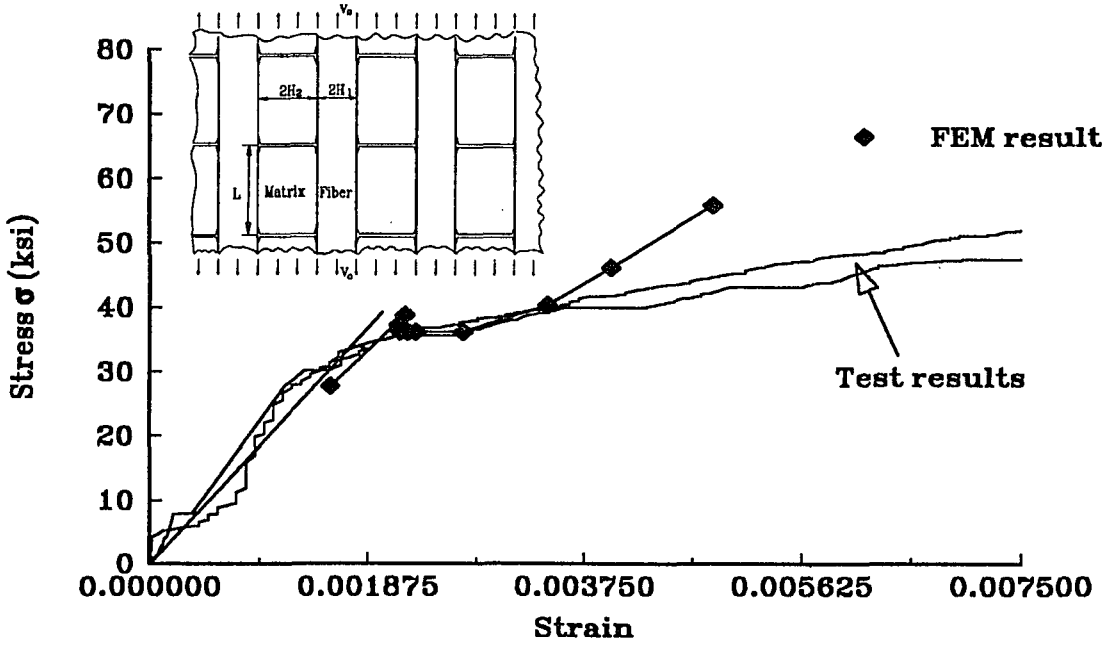

FIGURE 3.14 COMPARISON OF TENSILE TEST AND FEA RESULTS FOR SPECIMENS WITH V_f=40% AT ROOM TEMPERATURE ($L/2H_2$=3.0)

Appendix A

From eqns(1.9ab), one obtains:

$$\frac{\partial u_1(H_1,y)}{\partial y} = -\frac{4}{\pi}\int_0^\infty [A(\alpha)\sinh(w_1\alpha H_1) + C(\alpha)\sinh(w_3\alpha H_1)]\alpha\sin\alpha y d\alpha$$

$$+\frac{2}{\pi}\int_0^\infty\int_0^{a_1}\frac{\phi_1(t)}{\gamma_{13}}[-\frac{|w_1|}{\beta_5}e^{-|w_1|\alpha y/\beta_5} + \frac{|w_3|\gamma_{11}}{\beta_5\gamma_{12}})e^{-|w_3|\alpha y/\beta_5}]\sin\alpha t\sin\alpha H_1 dt d\alpha \quad (A.1)$$

$$\frac{\partial u_2(-H_2,y)}{\partial y} = \frac{4}{\pi}\int_0^\infty [A^*(\alpha)\sinh(w_1^*\alpha H_2) + C(\alpha)\sinh(w_3^*\alpha H_2)]\alpha\sin\alpha y d\alpha$$

$$+\frac{2}{\pi}\int_0^\infty\int_0^{a_2}\frac{\phi_2(t)}{\gamma_{13}^*}[-\frac{|w_1^*|}{\beta_5^*}e^{-|w_1^*|\alpha y/\beta_5^*} + \frac{|w_3^*|\gamma_{11}^*}{\beta_5^*\gamma_{12}^*}e^{-|w_3^*|\alpha y/\beta_5^*}]\sin\alpha t\sin\alpha H_2 dt d\alpha \quad (A.2)$$

$$\frac{\partial v_1(H_1,y)}{\partial y} = \frac{4}{\pi}\int_0^\infty [\beta_7 A(\alpha)\cosh(w_1\alpha H_1) + \beta_8 C(\alpha)\cosh(w_3\alpha H_1)]\alpha\cos\alpha y d\alpha$$

$$-\frac{2}{\pi}\int_0^\infty\int_0^{a_1}\frac{\phi_1(t)}{\gamma_{13}}[-\frac{|w_1|}{\beta_5}\beta_9\,\mathrm{sign}(w_1)e^{-|w_1|\alpha y/\beta_5}$$

$$+\frac{|w_3|\gamma_{11}}{\beta_5\gamma_{12}}\beta_{10}\,\mathrm{sign}(w_3)e^{-|w_3|\alpha y/\beta_5}]\sin\alpha t\cos\alpha H_1 dt d\alpha \quad (A.3)$$

$$\frac{\partial v_2(-H_2,y)}{\partial y} = \frac{4}{\pi}\int_0^\infty [\beta_7^* A^*(\alpha)\cosh(w_1^*\alpha H_2) + \beta_8^* C^*(\alpha)\cosh(w_3^*\alpha H_2)]\alpha\cos\alpha y d\alpha$$

$$-\frac{2}{\pi}\int_0^\infty\int_0^{a_2}\frac{\phi_2(t)}{\gamma_{13}^*}[-\frac{|w_1^*|}{\beta_5^*}\beta_9^*\,\mathrm{sign}(w_1^*)e^{-|w_1^*|\alpha y/\beta_5^*}$$

$$+\frac{|w_3^*|\gamma_{11}^*}{\beta_5^*\gamma_{12}^*}\beta_{10}^*\,\mathrm{sign}(w_3^*)e^{-|w_3^*|\alpha y/\beta_5^*}]\sin\alpha t\cos\alpha H_2 dt d\alpha \quad (A.4)$$

Using the following integral formulas:

$$\int_0^\infty e^{-at}\sin bt\,dt = \frac{b}{a^2+b^2} \qquad a>0 \qquad (A.5a)$$

and

$$\int_0^\infty e^{-at}\cos bt\,dt = \frac{a}{a^2+b^2} \qquad a>0 \qquad (A.5b)$$

equations (A.1-A.4) can be reduced to:

$$\frac{\partial u_1(H_1,y)}{\partial y} = -\frac{4}{\pi}\int_0^\infty [A(\alpha)\sinh(w_1\alpha H_1) + C(\alpha)\sinh(w_3\alpha H_1)]\alpha\sin\alpha y d\alpha$$

$$+\frac{2}{\pi}\int_0^{a_1}\frac{\phi_1(t)}{2\gamma_{13}}G_1(t,y)dt \qquad (A.1^*)$$

$$\frac{\partial u_2(-H_2,y)}{\partial y}=\frac{4}{\pi}\int_0^{\infty}[A^*(\alpha)\sinh(w_1^*\alpha H_2)+C^*(\alpha)\sinh(w_3^*\alpha H_2)]\alpha\sin\alpha y d\alpha$$

$$+\frac{2}{\pi}\int_0^{a_2}\frac{\phi_2(t)}{2\gamma_{13}^*}G_2(t,y)dt \qquad (A.2^*)$$

$$\frac{\partial v_1(H_1,y)}{\partial y}=\frac{4}{\pi}\int_0^{\infty}[\beta_7 A(\alpha)\cosh(w_1\alpha H_1)+\beta_8 C(\alpha)\cosh(w_3\alpha H_1)]\alpha\cos\alpha y d\alpha$$

$$-\frac{2}{\pi}\int_0^{a_1}\frac{\phi_1(t)}{2\gamma_{13}}G_3(t,y)dt \qquad (A.3^*)$$

$$\frac{\partial v_2(-H_2,y)}{\partial y}=\frac{4}{\pi}\int_0^{\infty}[\beta_7^* A^*(\alpha)\cosh(w_1^*\alpha H_2)+\beta_8^* C^*(\alpha)\cosh(w_3^*\alpha H_2)]\alpha\cos\alpha y d\alpha$$

$$-\frac{2}{\pi}\int_0^{a_2}\frac{\phi_2(t)}{2\gamma_{13}^*}G_4(t,y)dt \qquad (A.4^*)$$

where

$$G_1(t,y)=-\frac{|w_1|}{\beta_5}\left[\frac{\frac{|w_1|y}{\beta_5}}{\frac{(|w_1|y)^2}{\beta_5^2}+(H_1-t)^2}-\frac{\frac{|w_1|y}{\beta_5}}{\frac{(|w_1|y)^2}{\beta_5^2}+(H_1+t)^2}\right]$$

$$+\frac{|w_3|}{\beta_5}\left[\frac{\frac{|w_3|y}{\beta_5}}{\frac{(|w_3|y)^2}{\beta_5^2}+(H_1-t)^2}-\frac{\frac{|w_3|y}{\beta_5}}{\frac{(|w_3|y)^2}{\beta_5^2}+(H_1+t)^2}\right] \qquad (A.6a)$$

$$G_2(t,y)=-\frac{|w_1^*|}{\beta_5^*}\left[\frac{\frac{|w_1^*|y}{\beta_5^*}}{\frac{(|w_1^*|y)^2}{\beta_5^{*2}}+(H_1-t)^2}-\frac{\frac{|w_1^*|y}{\beta_5^*}}{\frac{(|w_1^*|y)^2}{\beta_5^{*2}}+(H_1+t)^2}\right]$$

$$+\frac{|w_3^*|}{\beta_5^*}\left[\frac{\frac{|w_3^*|y}{\beta_5^*}}{\frac{(|w_3^*|y)^2}{\beta_5^{*2}}+(H_1-t)^2}-\frac{\frac{|w_3^*|y}{\beta_5^*}}{\frac{(|w_3^*|y)^2}{\beta_5^{*2}}+(H_1+t)^2}\right] \qquad (A.6b)$$

$$G_3(t,y)=\frac{\beta_0\,\mathrm{sign}(w_1)|w_1|}{\beta_5}\left[\frac{H_1-t}{\frac{(|w_1|y)^2}{\beta_5^2}+(H_1-t)^2}-\frac{H_1+t}{\frac{(|w_1|y)^2}{\beta_5^2}+(H_1+t)^2}\right]$$

$$-\frac{\beta_{10}\text{sign}(w_3)|w_3|\gamma_{11}}{\beta_5}\left[\frac{H_1-t}{\frac{(|w_3|y)^2}{\beta_5^2}+(H_1-t)^2}-\frac{H_1+t}{\frac{(|w_3|y)^2}{\beta_5^2}+(H_1+t)^2}\right] \qquad \text{(A.6c)}$$

$$G_4(t,y)=\frac{\beta_0^*\text{sign}(w_1^*)|w_1^*|}{\beta_5^*}\left[\frac{H_2-t}{\frac{(|w_1^*|y)^2}{\beta_5^{*2}}+(H_2-t)^2}-\frac{H_2+t}{\frac{(|w_1^*|y)^2}{\beta_5^{*2}}+(H_2+t)^2}\right]$$

$$-\frac{\beta_{10}^*\text{sign}(w_3^*)|w_3^*|\gamma_{11}^*}{\beta_5^*}\left[\frac{H_2-t}{\frac{(|w_3^*|y)^2}{\beta_5^{*2}}+(H_2-t)^2}-\frac{H_2+t}{\frac{(|w_3^*|y)^2}{\beta_5^{*2}}+(H_2+t)^2}\right] \qquad \text{(A.6d)}$$

Applying (3.14ab) and (3.21cd) to eqns(A.1*)-(A.4*):

$$\phi_4(y)=-\frac{4}{\pi}\int_0^\infty [A(\alpha)\sinh(w_1\alpha H_1)+C(\alpha)\sinh(w_3\alpha H_1)$$

$$+A^*(\alpha)\sinh(w_1^*\alpha H_2)+C^*(\alpha)\sinh(w_3^*\alpha H_2)]\alpha\sin\alpha y d\alpha$$

$$+\frac{2}{\pi}\int_0^{a_1}\frac{\phi_1(t)}{2\gamma_{13}}G_1(t,y)dt+\frac{2}{\pi}\int_0^{a_2}\frac{\phi_2(t)}{2\gamma_{13}^*}G_2(t,y)dt \qquad \text{(A.7a)}$$

$$\phi_3(y)=\frac{4}{\pi}\int_0^\infty [\beta_7 A(\alpha)\cosh(w_1\alpha H_1)+\beta_8 C(\alpha)\cosh(w_3\alpha H_1)$$

$$-\beta_7^* A^*(\alpha)\cosh(w_1^*\alpha H_2)-\beta_8^* C^*(\alpha)\cosh(w_3^*\alpha H_2)]\alpha\cos\alpha y d\alpha$$

$$-\frac{2}{\pi}\int_0^{a_1}\frac{\phi_1(t)}{2\gamma_{13}}G_3(t,y)dt+\frac{2}{\pi}\int_0^{a_2}\frac{\phi_2(t)}{2\gamma_{13}^*}G_4(t,y)dt \qquad \text{(A.7b)}$$

Taking inverse cosine and sine Fourier transform for both sides of eqn (A.7a) and (A.7b) respectively, one gets:

$$A(\alpha)\sinh(w_1\alpha H_1)+C(\alpha)\sinh(w_3\alpha H_1)$$

$$+A^*(\alpha)\sinh(w_1^*\alpha H_2)+C^*(\alpha)\sinh(w_3^*\alpha H_2)=R_1(\alpha) \qquad \text{(A.8a)}$$

and

$$\beta_7 A(\alpha)\cosh(w_1\alpha H_1)+\beta_8 C(\alpha)\cosh(w_3\alpha H_1)$$

$$-\beta_7^* A^*(\alpha)\cosh(w_1^*\alpha H_2)-\beta_8^* C^*(\alpha)\cosh(w_3^*\alpha H_2)=R_2(\alpha) \qquad \text{(A.8b)}$$

where

$$R_1(\alpha) = -\frac{1}{2\alpha}\int_0^\infty \phi_4(y)\sin\alpha y dy + \frac{2}{\pi\alpha}\int_0^\infty \int_0^{a_1} \frac{\phi_1(t)}{4\gamma_{13}} G_1(t,y)\sin\alpha y dt dy$$

$$+ \frac{2}{\pi\alpha}\int_0^\infty \int_0^{a_2} \frac{\phi_2(t)}{4\gamma_{13}^*} G_2(t,y)\sin\alpha y dt dy \qquad \text{(A.9a)}$$

$$R_2(\alpha) = \frac{1}{2\alpha}\int_0^\infty \phi_3(y)\cos\alpha y dy + \frac{2}{\pi\alpha}\int_0^\infty \int_0^{a_1} \frac{\phi_1(t)}{4\gamma_{13}} G_3(t,y)\cos\alpha y dt dy$$

$$- \frac{2}{\pi\alpha}\int_0^\infty \int_0^{a_2} \frac{\phi_2(t)}{4\gamma_{13}^*} G_4(t,y)\cos\alpha y dt dy \qquad \text{(A.9b)}$$

Using the following integrals:

$$\int_0^\infty G_1(t,y)\sin\alpha y dy = -\frac{\pi}{2}(e^{-\alpha(H_1-t)\beta_5/|w_1|} - e^{-\alpha(H_1+t)\beta_5/|w_1|})$$

$$+ \frac{\pi\gamma_{11}}{2\gamma_{12}}(e^{-\alpha(H_1-t)\beta_5/|w_3|} - e^{-\alpha(H_1+t)\beta_5/|w_3|}) \qquad \text{(A.10a)}$$

$$\int_0^\infty G_2(t,y)\sin\alpha y dy = -\frac{\pi}{2}(e^{-\alpha(H_2-t)\beta_5^*/|w_1^*|} - e^{-\alpha(H_2+t)\beta_5^*/|w_1^*|})$$

$$+ \frac{\pi\gamma_{11}^*}{2\gamma_{12}^*}(e^{-\alpha(H_2-t)\beta_5^*/|w_3^*|} - e^{-\alpha(H_2+t)\beta_5^*/|w_3^*|}) \qquad \text{(A.10b)}$$

$$\int_0^\infty G_3(t,y)\cos\alpha y dy = \frac{\pi}{2}\text{sign}(w_1)\beta_9(e^{-\alpha(H_1-t)\beta_5/|w_1|} - e^{-\alpha(H_1+t)\beta_5/|w_1|})$$

$$- \frac{\pi}{2}\text{sign}(w_3)\beta_{10}\frac{\gamma_{11}}{\gamma_{12}}(e^{-\alpha(H_1-t)\beta_5/|w_3|} - e^{-\alpha(H_1+t)\beta_5/|w_3|}) \qquad \text{(A.10c)}$$

$$\int_0^\infty G_4(t,y)\cos\alpha y dy = \frac{\pi}{2}\text{sign}(w_1^*)\beta_9^*(e^{-\alpha(H_2-t)\beta_5^*/|w_1^*|} - e^{-\alpha(H_2+t)\beta_5^*/|w_1^*|}$$

$$- \frac{\pi}{2}\text{sign}(w_3^*)\beta_{10}^*\frac{\gamma_{11}^*}{\gamma_{12}^*}(e^{-\alpha(H_2-t)\beta_5^*/|w_3^*|} - e^{-\alpha(H_2+t)\beta_5^*/|w_3^*|}) \qquad \text{(A.10d)}$$

eqns(A.9a) and (A.9b) are finally reduced to:

$$R_1(\alpha) = -\frac{1}{2\alpha}\int_{b_1}^{b_2} \phi_4(y)\sin\alpha y dy$$

$$+\frac{1}{4\alpha\gamma_{13}}\int_{-a_1}^{a_1}\phi_1(t)[-e^{-\alpha(H_1-t)\beta_5/|w_1|}+\frac{\gamma_{11}}{\gamma_{12}}e^{-\alpha(H_1-t)\beta_5/|w_3|}]dt$$

$$+\frac{1}{4\alpha\gamma_{13}^*}\int_{-a_2}^{a_2}\phi_2(t)[-e^{-\alpha(H_2-t)\beta_5^*/|w_1^*|}+\frac{\gamma_{11}^*}{\gamma_{12}^*}(e^{-\alpha(H_2-t)\beta_5^*/|w_3^*|}]dt \qquad \text{(A.11a)}$$

and

$$R_2(a)=\frac{1}{2\alpha}\int_{b_1}^{b_2}\phi_3(y)\cos\alpha y dy$$

$$+\frac{1}{4\alpha\gamma_{13}}\int_{-a_1}^{a_1}\phi_1(t)[\text{sign}(w_1)\beta_9 e^{-\alpha(H_1-t)\beta_5/|w_1|}-\text{sign}(w_3)\beta_{10}\frac{\gamma_{11}}{\gamma_{12}}e^{-\alpha(H_1-t)\beta_5/|w_3|}]dt$$

$$-\frac{1}{4\alpha\gamma_{13}^*}\int_{-a_2}^{a_2}\phi_2(t)[\text{sign}(w_1^*)\beta_9^* e^{-\alpha(H_2-t)\beta_5^*/|w_1^*|}$$

$$-\text{sign}(w_3^*)\beta_{10}^*\frac{\gamma_{11}^*}{\gamma_{12}^*}e^{-\alpha(H_2-t)\beta_5^*/|w_3^*|}]dt \qquad \text{(A.11b)}$$

Similarly, applying the continuity conditions (3.13ab) and (3.14ab), one derives the following:

$$\int_0^\infty 2[\gamma_3 A(\alpha)\cosh(w_1\alpha H_1)+\gamma_4 C(\alpha)\cosh(w_3\alpha H_1)$$

$$-\lambda_1\gamma_3^* A^*(\alpha)\cosh(w_1^*\alpha H_2)-\lambda_1\gamma_4^* C^*(\alpha)\cosh(w_3^*\alpha H_2)]\alpha\cos\alpha y d\alpha$$

$$=-\int_0^\infty\int_0^{a_1}\frac{\phi_1(t)}{\gamma_{13}}\sin\alpha t dt[\gamma_1 e^{-|w_1|\alpha y/\beta_5}-\gamma_2\frac{\gamma_{11}}{\gamma_{12}}e^{-|w_3|\alpha y/\beta_5}]\cos\alpha H_1 d\alpha$$

$$+\int_0^\infty\int_0^{a_2}\frac{\lambda_1\phi_2(t)}{\gamma_{13}^*}\sin\alpha t dt[\gamma_1^* e^{-|w_1^*|\alpha y/\beta_5^*}-\gamma_2^*\frac{\gamma_{11}^*}{\gamma_{12}^*}e^{-|w_3^*|\alpha y/\beta_5^*}]\cos\alpha H_2 d\alpha \qquad \text{(A.12a)}$$

and

$$\int_0^\infty 2[\gamma_9 A(\alpha)\sinh(w_1\alpha H_1)+\gamma_{10} C(\alpha)\sinh(w_3\alpha H_1)$$

$$+\lambda_2\gamma_9^* A^*(\alpha)\sinh(w_1^*\alpha H_2)+\lambda_2\gamma_{10}^* C^*(\alpha)\sinh(w_3^*\alpha H_2)]\alpha\sin\alpha y d\alpha$$

$$= -\int_0^{\infty}\int_0^{a_1} \frac{\phi_1(t)}{\gamma_{13}} \sin\alpha t dt \gamma_{11}[e^{-|w_1|\alpha y/\beta_5} - e^{-|w_3|\alpha y/\beta_5}]\sin\alpha H_1 d\alpha$$

$$-\int_0^{\infty}\int_0^{a_2} \frac{\lambda_2\phi_2(t)}{\gamma_{13}^*} \sin\alpha t dt \gamma_{11}^*[e^{-|w_1^*|\alpha y/\beta_5^*} - e^{-|w_3^*|\alpha y/\beta_5^*}]\sin\alpha H_2 d\alpha \qquad \text{(A.12b)}$$

Applying inverse Fourier cosine and sine transform to (A.12ab) respectively, we have:

$$[\gamma_3 A(\alpha)\cosh(w_1\alpha H_1) + \gamma_4 C(\alpha)\cosh(w_3\alpha H_1)$$
$$-\lambda_1\gamma_3^* A^*(\alpha)\cosh(w_1^*\alpha H_2) - \lambda_1\gamma_4^* C^*(\alpha)\cosh(w_3^*\alpha H_2)]\alpha = R_3(\alpha) \qquad \text{(A.13a)}$$

and

$$[\gamma_9 A(\alpha)\sinh(w_1\alpha H_1) + \gamma_{10} C(\alpha)\sinh(w_3\alpha H_1)$$
$$+\lambda_2\gamma_9^* A^*(\alpha)\sinh(w_1^*\alpha H_2) + \lambda_2\gamma_{10}^* C^*(\alpha)\sinh(w_3^*\alpha H_2)]\alpha = R_4(\alpha) \qquad \text{(A.13b)}$$

where

$$R_3(\alpha) = -\frac{2}{\pi}\int_0^{\infty}\int_0^{a_1} \frac{\phi_1(t)}{4\gamma_{13}} S_1(t,y)\cos\alpha y dt dy + \frac{2}{\pi}\int_0^{\infty}\int_0^{a_2} \frac{\lambda_1\phi_2(t)}{4\gamma_{13}^*} S_2(t,y)\cos\alpha y dt dy \qquad \text{(A.14a)}$$

$$R_4(\alpha) = -\frac{2}{\pi}\int_0^{\infty}\int_0^{a_1} \frac{\phi_1(t)}{4\gamma_{13}} S_3(t,y)\sin\alpha y dt dy - \frac{2}{\pi}\int_0^{\infty}\int_0^{a_2} \frac{\lambda_2\phi_2(t)}{4\gamma_{13}^*} S_4(t,y)\sin\alpha y dt dy \qquad \text{(A.14b)}$$

and

$$S_1(t,y) = [-\gamma_1 \frac{H_1-t}{\frac{(|w_1|y)^2}{\beta_5^2}+(H_1-t)^2} + \gamma_2(\frac{\gamma_{11}}{\gamma_{12}} \frac{H_1-t}{\frac{(|w_3|y)^2}{\beta_5^2}+(H_1-t)^2}]$$
$$+ [\gamma_1 \frac{H_1+t}{\frac{(|w_1|y)^2}{\beta_5^2}+(H_1+t)^2} - \gamma_2(\frac{\gamma_{11}}{\gamma_{12}} \frac{H_1+t}{\frac{(|w_3|y)^2}{\beta_5^2}+(H_1+t)^2}] \qquad \text{(A.15a)}$$

$$S_2(t,y) = [-\gamma_1^* \frac{H_2-t}{\frac{(|w_1^*|y)^2}{\beta_5^{*2}}+(H_2-t)^2} + \gamma_2^*(\frac{\gamma_{11}^*}{\gamma_{12}^*} \frac{H_2-t}{\frac{(|w_3^*|y)^2}{\beta_5^{*2}}+(H_2-t)^2}]$$
$$+ [\gamma_1^* \frac{H_2+t}{\frac{(|w_1^*|y)^2}{\beta_5^{*2}}+(H_2+t)^2} - \gamma_2^*(\frac{\gamma_{11}^*}{\gamma_{12}^*} \frac{H_2+t}{\frac{(|w_3^*|y)^2}{\beta_5^{*2}}+(H_2+t)^2}] \qquad \text{(A.15b)}$$

$$S_3(t,y) = \gamma_{11}\left[\frac{\frac{|w_1|y}{\beta_5}}{\frac{(|w_1|y)^2}{\beta_5^2}+(H_1-t)^2} - \frac{\frac{|w_3|y}{\beta_5}}{\frac{(|w_3|y)^2}{\beta_5^2}+(H_1-t)^2}\right]$$

$$- \gamma_{11}\left[\frac{\frac{|w_1|y}{\beta_5}}{\frac{(|w_1|y)^2}{\beta_5^2}+(H_1+t)^2} - \frac{\frac{|w_3|y}{\beta_5}}{\frac{(|w_3|y)^2}{\beta_5^2}+(H_1+t)^2}\right] \qquad \text{(A.15c)}$$

$$S_4(t,y) = \gamma_{11}^*\left[\frac{\frac{|w_1^*|y}{\beta_5^*}}{\frac{(|w_1^*|y)^2}{\beta_5^{*2}}+(H_1-t)^2} - \frac{\frac{|w_3^*|y}{\beta_5^*}}{\frac{(|w_3^*|y)^2}{\beta_5^{*2}}+(H_1-t)^2}\right]$$

$$- \gamma_{11}^*\left[\frac{\frac{|w_1^*|y}{\beta_5^*}}{\frac{(|w_1^*|y)^2}{\beta_5^{*2}}+(H_1+t)^2} - \frac{\frac{|w_3^*|y}{\beta_5^*}}{\frac{(|w_3^*|y)^2}{\beta_5^{*2}}+(H_1+t)^2}\right] \qquad \text{(A.15d)}$$

With the help of the following integrals:

$$\int_0^\infty S_1(t,y)\cos\alpha y dy = -\frac{\pi\gamma_1\beta_5}{2|w_1|}\left(e^{-\alpha(H_1-t)\beta_5/|w_1|} - e^{-\alpha(H_1+t)\beta_5/|w_1|}\right)$$

$$+\frac{\pi\gamma_2\gamma_{11}\beta_5}{2\gamma_{12}|w_3|}\left(e^{-\alpha(H_1-t)\beta_5/|w_3|} - e^{-\alpha(H_1+t)\beta_5/|w_3|}\right) \qquad \text{(A.16a)}$$

$$\int_0^\infty S_2(t,y)\cos\alpha y dy = -\frac{\pi\gamma_1^*\beta_5^*}{2\,|w_1^*|}\left(e^{-\alpha(H_2-t)\beta_5^*/|w_1^*|} - e^{-\alpha(H_2+t)\beta_5^*/|w_1^*|}\right)$$

$$+\frac{\pi\gamma_2^*\gamma_{11}^*\beta_5^*}{2\,\gamma_{12}^*|w_3^*|}\left(e^{-\alpha(H_2-t)\beta_5^*/|w_3^*|} - e^{-\alpha(H_2+t)\beta_5^*/|w_3^*|}\right) \qquad \text{(A.16b)}$$

$$\int_0^\infty S_3(t,y)\sin\alpha y dy = +\frac{\pi\gamma_{11}\beta_5}{2\,|w_1|}\left(e^{-\alpha(H_1-t)\beta_5/|w_1|} - e^{-\alpha(H_1+t)\beta_5/|w_1|}\right)$$

$$-\frac{\pi\gamma_{11}\beta_5}{2\,|w_3|}\left(e^{-\alpha(H_1-t)\beta_5/|w_3|} - e^{-\alpha(H_1+t)\beta_5/|w_3|}\right) \qquad \text{(A.16c)}$$

$$\int_0^\infty S_4(t,y)\sin\alpha y dy = +\frac{\pi\gamma_{11}^*\beta_5^*}{2\,|w_1^*|}\left(e^{-\alpha(H_2-t)\beta_5^*/|w_1^*|} - e^{-\alpha(H_2+t)\beta_5^*/|w_1^*|}\right)$$

$$-\frac{\pi\gamma_{11}^*\beta_5^*}{2\,|w_3^*|}\left(e^{-\alpha(H_2-t)\beta_5^*/|w_3^*|} - e^{-\alpha(H_2+t)\beta_5^*/|w_3^*|}\right) \qquad \text{(A.16d)}$$

$R_3(\alpha)$ and $R_4(\alpha)$ are finally reduced to:

$$R_3(a) = \frac{1}{4\alpha\gamma_{13}}\int_{-a_1}^{a_1} \phi_1(t)[\frac{\gamma_1\beta_5}{|w_1|}e^{-\alpha(H_1-t)\beta_5/|w_1|} - \frac{\gamma_2\gamma_{11}\beta_5}{\gamma_{12}|w_3|}e^{-\alpha(H_1-t)\beta_5/|w_3|}]dt$$

$$+\frac{1}{4\alpha\gamma_{13}^*}\int_{-a_2}^{a_2} \phi_2(t)\lambda_1[-\frac{\gamma_1^*\beta_5^*}{|w_1^*|}e^{-\alpha(H_2-t)\beta_5^*/|w_1^*|} + \frac{\gamma_2^*\gamma_{11}^*\beta_5^*}{\gamma_{12}^*|w_3^*|}e^{-\alpha(H_2-t)\beta_5^*/|w_3^*|}]dt$$

(A.17a)

and

$$R_4(\alpha) = \frac{1}{4\alpha\gamma_{13}}\int_{-a_1}^{a_1} \phi_1(t)\gamma_{11}\beta_5[-\frac{1}{|w_1|}e^{-\alpha(H_1-t)\beta_5/|w_1|} + \frac{1}{|w_3|}e^{-\alpha(H_1-t)\beta_5/|w_3|}]dt$$

$$+\frac{1}{4\alpha\gamma_{13}^*}\int_{-a_2}^{a_2} \phi_2(t)\gamma_{11}^*\beta_5^*\lambda_2[-\frac{1}{|w_1^*|}e^{-\alpha(H_2-t)\beta_5^*/|w_1^*|} + \frac{1}{|w_3^*|}(e^{-\alpha(H_2-t)\beta_5^*/|w_3^*|}]dt$$

(A.17b)

Appendix B

Definition of material constants for both fiber and matrix strips. A superscript * will be used for the material in the matrix strip.

$$\gamma_1 = 1 + \frac{\nu_{yx} w_1 \beta_9}{\beta_5} \qquad \gamma_2 = 1 + \frac{\nu_{yx} w_3 \beta_{10}}{\beta_5} \qquad \gamma_3 = w_1 + \nu_{xy}\beta_7 \qquad \gamma_4 = w_3 + \nu_{yx}\beta_8$$

$$\gamma_5 = \nu_{xy} + \frac{\beta_9 w_1}{\beta_5} \qquad \gamma_6 = \nu_{xy} + \frac{\beta_{10} w_3}{\beta_5} \qquad \gamma_7 = \nu_{xy} w_1 + \beta_7 \qquad \gamma 8 = \nu_{xy} w_3 + \beta_8$$

$$\gamma_9 = -1 + \beta_7 w_1 \qquad \gamma_{10} = -1 + \beta_8 w_3 \qquad \gamma_{11} = -\frac{|w_1|}{\beta_5} + \text{sign}(w_1)\beta_9$$

$$\gamma_{12} = -\frac{|w_3|}{\beta_5} + \text{sign}(w_3)\beta_{10} \qquad \gamma_{13} = \text{sign}(w_1)\beta_9 - \frac{\gamma_{11}}{\gamma_{12}}\text{sign}(w_3)\beta_{10}$$

$$\gamma_{14} = \frac{1}{2}\left[\frac{\gamma_5}{\gamma_{13}} - \frac{\gamma_6}{\gamma_{13}}\frac{\gamma_{11}}{\gamma_{12}}\right] \qquad \lambda_1 = \frac{E_x^*}{E_x}\frac{1-\nu_{xy}\nu_{yx}}{1-\nu_{xy}^*\nu_{yx}^*} \qquad \lambda_2 = \frac{G_{xy}^*}{G_{xy}}$$

$$\lambda_3 = \beta_8\gamma_3 - \beta_7\gamma_4 \qquad \lambda_4 = \lambda_1\gamma_3^*\beta_7 - \beta_7^*\gamma_3 \qquad \lambda_5 = \lambda_1\gamma_4^*\beta_7 - \beta_8^*\gamma_3$$

$$\lambda_6 = \gamma_9 - \gamma_{10} \qquad \lambda_7 = \gamma_9 - \gamma_9^*\lambda_2 \qquad \lambda_8 = \gamma_9 - \gamma_{10}^*\lambda_2$$

$$\lambda_9 = \lambda_3\lambda_7 \qquad \lambda_{10} = \lambda_3\lambda_8 \qquad \lambda_{11} = \lambda_3\gamma_9$$

$$\lambda_{12} = \lambda_6\lambda_4 \qquad \lambda_{13} = \lambda_5\lambda_6 \qquad \lambda_{14} = \lambda_6\gamma_3$$

$$\lambda_{15} = \lambda_6\beta_7 \qquad \lambda_{16} = \lambda_3\beta_7 \qquad \lambda_{17} = \lambda_3\beta_7^* + \lambda_4\beta_8$$

$$\lambda_{18} = \lambda_4\beta_7 \qquad \lambda_{19} = \lambda_3\beta_8^* + \lambda_5)\beta_8 \qquad \lambda_{20} = \lambda_5\beta_7$$

$$\lambda_{21} = \lambda_3 - \gamma_3\beta_8 \qquad \lambda_{22} = \gamma_3\beta_7 \qquad \lambda_{23} = \beta_7\beta_8$$

$$\lambda_{24} = \lambda_{10}\lambda_{16} - \lambda_9\lambda_{16} \qquad \lambda_{25} = \lambda_{10}\lambda_{17} \qquad \lambda_{26} = \lambda_{12}\lambda_{16} - \lambda_{10}\lambda_{18}$$

$$\lambda_{27} = \lambda_9\lambda_{20} - \lambda_{13}\lambda_{16} \qquad \lambda_{28} = \lambda_9\lambda_{19} \qquad \lambda_{29} = \lambda_{12}\lambda_{19} - \lambda_{13}\lambda_{17}$$

$$\lambda_{30} = \lambda_{13}\lambda_{18} - \lambda_{12}\lambda_{20} \qquad \lambda_{31} = \lambda_{11}\lambda_{16} - \lambda_9\lambda_{16} \qquad \lambda_{32} = \lambda_{11}\lambda_{17}$$

$\lambda_{33} = \lambda_{16}\lambda_{12} - \lambda_{11}\lambda_{18}$ $\lambda_{34} = \lambda_9\lambda_{22} - \lambda_{14}\lambda_{16}$ $\lambda_{35} = \lambda_9\lambda_{21}$

$\lambda_{36} = -\lambda_{14}\lambda_{17} - \lambda_{21}\lambda_{12}\lambda_{37} = \lambda_{14}\lambda_{18} - \lambda_{22}\lambda_{12}$ $\lambda_{38} = \lambda_{15}\lambda_{16} - \beta_7\beta_7\lambda_9$

$\lambda_{39} = \lambda_9\lambda_{23}$ $\lambda_{40} = \lambda_{15}\lambda_{17} - \lambda_{12}\lambda_{23}$ $\lambda_{41} = \beta_7\beta_7\lambda_{12} - \lambda_{15}\lambda_{18}$

$\lambda_{42} = \lambda_3\lambda_{16}$ $\lambda_{43} = \lambda_3\lambda_{17}$ $\lambda_{44} = \lambda_3\lambda_{18}$

$\lambda_{45} = \lambda_{10}\lambda_{16} - \lambda_{11}\lambda_{16}$ $\lambda_{46} = \lambda_{11}\lambda_{20} - \lambda_{13}\lambda_{16}$ $\lambda_{47} = -\lambda_{11}\lambda_{19}$

$\lambda_{48} = \lambda_{14}\lambda_{16} - \lambda_{10}\lambda_2$ $\lambda_{49} = \lambda_{13}\lambda_{22} - \lambda_{14}\lambda_{20}$ $\lambda_{50} = -\lambda_{10}\lambda_{21}$

$\lambda_{51} = \lambda_{14}\lambda_{19} + \lambda_{13}\lambda_{21}$ $\lambda_{52} = \lambda_{10}\beta_7\beta_7 - \lambda_{15}\lambda_{16}\lambda_{53} = \lambda_{15}\lambda_{20} - \lambda_{13}\beta_7\beta_7$

$\lambda_{54} = -\lambda_{10}\lambda_{23}$ $\lambda_{55} = \lambda_{13}\lambda_{23} - \lambda_{15}\lambda_{19}$ $\lambda_{56} = -\lambda_3\lambda_{20}$

$\lambda_{57} = \lambda_3\lambda_{19}$ $\lambda_{58} = -\lambda_4\lambda_{16}(\lambda_8 - \gamma_9)$ $\lambda_{59} = -\lambda_5\lambda_{16}(\gamma_9 - \lambda_7)$

$\lambda_{60} = \gamma_9(\lambda_4\lambda_{19} - \lambda_5\lambda_{17})$ $\lambda_{61} = \gamma_3\beta_7(\lambda_{10} - \lambda_9)$ $\lambda_{62} = \lambda_8(\gamma_3\lambda_{17} + \lambda_4\lambda_{21})$

$\lambda_{63} = -\lambda_9(\gamma_3\beta_8^* + \lambda_5)$ $\lambda_{64} = -\beta_7\beta_7(\lambda_{10} - \lambda_9)$ $\lambda_{65} = \lambda_8(\lambda_4\lambda_{23} - \beta_7\lambda_{17})$

$\lambda_{66} = \lambda_7(\beta_7\lambda_{19} - \lambda_5\lambda_{23})$ $\lambda_{67} = -\lambda_4\lambda_{16}$ $\lambda_{68} = \lambda_5\lambda_{16}$

$\lambda_{69} = \lambda_5\lambda_{17} - \lambda_4\lambda_{19}$ $\lambda_{70} = \lambda_3(\beta_7^*(\lambda_{10} - \lambda_{11}) + \beta_8\lambda_4(\lambda_8 - \gamma_9))$

$\lambda_{71} = \lambda_3(\beta_8^*(\lambda_{11} - \lambda_9) + \beta_8\lambda_5(\gamma_9 - \lambda_7))$ $\lambda_{72} = \beta_7^*(\lambda_{11}\lambda_5 - \lambda_3\lambda_{13}) + \beta_8^*(\lambda_3\lambda_{12} - \lambda_{11}\lambda_4)$

$\lambda_{73} = \lambda_{21}(\lambda_{10} - \lambda_9)$ $\lambda_{74} = \lambda_{12}\lambda_3 - \lambda_{10}\lambda_4 + \beta_7^*(\lambda_{14}\lambda_3 - \lambda_{10}\gamma_3)$

$\lambda_{75} = \lambda_9\lambda_5 - \lambda_{13}\lambda_3 + \beta_8^*(\lambda_9\gamma_3 - \lambda_{14}\lambda_3)$ $\lambda_{76} = \lambda_{23}(\lambda_{10} - \lambda_9)$

$\lambda_{77} = \beta_7^*(\lambda_{10}\beta_7 - \lambda_{15}\lambda_3)$ $\lambda_{78} = \beta_8^*(\lambda_{15}\lambda_3 - \beta_7\lambda_9)$

$\lambda_{79} = \lambda_3(\lambda_4\beta_8^* - \lambda_5\beta_7^*)$ $\lambda_{80} = \lambda_{24} + \lambda_{25} + \lambda_{26} + \lambda_{27} - \lambda_{28} + \lambda_{29}$

$$\lambda_{81} = -\lambda_{70} - \lambda_{71} - \lambda_{72} + \text{sign}(w_1)\beta_9(\lambda_{73} + \lambda_{74} + \lambda_{75}) + \frac{\beta_5\gamma_1}{|w_1|}(\lambda_{76} + \lambda_{77} + \lambda_{78}) - \frac{\gamma_{11}\beta_5}{|w_1|}(\lambda_{43} - \lambda_{57} + \lambda_{79})$$

$$\lambda_{82} = -\lambda_{58} - \lambda_{59} - \lambda_{60} + \text{sign}(w_1)\beta_9(\lambda_{61} + \lambda_{62} + \lambda_{63})$$

$$+ \frac{\beta_5\gamma_1}{|w_1|}(\lambda_{64} + \lambda_{65} + \lambda_{66}) - \frac{\gamma_{11}\beta_5}{|w_1|}(\lambda_{67} + \lambda_{68} + \lambda_{69})$$

$$\lambda_{83} = \frac{\gamma_{11}}{\gamma_{12}}(\lambda_{70} + \lambda_{71} + \lambda_{72}) - \frac{\gamma_{11}}{\gamma_{12}}\text{sign}(w_3)\beta_{10}(\lambda_{73} + \lambda_{74} + \lambda_{75})$$

$$- \frac{\gamma_{11}}{\gamma_{12}}\frac{\beta_5\gamma_2}{|w_3|}(\lambda_{76} + \lambda_{77} + \lambda_{78}) + \frac{\gamma_{11}\beta_5}{|w_3|}(\lambda_{43} - \lambda_{57} + \lambda_{79})$$

$$\lambda_{84} = \frac{\gamma_{11}}{\gamma_{12}}(\lambda_{58} + \lambda_{59} + \lambda_{60}) - \frac{\gamma_{11}}{\gamma_{12}}\text{sign}(w_3)\beta_{10}(\lambda_{61} + \lambda_{62} + \lambda_{63})$$

$$- \frac{\gamma_{11}}{\gamma_{12}}\frac{\beta_5\gamma_2}{|w_3|}(\lambda_{64} + \lambda_{65} + \lambda_{66}) + \frac{\gamma_{11}\beta_5}{|w_3|}(\lambda_{67} + \lambda_{68} + \lambda_{69})$$

$$\lambda_{85} = \gamma_7\lambda_{81}\frac{1}{\gamma_{13}\gamma_{14}\lambda_{80}} \quad \lambda_{86} = \gamma_8\lambda_{82}\frac{1}{\gamma_{13}\gamma_{14}\lambda_{80}} \quad \lambda_{87} = \gamma_7\lambda_{83}\frac{1}{\gamma_{13}\gamma_{14}\lambda_{80}} \quad \lambda_{88} = \gamma_7\lambda_{84}\frac{1}{\gamma_{13}\gamma_{14}\lambda_{80}}$$

$$\lambda_{89} = -\lambda_{70} - \lambda_{71} - \lambda_{72} - \text{sign}(w_1^*)\beta_9^*(\lambda_{73} + \lambda_{74} + \lambda_{75})$$

$$- \lambda_1\gamma_1^*\frac{\beta_5^*}{|w_1^*|}(\lambda_{76} + \lambda_{77} + \lambda_{78}) - \lambda_2\gamma_{11}^*\frac{\beta_5^*}{|w_1^*|}(\lambda_{43} - \lambda_{57} + \lambda_{79})$$

$$\lambda_{90} = -\lambda_{58} - \lambda_{59} - \lambda_{60} - \text{sign}(w_1^*)\beta_9^*(\lambda_{61} + \lambda_{62} + \lambda_{63})$$

$$- \lambda_1\gamma_1^*\frac{\beta_5^*}{|w_1^*|}(\lambda_{64} + \lambda_{65} + \lambda_{66}) - \lambda_2\gamma_{11}^*\frac{\beta_5^*}{|w_1^*|}(\lambda_{67} + \lambda_{68} + \lambda_{69})$$

$$\lambda_{91} = \frac{\gamma_{11}^*}{\gamma_{12}^*}(\lambda_{70} + \lambda_{71} + \lambda_{72}) + \frac{\gamma_{11}^*}{\gamma_{12}^*}\text{sign}(w_3^*)\beta_{10}^*(\lambda_{73} + \lambda_{74} + \lambda_{75})$$

$$+ \lambda_1\gamma_2^*\frac{\gamma_{11}^*}{\gamma_{12}^*}\frac{\beta_5^*}{|w_3^*|}(\lambda_{76} + \lambda_{77} + \lambda_{78}) + \lambda_2\gamma_{11}^*\frac{\beta_5^*}{|w_3^*|}(\lambda_{43} - \lambda_{57} + \lambda_{79})$$

$$\lambda_{92} = \frac{\gamma_{11}^*}{\gamma_{12}^*}(\lambda_{58} + \lambda_{59} + \lambda_{60}) + \frac{\gamma_{11}^*}{\gamma_{12}^*}\text{sign}(w_3^*)\beta_{10}^*(\lambda_{61} + \lambda_{62} + \lambda_{63})$$

$$+ \lambda_1 \gamma_2^* \frac{\gamma_{11}^*}{\gamma_{12}^*} \frac{\beta_5^*}{|w_3^*|}(\lambda_{64} + \lambda_{65} + \lambda_{66}) + \lambda_2 \gamma_{11}^* \frac{\beta_5^*}{|w_3^*|}(\lambda_{67} + \lambda_{68} + \lambda_{69})$$

$$\lambda_{93} = \gamma_7 \lambda_{89} \frac{1}{\gamma_{13}^* \gamma_{14} \lambda_{80}} \quad \lambda_{94} = \gamma_8 \lambda_{90} \frac{1}{\gamma_{13}^* \gamma_{14} \lambda_{80}} \quad \lambda_{95} = \gamma_7 \lambda_{91} \frac{1}{\gamma_{13}^* \gamma_{14} \lambda_{80}} \quad \lambda_{96} = \gamma_8 \lambda_{92} \frac{1}{\gamma_{13}^* \gamma_{14} \lambda_{80}}$$

$$\lambda_{97} = -\lambda_{45} - \lambda_{46} - \lambda_{47} + \text{sign}(w_1)\beta_9(\lambda_{48} + \lambda_{50} + \lambda_{51})$$

$$+ \frac{\beta_5 \gamma_1}{|w_1|}(\lambda_{52} + \lambda_{54} + \lambda_{55}) - \frac{\gamma_{11} \beta_5}{|w_1|}(\lambda_{42} + \lambda_{56} + \lambda_{57})$$

$$\lambda_{98} = -\lambda_{31} - \lambda_{32} - \lambda_{33} + \text{sign}(w_1)\beta_9(\lambda_{34} + \lambda_{35} + \lambda_{36})$$

$$+ \frac{\beta_5 \gamma_1}{|w_1|}(\lambda_{38} + \lambda_{39} + \lambda_{40}) - \frac{\gamma_{11} \beta_5}{|w_1|}(\lambda_{42} + \lambda_{43} + \lambda_{44})$$

$$\lambda_{99} = \frac{\gamma_{11}}{\gamma_{12}}(\lambda_{45} + \lambda_{46} + \lambda_{47}) - \frac{\gamma_{11}}{\gamma_{12}} \text{sign}(w_3)\beta_{10}(\lambda_{48} + \lambda_{50} + \lambda_{51})$$

$$- \frac{\gamma_{11}}{\gamma_{12}} \frac{\beta_5 \gamma_2}{|w_3|}(\lambda_{52} + \lambda_{54} + \lambda_{55}) + \frac{\gamma_{11} \beta_5}{|w_3|}(\lambda_{42} + \lambda_{56} + \lambda_{57})$$

$$\lambda_{100} = \frac{\gamma_{11}}{\gamma_{12}}(\lambda_{31} + \lambda_{32} + \lambda_{33}) - \frac{\gamma_{11}}{\gamma_{12}} \text{sign}(w_3)\beta_{10}(\lambda_{34} + \lambda_{35} + \lambda_{36})$$

$$- \frac{\gamma_{11}}{\gamma_{12}} \frac{\beta_5 \gamma_2}{|w_3|}(\lambda_{38} + \lambda_{39} + \lambda_{40}) + \frac{\gamma_{11} \beta_5}{|w_3|}(-\lambda_{42} - \lambda_{43} + \lambda_{44})$$

$$\lambda_{101} = \lambda_{97} \gamma_7^* \frac{1}{\gamma_{13} \gamma_{14}^* \lambda_{80}} \qquad \lambda_{102} = \lambda_{98} \gamma_8^* \frac{1}{\gamma_{13} \gamma_{14}^* \lambda_{80}}$$

$$\lambda_{103} = \lambda_{99} \gamma_7^* \frac{1}{\gamma_{13} \gamma_{14}^* \lambda_{80}} \qquad \lambda_{104} = \lambda_{100} \gamma_8^* \frac{1}{\gamma_{13} \gamma_{14}^* \lambda_{80}}$$

$$\lambda_{105} = -\lambda_{45} - \lambda_{46} - \lambda_{47} - \text{sign}(w_1^*)\beta_9^*(\lambda_{48} + \lambda_{50} + \lambda_{51})$$

$$- \lambda_1 \gamma_1^* \frac{\beta_5^*}{|w_1^*|}(\lambda_{52} + \lambda_{54} + \lambda_{55}) - \lambda_2 \gamma_{11}^* \frac{\beta_5^*}{|w_1^*|}(\lambda_{42} + \lambda_{56} + \lambda_{57})$$

$$\lambda_{106} = -\lambda_{31} - \lambda_{32} - \lambda_{33} - \text{sign}(w_1^*)\beta_9^*(\lambda_{34} + \lambda_{35} + \lambda_{36})$$

$$- \lambda_1 \gamma_1^* \frac{\beta_5^*}{|w_1^*|}(\lambda_{38} + \lambda_{39} + \lambda_{40}) - \lambda_2 \gamma_{11}^* \frac{\beta_5^*}{|w_1^*|}(-\lambda_{42} - \lambda_{43} + \lambda_{44})$$

$$\lambda_{107} = \frac{\gamma_{11}^*}{\gamma_{12}^*}(\lambda_{45} + \lambda_{46} + \lambda_{47}) + \frac{\gamma_{11}^*}{\gamma_{12}^*}\text{sign}(w_3^*)\beta_{10}^*(\lambda_{48} + \lambda_{50} + \lambda_{51})$$

$$+ \lambda_1 \gamma_2^* \frac{\gamma_{11}^*}{\gamma_{12}^*} \frac{\beta_5^*}{|w_3^*|}(\lambda_{52} + \lambda_{54} + \lambda_{55}) + \lambda_2 \gamma_{11}^* \frac{\beta_5^*}{|w_3^*|}(\lambda_{42} + \lambda_{56} + \lambda_{57})$$

$$\lambda_{108} = \frac{\gamma_{11}^*}{\gamma_{12}^*}(\lambda_{31} + \lambda_{32} + \lambda_{33}) + \frac{\gamma_{11}^*}{\gamma_{12}^*}\text{sign}(w_3^*)\beta_{10}^*(\lambda_{34} + \lambda_{35} + \lambda_{36})$$

$$+ \lambda_1 \gamma_2^* \frac{\gamma_{11}^*}{\gamma_{12}^*} \frac{\beta_5^*}{|w_3^*|}(\lambda_{38} + \lambda_{39} + \lambda_{40}) + \lambda_2 \gamma_{11}^* \frac{\beta_5^*}{|w_3^*|}(-\lambda_{42} - \lambda_{43} + \lambda_{44}) \qquad 1$$

$$\lambda_{109} = \lambda_{105}\gamma_7^* \frac{1}{\gamma_{13}^*\gamma_{14}^*\lambda_{80}} \qquad \lambda_{110} = \lambda_{106}\gamma_8^* \frac{1}{\gamma_{13}^*\gamma_{14}^*\lambda_{80}}$$

$$\lambda_{111} = \lambda_{107}\gamma_7^* \frac{1}{\gamma_{13}^*\gamma_{14}^*\lambda_{80}} \qquad \lambda_{112} = \lambda_{108}\gamma_8^* \frac{1}{\gamma_{13}^*\gamma_{14}^*\lambda_{80}}$$

$$\rho_5 = \frac{\gamma_3\lambda_{81} + \gamma_4\lambda_{82}}{\pi\gamma_{13}\lambda_{80}} \qquad \rho_6 = \frac{\gamma_3\lambda_{83} + \gamma_4\lambda_{84}}{\pi\gamma_{13}\lambda_{80}} \qquad \rho_7 = \frac{\gamma_3\lambda_{89} + \gamma_4\lambda_{90}}{\pi\gamma_{13}^*\lambda_{80}}$$

$$\rho_8 = \frac{\gamma_3\lambda_{91} + \gamma_4\lambda_{92}}{\pi\gamma_{13}^*\lambda_{80}} \qquad \rho_9 = \frac{\gamma_9\lambda_{81} + \gamma_{10}\lambda_{82}}{\pi\gamma_{13}\lambda_{80}} \qquad \rho_{10} = \frac{\gamma_9\lambda_{83} + \gamma_{10}\lambda_{84}}{\pi\gamma_{13}\lambda_{80}}$$

$$\rho_{11} = \frac{\gamma_9\lambda_{89} + \gamma_{10}\lambda_{90}}{\pi\gamma_{13}^*\lambda_{80}} \qquad \rho_{12} = \frac{\gamma_9\lambda_{91} + \gamma_{10}\lambda_{92}}{\pi\gamma_{13}^*\lambda_{80}} \qquad \rho_{13} = \frac{\gamma_7(\lambda_{73} + \lambda_{74} + \lambda_{75})}{\pi\gamma_{14}\lambda_{80}}$$

$$\rho_{14} = \frac{\gamma_8(\lambda_{61} + \lambda_{62} + \lambda_{63})}{\pi\gamma_{14}\lambda_{80}} \qquad \rho_{15} = \frac{\gamma_7(\lambda_{70} + \lambda_{71} + \lambda_{72})}{\pi\gamma_{14}\lambda_{80}} \qquad \rho_{16} = \frac{\gamma_8(\lambda_{58} + \lambda_{59} + \lambda_{60})}{\pi\gamma_{14}\lambda_{80}}$$

$$\rho_{17} = \frac{\gamma_7^*(\lambda_{48} + \lambda_{50} + \lambda_{51})}{\pi\gamma_{14}^*\lambda_{80}} \qquad \rho_{18} = \frac{\gamma_8^*(\lambda_{34} + \lambda_{35} + \lambda_{36})}{\pi\gamma_{14}^*\lambda_{80}} \qquad \rho_{19} = \frac{\gamma_7^*(\lambda_{45} + \lambda_{46} + \lambda_{47})}{\pi\gamma_{14}^*\lambda_{80}}$$

$$\rho_{20} = \frac{\gamma_8^*(\lambda_{31} + \lambda_{32} + \lambda_{33})}{\pi\gamma_{14}^*\lambda_{80}}$$

Appendix C

$f_1(\alpha) = \tanh(w^*_1 \alpha H_2)\tanh(w^*_3 \alpha H_2)$ $f_2(\alpha) = \tanh(w^*_3 \alpha H_2)\tanh(w_1 \alpha H_1)$

$f_3(\alpha) = \tanh(w^*_3 \alpha H_2)\tanh(w_3 \alpha H_1)$ $f_4(\alpha) = \tanh(w^*_1 \alpha H_2)\tanh(w_3 \alpha H_1)$

$f_5(\alpha) = \tanh(w^*_1 \alpha H_2)\tanh(w_1 \alpha H_1)$ $f_6(\alpha) = \tanh(w_1 \alpha H_1)\tanh(w_3 \alpha H_1)$

$f(\alpha) = \lambda_{24} f_1(\alpha) + \lambda_{25} f_2(\alpha) + \lambda_{26} f_3(\alpha) + \lambda_{27} f_4(\alpha) - \lambda_{28} f_5(\alpha) + \lambda_{29} f_6(\alpha)$

$g_1(\alpha) = \lambda_{70}\tanh(w^*_3 \alpha H_2) + \lambda_{71}\tanh(w^*_1 \alpha H_2) + \lambda_{72}\tanh(w_3 \alpha H_1)$

$h_1(\alpha) = \lambda_{73} f_1(\alpha) + \lambda_{74} f_3(\alpha) + \lambda_{75} f_4(\alpha)$

$m_1(\alpha) = \lambda_{76} f_1(\alpha) + \lambda_{77} f_3(\alpha) + \lambda_{78} f_4(\alpha)$

$n_1(\alpha) = \lambda_{43}\tanh(w^*_3 \alpha H_2) - \lambda_{57}\tanh(w^*_1 \alpha H_2) + \lambda_{79}\tanh(w_3 \alpha H_1)$

$g_2(\alpha) = \lambda_{58}\tanh(w^*_3 \alpha H_2) + \lambda_{59}\tanh(w^*_1 \alpha H_2) + \lambda_{60}\tanh(w_1 \alpha H_1)$

$h_2(\alpha) = \lambda_{61} f_1(\alpha) + \lambda_{62} f_2(\alpha) + \lambda_{63} f_5(\alpha)$

$m_2(\alpha) = \lambda_{64} f_1(\alpha) + \lambda_{65} f_2(\alpha) + \lambda_{66} f_5(\alpha)$

$n_2(\alpha) = \lambda_{67}\tanh(w^*_3 \alpha H_2) + \lambda_{68}\tanh(w^*_1 \alpha H_2) + \lambda_{69}\tanh(w_1 \alpha H_1)$

$g_3(\alpha) = \lambda_{45}\tanh(w^*_3 \alpha H_2) + \lambda_{46}\tanh(w_3 \alpha H_1) + \lambda_{47}\tanh(w_1 \alpha H_1)$

$h_3(\alpha) = \lambda_{48} f_3(\alpha) + \lambda_{50} f_2(\alpha) + \lambda_{51} f_6(\alpha)$

$m_3(\alpha) = \lambda_{52} f_3(\alpha) + \lambda_{54} f_2(\alpha) + \lambda_{55} f_6(\alpha)$

$n_3(\alpha) = \lambda_{42}\tanh(w^*_3 \alpha H_2) + \lambda_{56}\tanh(w_3 \alpha H_1) + \lambda_{57}\tanh(w_1 \alpha H_1)$

$g_4(\alpha) = \lambda_{31}\tanh(w^*_1 \alpha H_2) + \lambda_{32}\tanh(w_1 \alpha H_1) + \lambda_{33}\tanh(w_3 \alpha H_1)$

$h_4(\alpha) = \lambda_{34} f_4(\alpha) + \lambda_{35} f_5(\alpha) + \lambda_{36} f_6(\alpha)$

$m_4(\alpha) = \lambda_{38} f_4(\alpha) + \lambda_{39} f_5(\alpha) + \lambda_{40} f_6(\alpha)$

$n_4(\alpha) = -\lambda_{42}\tanh(w^*_1 \alpha H_2) - \lambda_{43}\tanh(w_1 \alpha H_1) + \lambda_{44}\tanh(w_3 \alpha H_1)$

$$k_1(x_1,\alpha) = \frac{\gamma_7\cosh(w_1\alpha x_1)}{2\cosh(w_1\alpha H_1)f(\alpha)\gamma_{13}}[\,-g_1(\alpha) + \mathrm{sign}(w_1)\beta_9 h_1(\alpha)$$

$$+ \frac{\gamma_1\beta_5}{|w_1|}m_1(\alpha) - \frac{\gamma_{11}\beta_5}{|w_1|}n_1(\alpha)\,] \quad + \frac{\gamma_8\cosh(w_3\alpha x_1)}{2\cosh(w_3\alpha H_1)f(\alpha)\gamma_{13}}[\,-g_2(\alpha)$$

$$+ \mathrm{sign}(w_1)\beta_9 h_2(\alpha) + \frac{\gamma_1\beta_5}{|w_1|}m_2(\alpha) - \frac{\gamma_{11}\beta_5}{|w_1|}n_2(\alpha)\,]$$

$$k_2(x_1,\alpha) = \frac{\gamma_7\cosh(w_1\alpha x_1)}{2\cosh(w_1\alpha H_1)f(\alpha)\gamma_{13}}[\,\frac{\gamma_{11}}{\gamma_{12}}g_1(\alpha) - \frac{\gamma_{11}}{\gamma_{12}}\mathrm{sign}(w_3)\beta_{10}h_1(\alpha)$$

$$- \frac{\gamma_{11}\gamma_2\beta_5}{\gamma_{12}|w_3|}m_1(\alpha) + \frac{\gamma_{11}\beta_5}{|w_3|}n_1(\alpha)\,] + \frac{\gamma_8\cosh(w_3\alpha x_1)}{2\cosh(w_3\alpha H_1)f(\alpha)\gamma_{13}}[\,\frac{\gamma_{11}}{\gamma_{12}}g_2(\alpha)$$

$$- \frac{\gamma_{11}}{\gamma_{12}}\mathrm{sign}(w_3)\beta_{10}h_2(\alpha) - \frac{\gamma_{11}\gamma_2\beta_5}{\gamma_{12}|w_3|}m_2(\alpha) + \frac{\gamma_{11}\beta_5}{|w_3|}n_2(\alpha)\,]$$

$$k_3(x_1,\alpha) = \frac{\gamma_7\cosh(w_1\alpha x_1)}{2\cosh(w_1\alpha H_1)f(\alpha)\gamma_{13}^*}[\,-g_1(\alpha) - \mathrm{sign}(w_1^*)\beta_9^* h_1(\alpha)$$

$$- \frac{\gamma_1^*\lambda_1\beta_5^*}{|w_1^*|}m_1(\alpha) - \frac{\gamma_{11}^*\lambda_2\beta_5^*}{|w_1^*|}n_1(\alpha)\,] + \frac{\gamma_8\cosh(w_3\alpha x_1)}{2\cosh(w_3\alpha H_1)f(\alpha)\gamma_{13}^*}[\,-g_2(\alpha)$$

$$- \mathrm{sign}(w_1^*)\beta_9^* h_2(\alpha) - \frac{\gamma_1^*\lambda_1\beta_5^*}{|w_1^*|}m_2(\alpha) - \frac{\gamma_{11}^*\lambda_2\beta_5^*}{|w_1^*|}n_2(\alpha)\,]$$

$$k_4(x_1,\alpha) = \frac{\gamma_7\cosh(w_1\alpha x_1)}{2\cosh(w_1\alpha H_1)f(\alpha)\gamma_{13}^*}[\,\frac{\gamma_{11}^*}{\gamma_{12}^*}g_1(\alpha) + \frac{\gamma_{11}^*}{\gamma_{12}^*}\mathrm{sign}(w_3^*)\beta_{10}^* h_1(\alpha)$$

$$+ \frac{\gamma_{11}^*\gamma_2^*\lambda_1\beta_5^*}{\gamma_{12}^*\,|w_3^*|}m_1(\alpha) + \frac{\gamma_{11}^*\lambda_2\beta_5^*}{|w_1^*|}n_1(\alpha)\,] + \frac{\gamma_8\cosh(w_3\alpha x_1)}{2\cosh(w_3\alpha H_1)f(\alpha)\gamma_{13}^*}[\,\frac{\gamma_{11}^*}{\gamma_{12}^*}g_2(\alpha)$$

$$+ \frac{\gamma_{11}^*}{\gamma_{12}^*}\mathrm{sign}(w_3^*)\beta_{10}^* h_2(\alpha) + \frac{\gamma_{11}^*\gamma_2^*\lambda_1\beta_5^*}{\gamma_{12}^*\,|w_3^*|}m_2(\alpha) + \frac{\gamma_{11}^*\lambda_2\beta_5^*}{|w_3^*|}n_2(\alpha)\,]$$

$$J_1(x_1,\alpha) = \frac{\gamma_7\cosh(w_1\alpha x_1)h_1(\alpha)}{\cosh(w_1\alpha H_1)f(\alpha)} \qquad J_2(x_1,\alpha) = \frac{\gamma_8\cosh(w_3\alpha x_1)h_2(\alpha)}{\cosh(w_3\alpha H_1)f(\alpha)}$$

$$J_3(x_1,\alpha) = -\frac{\gamma_7\cosh(w_1\alpha x_1)g_1(\alpha)}{\cosh(w_1\alpha H_1)f(\alpha)} \qquad J_4(x_1,\alpha) = -\frac{\gamma_8\cosh(w_3\alpha x_1)g_2(\alpha)}{\cosh(w_3\alpha H_1)f(\alpha)}$$

$$k_5(x_2,\alpha) = \frac{\gamma_7^*\cosh(w_1^*\alpha x_2)}{2\cosh(w_1^*\alpha H_2)f(\alpha)\gamma_{13}}[\,-g_3(\alpha) + \mathrm{sign}(w_1)\beta_9 h_3(\alpha)$$

$$+\frac{\gamma_1\beta_5}{|w_1|}m_3(\alpha) - \frac{\gamma_{11}\beta_5}{|w_1|}n_3(\alpha)\,] + \frac{\gamma_8^*\cosh(w_3^*\alpha x_2)}{2\cosh(w_3^*\alpha H_2)f(\alpha)\gamma_{13}}[\,-g_4(\alpha)$$

$$+\mathrm{sign}(w_1)\beta_9 h_4(\alpha) + \frac{\gamma_1\beta_5}{|w_1|}m_4(\alpha) - \frac{\gamma_{11}\beta_5}{|w_1|}n_4(\alpha)\,]$$

$$k_6(x_2,\alpha) = \frac{\gamma_7^*\cosh(w_1^*\alpha x_2)}{2\cosh(w_1^*\alpha H_2)f(\alpha)\gamma_{13}}[\,\frac{\gamma_{11}}{\gamma_{12}}g_3(\alpha) - \frac{\gamma_{11}}{\gamma_{12}}\mathrm{sign}(w_3)\beta_{10}h_3(\alpha)$$

$$-\frac{\gamma_{11}\gamma_2\beta_5}{\gamma_{12}|w_3|}m_3(\alpha) + \frac{\gamma_{11}\beta_5}{|w_3|}n_3(\alpha)\,] + \frac{\gamma_8^*\cosh(w_3^*\alpha x_2)}{2\cosh(w_3^*\alpha H_2)f(\alpha)\gamma_{13}}[\,\frac{\gamma_{11}}{\gamma_{12}}g_4(\alpha)$$

$$-\frac{\gamma_{11}}{\gamma_{12}}\mathrm{sign}(w_3)\beta_{10}h_4(\alpha) - \frac{\gamma_{11}\gamma_1\beta_5}{\gamma_{12}|w_3|}m_4(\alpha) + \frac{\gamma_{11}\beta_5}{|w_3|}n_4(\alpha)\,]$$

$$k_7(x_2,\alpha) = \frac{\gamma_7^*\cosh(w_1^*\alpha x_2)}{2\cosh(w_1^*\alpha H_2)f(\alpha)\gamma_{13}^*}[\,-g_3(\alpha) - \mathrm{sign}(w_1^*)\beta_9^* h_3(\alpha)$$

$$-\frac{\gamma_1^*\lambda_1\beta_5^*}{|w_1^*|}m_3(\alpha) - \frac{\gamma_{11}^*\lambda_2\beta_5^*}{|w_1^*|}n_3(\alpha)\,] + \frac{\gamma_8^*\cosh(w_3^*\alpha x_2)}{2\cosh(w_3^*\alpha H_2)f(\alpha)\gamma_{13}^*}[\,-g_4(\alpha)$$

$$-\mathrm{sign}(w_1^*)\beta_9^* h_4(\alpha) - \frac{\gamma_1^*\lambda_1\beta_5^*}{|w_1^*|}m_4(\alpha) - \frac{\gamma_{11}^*\lambda_2\beta_5^*}{|w_1^*|}n_4(\alpha)\,]$$

$$k_8(x_2,\alpha) = \frac{\gamma_7^*\cosh(w_1^*\alpha x_2)}{2\cosh(w_1^*\alpha H_2)f(\alpha)\gamma_{13}^*}[\,\frac{\gamma_{11}^*}{\gamma_{12}^*}g_3(\alpha) + \frac{\gamma_{11}^*}{\gamma_{12}^*}\mathrm{sign}(w_3^*)\beta_{10}^* h_3(\alpha)$$

$$+\frac{\gamma_{11}^*\gamma_2^*\lambda_1\beta_5^*}{\gamma_{12}^*\ |w_3^*|}m_3(\alpha) + \frac{\gamma_{11}^*\lambda_2\beta_5^*}{|w_1^*|}n_3(\alpha)\,] + \frac{\gamma_8^*\cosh(w_3^*\alpha x_2)}{2\cosh(w_3^*\alpha H_2)f(\alpha)\gamma_{13}^*}[\,\frac{\gamma_{11}^*}{\gamma_{12}^*}g_4(\alpha)$$

$$+\frac{\gamma_{11}^*}{\gamma_{12}^*}\mathrm{sign}(w_3^*)\beta_{10}^* h_4(\alpha) + \frac{\gamma_{11}^*\gamma_2^*\lambda_1\beta_5^*}{\gamma_{12}^*\ |w_3^*|}m_4(\alpha) + \frac{\gamma_{11}^*\lambda_2\beta_5^*}{|w_3^*|}n_4(\alpha)\,]$$

$$J_5(x_2,\alpha) = \frac{\gamma_7^* \cosh(w_1^* \alpha x_2) h_3(\alpha)}{\cosh(w_1^* \alpha H_2) f(\alpha)} \qquad J_6(x_2,\alpha) = \frac{\gamma_8^* \cosh(w_3^* \alpha x_2) h_4(\alpha)}{\cosh(w_3^* \alpha H_2) f(\alpha)}$$

$$J_7(x_2,\alpha) = -\frac{\gamma_7^* \cosh(w_1^* \alpha x_2) g_3(\alpha)}{\cosh(w_1^* \alpha H_2) f(\alpha)} \qquad J_8(x_2,\alpha) = -\frac{\gamma_8^* \cosh(w_3^* \alpha x_2) g_4(\alpha)}{\cosh(w_3^* \alpha H_2) f(\alpha)}$$

$$k_9(y,x_1,\alpha) = \frac{\gamma_3 \cos\alpha y}{2f(\alpha)\gamma_{13}} \frac{\cosh(w_1 \alpha x_1)}{\cosh(w_1 \alpha H_1)} [\, -g_1(\alpha) + \text{sign}(w_1)\beta_9 h_1(\alpha) + \frac{\gamma_1 \beta_5}{|w_1|} m_1(\alpha)$$

$$- \frac{\gamma_{11}\beta_5}{|w_1|} n_1(\alpha)\,] + \frac{\gamma_4 \cos\alpha y}{2f(\alpha)\gamma_{13}} \frac{\cosh(w_3 \alpha x_1)}{\cosh(w_3 \alpha H_1)} [\, -g_2(\alpha) + \text{sign}(w_1)\beta_9 h_2(\alpha)$$

$$+ \frac{\gamma_1 \beta_5}{|w_1|} m_2(\alpha) - \frac{\gamma_{11}\beta_5}{|w_1|} n_2(\alpha)\,]$$

$$k_{10}(y,x_1,\alpha) = \frac{\gamma_3 \cos\alpha y}{2f(\alpha)\gamma_{13}} \frac{\cosh(w_1 \alpha x_1)}{\cosh(w_1 \alpha H_1)} [\, \frac{\gamma_{11}}{\gamma_{12}} g_1(\alpha) - \frac{\gamma_{11}}{\gamma_{12}} \text{sign}(w_3)\beta_{10} h_1(\alpha)$$

$$- \frac{\gamma_{11}\gamma_2\beta_5}{\gamma_{12}|w_3|} m_1(\alpha) + \frac{\gamma_{11}\beta_5}{|w_3|} n_1(\alpha)] + \frac{\gamma_4 \cos\alpha y}{2f(\alpha)\gamma_{13}} \frac{\cosh(w_3 \alpha x_1)}{\cosh(w_3 \alpha H_1)} [\, \frac{\gamma_{11}}{\gamma_{12}} g_2(\alpha)$$

$$- \frac{\gamma_{11}}{\gamma_{12}} \text{sign}(w_3)\beta_{10} h_2(\alpha) - \frac{\gamma_{11}}{\gamma_{12}} \frac{\gamma_2\beta_5}{|w_3|} m_2(\alpha) + \frac{\gamma_{11}\beta_5}{|w_3|} n_2(\alpha)\,]$$

$$k_{11}(y,x_1,\alpha) = \frac{\gamma_3 \cos\alpha y}{2f(\alpha)\gamma_{13}^*} \frac{\cosh(w_1 \alpha x_1)}{\cosh(w_1 \alpha H_1)} [\, - g_1(\alpha) - \text{sign}(w_1^*)\beta_9^* h_1(\alpha)$$

$$- \frac{\gamma_1^* \lambda_1 \beta_5^*}{|w_1^*|} m_1(\alpha) - \frac{\gamma_{11}^* \lambda_2 \beta_5^*}{|w_1^*|} n_1(\alpha)] + \frac{\gamma_4 \cos\alpha y}{2f(\alpha)\gamma_{13}^*} \frac{\cosh(w_3 \alpha x_1)}{\cosh(w_3 \alpha H_1)} [\, -g_2(\alpha)$$

$$- \text{sign}(w_1^*)\beta_9^* h_2(\alpha) - \frac{\gamma_1^* \lambda_1 \beta_5^*}{|w_1^*|} m_2(\alpha) - \frac{\gamma_{11}^* \lambda_2 \beta_5^*}{|w_1^*|} n_2(\alpha)\,]$$

$$k_{12}(y,x_1,\alpha) = \frac{\gamma_3 \cos\alpha y}{2f(\alpha)\gamma_{13}^*} \frac{\cosh(w_1 \alpha x_1)}{\cosh(w_1 \alpha H_1)} [\, \frac{\gamma_{11}^*}{\gamma_{12}^*} g_1(\alpha) + \frac{\gamma_{11}^*}{\gamma_{12}^*} \text{sign}(w_3^*)\beta_{10}^* h_1(\alpha)$$

$$+\frac{\gamma_{11}^{*}\gamma_{2}^{*}\lambda_{1}\beta_{5}^{*}}{\gamma_{12}^{*}\ |w_3^{*}|}m_1(\alpha)+\frac{\gamma_{11}^{*}\lambda_{2}\beta_{5}^{*}}{|w_1^{*}|}n_1(\alpha)\ ]+\frac{\gamma_4\cos\alpha y}{2f(\alpha)\gamma_{13}^{*}}\frac{\cosh(w_3\alpha x_1)}{\cosh(w_3\alpha H_1)}[\ \frac{\gamma_{11}^{*}}{\gamma_{12}^{*}}g_2(\alpha)$$

$$+\frac{\gamma_{11}^{*}}{\gamma_{12}^{*}}\text{sign}(w_3^{*})\beta_{10}^{*}h_2(\alpha)+\frac{\gamma_{11}^{*}\gamma_{2}^{*}\lambda_{1}\beta_{5}^{*}}{\gamma_{12}^{*}\ |w_3^{*}|}m_2(\alpha)+\frac{\gamma_{11}^{*}\lambda_{2}\beta_{5}^{*}}{|w_3^{*}|}n_2(\alpha)\ ]$$

$$J_9(y,\alpha)=\frac{\gamma_3 h_1(\alpha)}{f(\alpha)}\cos\alpha y \qquad J_{10}(y,\alpha)=\frac{\gamma_4 h_2(\alpha)}{f(\alpha)}\cos\alpha y$$

$$J_{11}(y,\alpha)=-\frac{\gamma_3 g_1(\alpha)}{f(\alpha)}\cos\alpha y \qquad J_{12}(y,\alpha)=-\frac{\gamma_4 g_2(\alpha)}{f(\alpha)}\cos\alpha y$$

$$k_{13}(y,x_1,\alpha)=\frac{\gamma_9\sin\alpha y}{2f(\alpha)\gamma_{13}}\frac{\sinh(w_1\alpha x_1)}{\cosh(w_1\alpha H_1)}\ [\ -g_1(\alpha)+\text{sign}(w_1)\beta_9 h_1(\alpha)+\frac{\gamma_1\beta_5}{|w_1|}m_1(\alpha)$$

$$-\frac{\gamma_{11}\beta_5}{|w_1|}n_1(\alpha)\ ]+\frac{\gamma_{10}\sin\alpha y}{2f(\alpha)\gamma_{13}}\frac{\sinh(w_3\alpha x_1)}{\cosh(w_3\alpha H_1)}\ [\ -g_2(\alpha)+\text{sign}(w_1)\beta_9 h_2(\alpha)$$

$$+\frac{\gamma_1\beta_5}{|w_1|}m_2(\alpha)-\frac{\gamma_{11}\beta_5}{|w_1|}n_2(\alpha)\ ]$$

$$k_{14}(y,x_1,\alpha)=\frac{\gamma_9\sin\alpha y}{2f(\alpha)\gamma_{13}}\frac{\sinh(w_1\alpha x_1)}{\cosh(w_1\alpha H_1)}\ [\ \frac{\gamma_{11}}{\gamma_{12}}g_1(\alpha)-\frac{\gamma_{11}}{\gamma_{12}}\text{sign}(w_3)\beta_{10}h_1(\alpha)$$

$$-\frac{\gamma_{11}\gamma_2\beta_5}{\gamma_{12}|w_3|}m_1(\alpha)+\frac{\gamma_{11}\beta_5}{|w_3|}n_1(\alpha)\ ]+\frac{\gamma_{10}\sin\alpha y}{2f(\alpha)\gamma_{13}}\frac{\sinh(w_3\alpha x_1)}{\cosh(w_3\alpha H_1)}\ [\ \frac{\gamma_{11}}{\gamma_{12}}g_2(\alpha)$$

$$-\frac{\gamma_{11}}{\gamma_{12}}\text{sign}(w_3)\beta_{10}h_2(\alpha)-\frac{\gamma_{11}\gamma_2\beta_5}{\gamma_{12}\ |w_3|}m_2(\alpha)+\frac{\gamma_{11}\beta_5}{|w_3|}n_2(\alpha)\ ]$$

$$k_{15}(y,x_1,\alpha)=\frac{\gamma_9\sin\alpha y}{2f(\alpha)\gamma_{13}^{*}}\frac{\sinh(w_1\alpha x_1)}{\cosh(w_1\alpha H_1)}\ [\ -g_1(\alpha)-\text{sign}(w_1^{*})\beta_9^{*}h_1(\alpha)$$

$$-\frac{\gamma_1^{*}\lambda_1\beta_5^{*}}{|w_1^{*}|}m_1(\alpha)-\frac{\gamma_{11}^{*}\lambda_2\beta_5^{*}}{|w_1^{*}|}n_1(\alpha)\ ]+\frac{\gamma_{10}\sin\alpha y}{2f(\alpha)\gamma_{13}^{*}}\frac{\sinh(w_3\alpha x_1)}{\cosh(w_3\alpha H_1)}\ [\ -g_2(\alpha)$$

$$- \text{sign}(w_1^*)\beta_9^* h_2(\alpha) - \frac{\gamma_1^*\lambda_1\beta_5^*}{|w_1^*|} m_2(\alpha) - \frac{\gamma_{11}^*\lambda_2\beta_5^*}{|w_1^*|} n_2(\alpha) \Big]$$

$$k_{16}(y,x_1,\alpha) = \frac{\gamma_9 \sin\alpha y}{2f(\alpha)\gamma_{13}^*} \frac{\sinh(w_1\alpha x_1)}{\cosh(w_1\alpha H_1)} \Big[\frac{\gamma_{11}^*}{\gamma_{12}^*} g_1(\alpha) + \frac{\gamma_{11}^*}{\gamma_{12}^*} \text{sign}(w_3^*)\beta_{10}^* h_1(\alpha)$$

$$+ \frac{\gamma_{11}^*\gamma_2^*\lambda_1\beta_5^*}{\gamma_{12}^* |w_3^*|} m_1(\alpha) + \frac{\gamma_{11}^*\lambda_2\beta_5^*}{|w_3^*|} n_1(\alpha)] + \frac{\gamma_{10}\sin\alpha y}{2f(\alpha)\gamma_{13}^*} \frac{\sinh(w_3\alpha x_1)}{\cosh(w_3\alpha H_1)} [\frac{\gamma_{11}^*}{\gamma_{12}^*} g_2(\alpha)$$

$$+ \frac{\gamma_{11}^*}{\gamma_{12}^*} \text{sign}(w_3^*)\beta_{10}^* h_2(\alpha) + \frac{\gamma_{11}^*\gamma_2^*\lambda_1\beta_5^*}{\gamma_{12}^* |w_3^*|} m_2(\alpha) - \frac{\gamma_{11}^*\lambda_2\beta_5^*}{|w_3^*|} n_2(\alpha) \Big]$$

$$J_{13}(y,\alpha) = \frac{\gamma_9 h_1(\alpha)}{f(\alpha)} \sin\alpha y \qquad J_{14}(y,\alpha) = \frac{\gamma_{10} h_2(\alpha)}{f(\alpha)} \sin\alpha y$$

$$J_{15}(y,\alpha) = -\frac{\gamma_9 g_1(\alpha)}{f(\alpha)} \sin\alpha y \qquad J_{16}(y,\alpha) = -\frac{\gamma_{10} g_2(\alpha)}{f(\alpha)} \sin\alpha y$$

Appendix D Asymptotic analysis of the kernels

Depending on the crack geometries, some or all of the kernels might be unbounded as $\alpha \to \infty$. The unbounded kernels will affect the values of singularities at crack tips. Therefore an asymptotic analysis is necessary to determine what kind of geometries will result in the unbounded kernels.

First the singular behaviors of the following integrals in eqns(1.29cd) are considered:

$$\int_{b_1}^{b_2} K_{33}'(y,t)\phi_3(t)dt \qquad \int_{b_1}^{b_2} K_{34}'(y,t)\phi_4(t)dt$$

$$\int_{b_1}^{b_2} K_{43}'(y,t)\phi_3(t)dt \qquad \int_{b_1}^{b_2} K_{44}'(y,t)\phi_4(t)dt \qquad \text{(D.1abcd)}$$

where

$$K_{33}'(y,t) = \lim_{x_1 \to H_1} \frac{1}{\pi}\int_0^\infty \left[\frac{ch(w_1\alpha x_1)}{ch(w_1\alpha H_1)}J_9(y,\alpha) + \frac{ch(w_3\alpha x_1)}{ch(w_3\alpha H_1)}J_{10}(y,\alpha)\right]\cos\alpha t d\alpha$$

$$= \lim_{x_1 \to H_1} \frac{1}{\pi}\int_0^\infty \left[\frac{ch(w_1\alpha x_1)\gamma_3 h_1(\alpha)}{ch(w_1\alpha H_1)\ f(\alpha)} + \frac{ch(w_3\alpha x_1)\ \gamma_4 h_2(\alpha)}{ch(w_3\alpha H_1)\ f(\alpha)}\right]\cos\alpha y\cos\alpha t d\alpha$$

$$= \lim_{x_1 \to H_1} \frac{1}{2\pi}\int_0^\infty \left[\frac{ch(w_1\alpha x_1)\gamma_3 h_1(\alpha)}{ch(w_1\alpha H_1)\ f(\alpha)} + \frac{ch(w_3\alpha x_1)\ \gamma_4 h_2(\alpha)}{ch(w_3\alpha H_1)\ f(\alpha)}\right][\cos\alpha(t-y)+\cos\alpha(t+y)]d\alpha \qquad \text{(D.2a)}$$

$$K_{34}'(y,t) = \lim_{x_1 \to H_1} \frac{1}{\pi}\int_0^\infty \left[\frac{ch(w_1\alpha x_1)}{ch(w_1\alpha H_1)}J_{11}(y,\alpha) + \frac{ch(w_3\alpha x_1)}{ch(w_3\alpha H_1)}J_{12}(y,\alpha)\right]\sin\alpha t d\alpha$$

$$= -\lim_{x_1 \to H_1} \frac{1}{\pi}\int_0^\infty \left[\frac{ch(w_1\alpha x_1)\gamma_3 g_1(\alpha)}{ch(w_1\alpha H_1)\ f(\alpha)} + \frac{ch(w_3\alpha x_1)\gamma_4 g_2(\alpha)}{ch(w_3\alpha H_1)\ f(\alpha)}\right]\cos\alpha y\sin\alpha t d\alpha$$

$$= -\lim_{x_1 \to H_1} \frac{1}{2\pi} \int_0^\infty \left[\frac{ch(w_1 \alpha x_1)\gamma_3 g_1(\alpha)}{ch(w_1 \alpha H_1)\ f(\alpha)} + \frac{ch(w_3 \alpha x_1)\gamma_4 g_2(\alpha)}{ch(w_3 \alpha H_1)\ f(\alpha)} \right] [\sin\alpha(t-y)+\sin\alpha(t+y)]d\alpha \qquad (D.2b)$$

$$K_{43}'(y,t) = \lim_{x_1 \to H_1} \frac{1}{\pi} \int_0^\infty \left[\frac{sh(w_1 \alpha x_1)}{ch(w_1 \alpha H_1)} J_{13}(y,\alpha) + \frac{sh(w_3 \alpha x_1)}{ch(w_3 \alpha H_1)} J_{14}(y,\alpha) \right] \cos\alpha t d\alpha$$

$$= \lim_{x_1 \to H_1} \frac{1}{\pi} \int_0^\infty \left[\frac{sh(w_1 \alpha x_1)\gamma_9 h_1(\alpha)}{ch(w_1 \alpha H_1)\ f(\alpha)} + \frac{sh(w_3 \alpha x_1)\gamma_{10} h_2(\alpha)}{ch(w_3 \alpha H_1)\ f(\alpha)} \right] \sin\alpha y \cos\alpha t d\alpha$$

$$= \lim_{x_1 \to H_1} \frac{1}{2\pi} \int_0^\infty \left[\frac{sh(w_1 \alpha x_1)\gamma_9 h_1(\alpha)}{ch(w_1 \alpha H_1)\ f(\alpha)} + \frac{sh(w_3 \alpha x_1)\gamma_{10} h_2(\alpha)}{ch(w_3 \alpha H_1)\ f(\alpha)} \right] [-\sin\alpha(t-y)+\sin\alpha(t+y)]d\alpha \qquad (D.2c)$$

$$K_{44}'(y,t) = \lim_{x_1 \to H_1} \frac{1}{\pi} \int_0^\infty \left[\frac{sh(w_1 \alpha x_1)}{ch(w_1 \alpha H_1)} J_{15}(y,\alpha) + \frac{sh(w_3 \alpha x_1)}{ch(w_3 \alpha H_1)} J_{16}(y,\alpha) \right] \sin\alpha t d\alpha$$

$$= -\lim_{x_1 \to H_1} \frac{1}{\pi} \int_0^\infty \left[\frac{sh(w_1 \alpha x_1)\gamma_9 g_1(\alpha)}{ch(w_1 \alpha H_1)\ f(\alpha)} + \frac{sh(w_3 \alpha x_1)\ \gamma_{10} g_2(\alpha)}{ch(w_3 \alpha H_1)\ f(\alpha)} \right] \sin\alpha y \sin\alpha t d\alpha$$

$$= -\lim_{x_1 \to H_1} \frac{1}{2\pi} \int_0^\infty \left[\frac{sh(w_1 \alpha x_1)\gamma_9 g_1(\alpha)}{ch(w_1 \alpha H_1)\ f(\alpha)} + \frac{sh(w_3 \alpha x_1)\ \gamma_{10} g_2(\alpha)}{ch(w_3 \alpha H_1)\ f(\alpha)} \right] [\cos\alpha(t-y)-\cos\alpha(t+y)]d\alpha \qquad (D.2d)$$

As α approaches infinity, we have:

$$\left[\frac{ch(w_1 \alpha x_1)\gamma_3 h_1(\alpha)}{ch(w_1 \alpha H_1)\ f(\alpha)} + \frac{ch(w_3 \alpha x_1)\ \gamma_4 h_2(\alpha)}{ch(w_3 \alpha H_1)\ f(\alpha)} \right] \cong \xi_1 e^{-\alpha w_1 (H_1 - x_1)} + \xi_2 e^{-\alpha w_3 (H_1 - x_1)} \qquad (D.3a)$$

$$\left[\frac{ch(w_1 \alpha x_1)\gamma_3 g_1(\alpha)}{ch(w_1 \alpha H_1)\ f(\alpha)} + \frac{ch(w_3 \alpha x_1)\gamma_4 g_2(\alpha)}{ch(w_3 \alpha H_1)\ f(\alpha)} \right] \cong \xi_3 e^{-\alpha w_1 (H_1 - x_1)} + \xi_4 e^{-\alpha w_3 (H_1 - x_1)} \qquad (D.3b)$$

$$\left[\frac{sh(w_1 \alpha x_1)\gamma_9 h_1(\alpha)}{ch(w_1 \alpha H_1)\ f(\alpha)} + \frac{sh(w_3 \alpha x_1)\gamma_{10} h_2(\alpha)}{ch(w_3 \alpha H_1)\ f(\alpha)} \right] \cong \xi_5 e^{-\alpha w_1 (H_1 - x_1)} + \xi_6 e^{-\alpha w_3 (H_1 - x_1)} \qquad (D.3c)$$

$$\left[\frac{sh(w_1 \alpha x_1)\gamma_9 g_1(\alpha)}{ch(w_1 \alpha H_1)\ f(\alpha)} + \frac{sh(w_3 \alpha x_1)\ \gamma_{10} g_2(\alpha)}{ch(w_3 \alpha H_1)\ f(\alpha)} \right] \cong \xi_7 e^{-\alpha w_1 (H_1 - x_1)} + \xi_8 e^{-\alpha w_3 (H_1 - x_1)} \qquad (D.3d)$$

where ξ_i(i=1-8) are material constants and are expressed as:

$$\xi_1 = \frac{\gamma_3(\lambda_{73}+\lambda_{74}+\lambda_{75})}{\lambda_{24}+\lambda_{25}+\lambda_{26}+\lambda_{27}-\lambda_{28}+\lambda_{29}} \quad \text{(D.4a)}$$

$$\xi_2 = \frac{\gamma_4(\lambda_{61}+\lambda_{62}+\lambda_{63})}{\lambda_{24}+\lambda_{25}+\lambda_{26}+\lambda_{27}-\lambda_{28}+\lambda_{29}} \quad \text{(D.4b)}$$

$$\xi_3 = \frac{\gamma_3(\lambda_{70}+\lambda_{71}+\lambda_{72})}{\lambda_{24}+\lambda_{25}+\lambda_{26}+\lambda_{27}-\lambda_{28}+\lambda_{29}} \quad \text{(D.4c)}$$

$$\xi_4 = \frac{\gamma_4(\lambda_{58}+\lambda_{59}+\lambda_{60})}{\lambda_{24}+\lambda_{25}+\lambda_{26}+\lambda_{27}-\lambda_{28}+\lambda_{29}} \quad \text{(D.4d)}$$

$$\xi_5 = \frac{\gamma_9(\lambda_{73}+\lambda_{74}+\lambda_{75})}{\lambda_{24}+\lambda_{25}+\lambda_{26}+\lambda_{27}-\lambda_{28}+\lambda_{29}} \quad \text{(D.4e)}$$

$$\xi_6 = \frac{\gamma_{10}(\lambda_{61}+\lambda_{62}+\lambda_{63})}{\lambda_{24}+\lambda_{25}+\lambda_{26}+\lambda_{27}-\lambda_{28}+\lambda_{29}} \quad \text{(D.4f)}$$

$$\xi_7 = \frac{\gamma_9(\lambda_{70}+\lambda_{71}+\lambda_{72})}{\lambda_{24}+\lambda_{25}+\lambda_{26}+\lambda_{27}-\lambda_{28}+\lambda_{29}} \quad \text{(D.4g)}$$

$$\xi_8 = \frac{\gamma_{10}(\lambda_{58}+\lambda_{59}+\lambda_{60})}{\lambda_{24}+\lambda_{25}+\lambda_{26}+\lambda_{27}-\lambda_{28}+\lambda_{29}} \quad \text{(D.4h)}$$

Utilizing the following formulas:

$$\lim_{x_1 \to H_1} \int_0^\infty e^{-\alpha w_1(H_1-x_1)}[\cos\alpha(t-y) + \cos\alpha(t+y)]d\alpha = \pi[\delta(t-y) + \delta(t+y)] \quad \text{(D.5a)}$$

and $$\lim_{x_1 \to H_1} \int_0^\infty e^{-\alpha w_1(H_1-x_1)}[\sin\alpha(t-y) + \sin\alpha(t+y)]d\alpha = \left(\frac{1}{t-y} + \frac{1}{t+y}\right) \quad \text{(D.5b)}$$

The asymptotic values of eqns(D.2abcd) become:

$$\lim_{x_1 \to H_1} \frac{1}{2\pi} \int_0^\infty [\xi_1 e^{-\alpha w_1(H_1-x_1)} + \xi_2 e^{-\alpha w_3(H_1-x_1)}][\cos\alpha(t-y) + \cos\alpha(t+y)]d\alpha$$

$$= \frac{\rho_1}{2}[\delta(t-y) + \delta(t+y)] \tag{D.6a}$$

$$-\lim_{x_1 \to H_1} \frac{1}{2\pi}\int_0^\infty [\xi_3 e^{-\alpha w_1(H_1-x_1)} + \xi_4 e^{-\alpha w_3(H_1-x_1)}][\sin\alpha(t-y) + \sin\alpha(t+y)]d\alpha$$

$$= -\frac{\rho_2}{2\pi}\left(\frac{1}{t-y} + \frac{1}{t+y}\right) \tag{D.6b}$$

$$\lim_{x_1 \to H_1} \frac{1}{2\pi}\int_0^\infty [\xi_5 e^{-\alpha w_1(H_1-x_1)} + \xi_6 e^{-\alpha w_3(H_1-x_1)}][-\sin\alpha(t-y) + \sin\alpha(t+y)]d\alpha$$

$$= \frac{\rho_3}{2\pi}\left(-\frac{1}{t-y} + \frac{1}{t+y}\right) \tag{D.6c}$$

$$-\lim_{x_1 \to H_1} \frac{1}{2\pi}\int_0^\infty [\xi_7 e^{-\alpha w_1(H_1-x_1)} + \xi_8 e^{-\alpha w_3(H_1-x_1)}][\cos\alpha(t-y) - \cos\alpha(t+y)]d\alpha$$

$$= -\frac{\rho_4}{2}[\delta(t-y) - \delta(t+y)] \tag{D.6d}$$

where $\rho_1 = \xi_1 + \xi_2$, $\rho_2 = \xi_3 + \xi_4$, $\rho_3 = \xi_5 + \xi_6$ and $\rho_4 = \xi_7 + \xi_8$

For $0<b_1 \le t \le b_2$, one has the following relations:

$$\frac{\rho_1}{2}\int_{b_1}^{b_2} \phi_3(t)\delta(t-y)dt = \frac{\rho_1}{2}\phi_3(y) \tag{D.7a}$$

$$\frac{\rho_1}{2}\int_{b_1}^{b_2} \phi_3(t)\delta(t+y)dt = 0 \tag{D.7b}$$

$$\frac{\rho_4}{2}\int_{b_1}^{b_2} \phi_4(t)\delta(t-y)dt = \frac{\rho_4}{2}\phi_4(y) \tag{D.7c}$$

$$\frac{\rho_4}{2}\int_{b_1}^{b_2}\phi_4(t)\delta(t+y)dt = 0 \qquad \text{(D.7d)}$$

By adding and subtracting the asymptotic value under integral signs in eqns(D.2abcd), and substituting them back into eqns(D.1abcd) respectively, we obtain:

$$\int_{b_1}^{b_2} K_{33}'(y,t)\phi_3(t)dt = \frac{\rho_1}{2}\phi_3(y) + \int_{b_1}^{b_2} K_{33}(y,t)\phi_3(t)dt \qquad \text{(D.8a)}$$

$$\int_{b_1}^{b_2} K_{34}'(y,t)\phi_4(t)dt = -\frac{\rho_2}{2\pi}\int_{b_1}^{b_2}\left(\frac{1}{t-y}+\frac{1}{t+y}\right)\phi_4(t)dt + \int_{b_1}^{b_2} K_{34}(y,t)\phi_4(t)dt \qquad \text{(D.8b)}$$

$$\int_{b_1}^{b_2} K_{43}'(y,t)\phi_3(t)dt = \frac{\rho_3}{2\pi}\int_{b_1}^{b_2}\left(-\frac{1}{t-y}+\frac{1}{t+y}\right)\phi_3(t)dt + \int_{b_1}^{b_2} K_{43}(y,t)\phi_3(t)dt \qquad \text{(D.8c)}$$

$$\int_{b_1}^{b_2} K_{44}'(y,t)\phi_4(t)dt = -\frac{\rho_4}{2}\phi_4(y) + \int_{b_1}^{b_2} K_{44}(y,t)\phi_4(t)dt \qquad \text{(D.8d)}$$

where

$$K_{33}(y,t) = \lim_{x_1\to H_1}\frac{1}{2\pi}\int_0^\infty \left\{\left[\frac{ch(w_1\alpha x_1)\gamma_3 h_1(\alpha)}{ch(w_1\alpha H_1)\ f(\alpha)} + \frac{ch(w_3\alpha x_1)\ \gamma_4 h_2(\alpha)}{ch(w_3\alpha H_1)\ f(\alpha)}\right]\right.$$

$$\left. - \left[\xi_1 e^{-\alpha w_1(H_1-x_1)} + \xi_2 e^{-\alpha w_3(H_1-x_1)}\right]\right\}\left[\cos\alpha(t-y) + \cos\alpha(t+y)\right]d\alpha \qquad \text{(D.9a)}$$

$$K_{34}(y,t) = -\lim_{x_1\to H_1}\frac{1}{2\pi}\int_0^\infty \left\{\left[\frac{ch(w_1\alpha x_1)\gamma_3 g_1(\alpha)}{ch(w_1\alpha H_1)\ f(\alpha)} + \frac{ch(w_3\alpha x_1)\gamma_4 g_2(\alpha)}{ch(w_3\alpha H_1)\ f(\alpha)}\right]\right.$$

$$\left. - \left[\xi_3 e^{-\alpha w_1(H_1-x_1)} + \xi_4 e^{-\alpha w_3(H_1-x_1)}\right]\right\}\left[\sin\alpha(t-y) + \sin\alpha(t+y)\right]d\alpha \qquad \text{(D.9b)}$$

$$K_{43}(y,t)= \lim_{x_1 \to H_1} \frac{1}{2\pi}\int_0^{\infty} \{[\frac{sh(w_1\alpha x_1)\gamma_9 h_1(\alpha)}{ch(w_1\alpha H_1)\ f(\alpha)} + \frac{sh(w_3\alpha x_1)\gamma_{10} h_2(\alpha)}{ch(w_3\alpha H_1)\ f(\alpha)}]$$

$$- [\xi_5 e^{-\alpha w_1(H_1-x_1)} + \xi_6 e^{-\alpha w_3(H_1-x_1)}]\}[-\sin\alpha(t-y) + \sin\alpha(t+y)]d\alpha \qquad (D.9c)$$

$$K_{44}(y,t)= -\lim_{x_1 \to H_1} \frac{1}{2\pi}\int_0^{\infty} \{[\frac{sh(w_1\alpha x_1)\gamma_9 g_1(\alpha)}{ch(w_1\alpha H_1)\ f(\alpha)} + \frac{sh(w_3\alpha x_1)\ \gamma_{10} g_2(\alpha)}{ch(w_3\alpha H_1)\ f(\alpha)}]$$

$$- [\xi_7 e^{-\alpha w_1(H_1-x_1)} + \xi_8 e^{-\alpha w_3(H_1-x_1)}]\}[\cos\alpha(t-y) - \cos\alpha(t+y)]d\alpha \qquad (D.9d)$$

Now consider rest of the singular kernels. If one decompose a kernel into two parts:

$$K_{ij} = K_{ijs} + K_{ijf} \qquad (i,j = 1,2,3,4) \qquad (D.10)$$

where K_{ijs} is unbounded part and K_{ijf} is bounded part of the kernel K_{ij}, then the asymptotic behaviors for the remaining kernels can be derived as follow.

Let $k_{i\infty}(x_1,\alpha)$ (i=1-8) be the asymptotic expression of $k_i(x_1,\alpha)$, then we have:

$$K_{11S}(x_1,t) = \frac{1}{\gamma_{14}\pi}\int_0^{\infty} [k_{1\infty}(x_1,\alpha)e^{-\alpha(H_1-t)\beta_5/|w_1|} + k_{2\infty}(x_1,\alpha)e^{-\alpha(H_1-t)\beta_5/|w_3|}]d\alpha$$

$$= \frac{\gamma_7\lambda_{81}}{\pi\gamma_{13}\gamma_{14}\lambda_{80}}\int_0^{\infty}\cosh(w_1\alpha x_1)e^{-\alpha[(H_1-t)\beta_5/|w_1|+H_1|w_1|]}d\alpha$$

$$+ \frac{\gamma_8\lambda_{82}}{\pi\gamma_{13}\gamma_{14}\lambda_{80}}\int_0^{\infty}\cosh(w_3\alpha x_1)e^{-\alpha[(H_1-t)\beta_5/|w_1|+H_1|w_3|]}d\alpha$$

$$+ \frac{\gamma_7\lambda_{83}}{\pi\gamma_{13}\gamma_{14}\lambda_{80}}\int_0^{\infty}\cosh(w_1\alpha x_1)e^{-\alpha[(H_1-t)\beta_5/|w_3|+H_1|w_1|]}d\alpha$$

$$+ \frac{\gamma_8\lambda_{84}}{\pi\gamma_{13}\gamma_{14}\lambda_{80}}\int_0^{\infty}\cosh(w_3\alpha x_1)e^{-\alpha[(H_1-t)\beta_5/|w_3|+H_1|w_3|]}d\alpha$$

$$= \frac{1}{\pi}\lambda_{85}\frac{(H_1-t)\beta_5/|w_1|+H_1|w_1|}{[(H_1-t)\beta_5/|w_1|+H_1|w_1|]^2-(w_1x_1)^2}$$

$$+ \frac{1}{\pi}\lambda_{86}\frac{(H_1-t)\beta_5/|w_1|+H_1|w_3|}{[(H_1-t)\beta_5/|w_1|+H_1|w_3|]^2-(w_3x_1)^2}$$

$$+ \frac{1}{\pi}\lambda_{87}\frac{(H_1-t)\beta_5/|w_3|+H_1|w_1|}{[(H_1-t)\beta_5/|w_3|+H_1|w_1|]^2-(w_1x_1)^2}$$

$$+ \frac{1}{\pi}\lambda_{88}\frac{(H_1-t)\beta_5/|w_3|+H_1|w_3|}{[(H_1-t)\beta_5/|w_3|+H_1|w_3|]^2-(w_3x_1)^2} \qquad \text{(D.11)}$$

Similarly one can derive:

$$K_{12S}(x_1,t) = \frac{1}{\pi}\lambda_{93}\frac{(H_2-t)\beta_5^*/|w_1^*|+H_1|w_1|}{[(H_2-t)\beta_5^*/|w_1^*|+H_1|w_1|]^2-(w_1x_1)^2}$$

$$+ \frac{1}{\pi}\lambda_{94}\frac{(H_2-t)\beta_5^*/|w_1^*|+H_1|w_3|}{[(H_2-t)\beta_5^*/|w_1^*|+H_1|w_3|]^2-(w_3x_1)^2}$$

$$+ \frac{1}{\pi}\lambda_{95}\frac{(H_2-t)\beta_5^*/|w_3^*|+H_1|w_1|}{[(H_2-t)\beta_5^*/|w_3^*|+H_1|w_1|]^2-(w_1x_1)^2}$$

$$+ \frac{1}{\pi}\lambda_{96}\frac{(H_2-t)\beta_5^*/|w_3^*|+H_1|w_3|}{[(H_2-t)\beta_5^*/|w_3^*|+H_1|w_3|]^2-(w_3x_1)^2} \qquad \text{(D.12)}$$

$$K_{21S}(x_2,t) = \frac{1}{\pi}\lambda_{101}\frac{(H_1-t)\beta_5/|w_1|+H_2|w_1^*|}{[(H_1-t)\beta_5/|w_1|+H_2|w_1^*|]^2-(w_1^*x_2)^2}$$

$$+ \frac{1}{\pi}\lambda_{102}\frac{(H_1-t)\beta_5/|w_1|+H_2|w_3^*|}{[(H_1-t)\beta_5/|w_1|+H_2|w_3^*|]^2-(w_3^*x_2)^2}$$

$$+ \frac{1}{\pi}\lambda_{103}\frac{(H_1-t)\beta_5/|w_3|+H_2|w_1^*|}{[(H_1-t)\beta_5/|w_3|+H_2|w_1^*|]^2-(w_1^*x_2)^2}$$

$$+ \frac{1}{\pi}\lambda_{104}\frac{(H_1-t)\beta_5/|w_3|+H_2|w_3^*|}{[(H_1-t)\beta_5/|w_3|+H_2|w_3^*|]^2-(w_3^*x_2)^2} \qquad \text{(D.13)}$$

$$K_{22S}(x_2,t) = \frac{1}{\pi}\lambda_{109}\frac{(H_2-t)\beta_5^*/|w_1^*|+H_2|w_1^*|}{[(H_2-t)\beta_5^*/|w_1^*|+H_2|w_1^*|]^2-(w_1^*x_2)^2}$$

$$+\frac{1}{\pi}\lambda_{110}\frac{(H_2-t)\beta_5^*/|w_1^*|+H_2|w_3^*|}{[(H_2-t)\beta_5^*/|w_1^*|+H_2|w_3^*|]^2-(w_3^*x_2)^2}$$

$$+\frac{1}{\pi}\lambda_{111}\frac{(H_2-t)\beta_5^*/|w_3^*|+H_2|w_1^*|}{[(H_2-t)\beta_5^*/|w_3^*|+H_2|w_1^*|]^2-(w_1^*x_2)^2}$$

$$+\frac{1}{\pi}\lambda_{112}\frac{(H_2-t)\beta_5^*/|w_3^*|+H_2|w_3^*|}{[(H_2-t)\beta_5^*/|w_3^*|+H_2|w_3^*|]^2-(w_3^*x_2)^2} \qquad \text{(D.14)}$$

The asymptotic expressions for $K_{31}(y,t)$, $K_{32}(y,t)$, $K_{41}(y,t)$ and $K_{42}(y,t)$ are derived as follow:

$$K_{31S}(y,t)=\frac{1}{2\gamma_{13}\pi}[-\gamma_1\frac{H_1\text{-}t}{\frac{(|w_1|y)^2}{\beta_5^2}+(H_1\text{-}t)^2}+\gamma_2(\frac{\gamma_{11}}{\gamma_{12}})\frac{H_1\text{-}t}{\frac{(|w_3|y)^2}{\beta_5^2}+(H_1\text{-}t)^2}]$$

$$+\lim_{x_1\to H_1}\frac{1}{\pi}\int_0^\infty[k_{9\infty}(y,x_1,\alpha)e^{-\alpha(H_1-t)\beta_5/|w_1|}+k_{10\infty}(y,x_1,\alpha)e^{-\alpha(H_1-t)\beta_5/|w_3|}]d\alpha$$

$$=\frac{1}{2\gamma_{13}\pi}[-\gamma_1\frac{H_1\text{-}t}{\frac{(|w_1|y)^2}{\beta_5^2}+(H_1\text{-}t)^2}+\gamma_2(\frac{\gamma_{11}}{\gamma_{12}})\frac{H_1\text{-}t}{\frac{(|w_3|y)^2}{\beta_5^2}+(H_1\text{-}t)^2}]$$

$$+\lim_{x_1\to H_1}\frac{\gamma_3\lambda_{81}+\gamma_4\lambda_{82}}{\pi\gamma_{13}\lambda_{80}}\int_0^\infty\cos(\alpha y)e^{-\alpha[(H_1-t)\beta_5/|w_1|+(H_1-x_1)|w_1|]}d\alpha$$

$$+\lim_{x_1\to H_1}\frac{\gamma_3\lambda_{83}+\gamma_4\lambda_{84}}{\pi\gamma_{13}\lambda_{80}}\int_0^\infty\cos(\alpha y)e^{-\alpha[(H_1-t)\beta_5/|w_3|+(H_1-x_1)|w_3|]}d\alpha$$

$$=\frac{1}{2\gamma_{13}\pi}[-\gamma_1\frac{H_1\text{-}t}{\frac{(|w_1|y)^2}{\beta_5^2}+(H_1\text{-}t)^2}+\gamma_2(\frac{\gamma_{11}}{\gamma_{12}})\frac{H_1\text{-}t}{\frac{(|w_3|y)^2}{\beta_5^2}+(H_1\text{-}t)^2}]$$

$$+\rho_5\frac{(H_1-t)\beta_5/|w_1|}{[(H_1-t)\beta_5/|w_1|]^2+y^2}+\rho_6\frac{(H_1-t)\beta_5/|w_3|}{[(H_1-t)\beta_5/|w_3|]^2+y^2} \qquad \text{(D.15)}$$

$$K_{32S}(y,t)=\rho_7\frac{(H_2-t)\beta_5^*/|w_1^*|}{[(H_2-t)\beta_5^*/|w_1^*|]^2+y^2}+\rho_8\frac{(H_2-t)\beta_5^*/|w_3^*|}{[(H_2-t)\beta_5^*/|w_3^*|]^2+y^2} \qquad \text{(D.16)}$$

$$K_{41S}(y,t) = \frac{\gamma_{11}}{2\gamma_{13}\pi}\left[\frac{\frac{|w_1|y}{\beta_5}}{\frac{(|w_1|y)^2}{\beta_5^2}+(H_1-t)^2} - \frac{\frac{|w_3|y}{\beta_5}}{\frac{(|w_3|y)^2}{\beta_5^2}+(H_1-t)^2}\right]$$

$$- \rho_9\frac{y}{[(H_1-t)\beta_5/|w_1|]^2+y^2} - \rho_{10}\frac{y}{[(H_1-t)\beta_5/|w_3|]^2+y^2} \qquad \text{(D.17)}$$

$$K_{42S}(y,t) = - \rho_{11}\frac{y}{[(H_2-t)\beta_5^*/|w_1^*|]^2+y^2} - \rho_{12}\frac{y}{[(H_2-t)\beta_5^*/|w_3^*|]^2+y^2} \qquad \text{(D.18)}$$

Let $J_{i\infty}(x_1,\alpha)$ (i= 1-8) be the asymptotic expressions of $J_i(x_1,\alpha)$, then we have:

$$K_{13S}(x_1,t) = \frac{1}{\gamma_{14}\pi}\int_0^\infty [J_{1\infty}(x_1,\alpha) + J_{2\infty}(x_1,\alpha)]\cos\alpha t d\alpha$$

$$= \frac{\gamma_7(\lambda_{73}+\lambda_{74}+\lambda_{75})}{\pi\gamma_{14}\lambda_{80}}\int_0^\infty \cos(\alpha t)e^{-\alpha w_1(H_1-x_1)}d\alpha$$

$$+ \frac{\gamma_8(\lambda_{61}+\lambda_{62}+\lambda_{63})}{\pi\gamma_{14}\lambda_{80}}\int_0^\infty \cos(\alpha t)e^{-\alpha w_3(H_1-x_1)}d\alpha$$

$$= \rho_{13}\frac{w_1(H_1-x_1)}{[w_1(H_1-x_1)]^2+t^2} + \rho_{14}\frac{w_3(H_1-x_1)}{[w_3(H_1-x_1)]^2+t^2} \qquad \text{(D.19)}$$

Using the same technique we can derive:

$$K_{14S}(x_1,t) = \rho_{15}\frac{t}{[w_1(H_1-x_1)]^2+t^2} + \rho_{16}\frac{t}{[w_3(H_1-x_1)]^2+t^2} \qquad \text{(D.20)}$$

$$K_{23S}(x_2,t) = \rho_{17}\frac{w_1^*(H_2-x_2)}{[w_1^*(H_2-x_2)]^2+t^2} + \rho_{18}\frac{w_3^*(H_2-x_2)}{[w_3^*(H_2-x_2)]^2+t^2} \qquad \text{(D.21)}$$

$$K_{24S}(x_2,t) = \rho_{19}\frac{t}{[w_1^*(H_2-x_2)]^2+t^2} + \rho_{20}\frac{t}{[w_3^*(H_2-x_2)]^2+t^2} \qquad \text{(D.22)}$$

The coefficients λ_i (i=85-112) and ρ_j (j=5-20) are given in Appendix B

Appendix E Derivations of stress intensity factors and strain energy release rates

i) Case of embedded cracks

The stress intensity factors at the transverse crack tips are defined as:

at $x_1 = a_1$: $$k(a_1) = \lim_{x_1 \to a_1} \sqrt{2(x_1 - a_1)}\,\sigma_{1y}(x_1,0) \tag{E.1a}$$

at $x_2 = a_2$: $$k(a_2) = \lim_{x_2 \to a_2} \sqrt{2(x_2 - a_2)}\,\sigma_{2y}(x_2,0) \tag{E.1b}$$

From eqns (3.29a), for $|x_1| > a_1$ we obtain:

$$\sigma_{1y}(x_1,0) = \frac{2\gamma_{14}E_y}{\pi(1-\nu_{xy}\nu_{yx})}\int_{-a_1}^{a_1}\frac{\phi_1(t)}{t-x_1}dt + \sigma^{o}_{1y}(x_1,0) \tag{E.2}$$

where $\sigma^{o}_{1y}(x_1,0)$ is bounded function. and

$$\phi(t) = \frac{F_1(t)}{\sqrt{a_1^2 - t^2}} = \frac{F_1(t)e^{i\pi/2}}{(t-a_1)^{1/2}(t+a_1)^{1/2}}$$

From [28], if we introduce a sectionally holomorphic function as

$$\varphi(z) = \frac{1}{\pi}\int_{-a_1}^{a_1}\frac{\phi_1(t)}{t-z}dt$$

then we have:

$$\varphi(z) = \frac{F_1(-a_1)e^{i\pi/2}}{(2a_1)^{1/2}(z+a_1)^{1/2}} - \frac{F_1(a_1)}{(2a_1)^{1/2}(z-a_1)^{1/2}} + \varphi_o(z) \tag{E.3}$$

Substituting (E.3) into (E.2) and from the definition of (E.1a), we have:

$$k(a_1) = -\frac{2\gamma_{14}E_y}{\pi(1-\nu_{xy}\nu_{yx})}\frac{1}{\sqrt{a_1}}F_1(a_1) = -\frac{2\gamma_{14}E_y}{\pi(1-\nu_{xy}\nu_{yx})}\sqrt{a_1}\,F_1^{o}(1) \tag{E.4}$$

Similarly

$$k(a_2) = -\frac{2\gamma^{*}_{14}E^{*}_y}{\pi(1-\nu^{*}_{xy}\nu^{*}_{yx})}\frac{1}{\sqrt{a_2}}F_2(a_2) = -\frac{2\gamma^{*}_{14}E^{*}_y}{\pi(1-\nu^{*}_{xy}\nu^{*}_{yx})}\sqrt{a_2}\,F_2^{o}(1) \tag{E.5}$$

Now consider the stress intensity factors on the interface. For $y < b_1$ and $y > b_2$, the stresses along the interface can be expressed as:

$$\sqrt{\frac{\rho_4}{\rho_1\rho_2\rho_3}}\frac{1-\nu_{xy}\nu_{yx}}{2E_x}\sigma_{xx}(H_1,y)+i\frac{1}{\rho_3}\frac{1}{2G_{xy}}\sigma_{xy}(H_1,y)=\frac{1}{\pi i}\int_{b_1}^{b_2}\frac{\psi_3(s)}{s-y}ds$$

where $$\psi_3(s)=\frac{F_3(s)e^{i\pi\beta_3}}{(b_1-s)^{\alpha_3}(s-b_2)^{\beta_3}}.$$

Again using the method given in [28], we have:

$$\frac{1}{\pi i}\int_{b_1}^{b_2}\frac{\psi_3(s)}{s-y}ds=i\sqrt{1-\zeta^2}\,[\frac{1}{(b_1-y)^{\alpha_3}(y-b_2)^{\beta_3}}F_3(y)+F_n(y)\,]$$

where $F_n(y)$ is the principal part of $\psi_3(s)$ at infinity and is bounded. Therefore, the stresses near points b_1 and b_2 can be expressed as:

$$\frac{1-\nu_{xy}\nu_{yx}}{2E_x}\sqrt{\frac{\rho_4}{\rho_1\rho_2\rho_3}}\sigma_{xx}(H_1,y)+i\frac{1}{\rho_3}\frac{1}{2G_{xy}}\sigma_{xy}(H_1,y)=i\sqrt{1-\zeta^2}\frac{1}{(b_1-y)^{\alpha_3}(y-b_2)^{\beta_3}}F_3(y)$$

Multiply both side of above equation by -i, then we have:

$$\frac{1}{\rho_3}\frac{1}{2G_{xy}}\sigma_{xy}(H_1,y)-i\frac{1-\nu_{xy}\nu_{yx}}{2E_x}\sqrt{\frac{\rho_4}{\rho_1\rho_2\rho_3}}\sigma_{xx}(H_1,y)=\sqrt{1-\zeta^2}\frac{1}{(b_1-y)^{\alpha_3}(y-b_2)^{\beta_3}}F_3(y) \qquad (E.6)$$

Now if we define the following stress intensity factors at the interface:

$$\frac{1}{\rho_3}\frac{1}{2G_{xy}}k_2(b_1)-i\sqrt{\frac{\rho_4}{\rho_1\rho_2\rho_3}}\frac{1-\nu_{xy}\nu_{yx}}{2E_x}k_1(b_1)$$

$$=\lim_{y\to b_1}(b_1-y)^{\alpha_3}(y-b_2)^{\beta_3}[\frac{1}{\rho_3}\frac{1}{2G_{xy}}\sigma_{1xy}(H_1,y)-i\sqrt{\frac{\rho_4}{\rho_1\rho_2\rho_3}}\frac{1-\nu_{xy}\nu_{yx}}{2E_x}\sigma_{1xx}(H_1,y)\,] \qquad (E.7a)$$

and

$$\frac{1}{\rho_3}\frac{1}{2G_{xy}}k_2(b_2) - i\sqrt{\frac{\rho_4}{\rho_1\rho_2\rho_3}}\frac{1-\nu_{xy}\nu_{yx}}{2E_x}k_1(b_2)$$

$$= \lim_{y\to b_2}(b_1-y)^{\alpha_3}(y-b_2)^{\beta_3}\left[\frac{1}{\rho_3}\frac{1}{2G_{xy}}\sigma_{1xy}(H_1,y) - i\sqrt{\frac{\rho_4}{\rho_1\rho_2\rho_3}}\frac{1-\nu_{xy}\nu_{yx}}{2E_x}\sigma_{1xx}(H_1,y)\right] \qquad \text{(E.7b)}$$

With the help of eqn (E.6), we obtain:

$$\frac{1}{\rho_3}\frac{1}{2G_{xy}}k_2(b_1) - i\sqrt{\frac{\rho_4}{\rho_1\rho_2\rho_3}}\frac{1-\nu_{xy}\nu_{yx}}{2E_x}k_1(b_1) = L\sqrt{1-\zeta^2}\,F_3^o(-1) \qquad \text{(E.8a)}$$

$$\frac{1}{\rho_3}\frac{1}{2G_{xy}}k_2(b_2) - i\sqrt{\frac{\rho_4}{\rho_1\rho_2\rho_3}}\frac{1-\nu_{xy}\nu_{yx}}{2E_x}k_1(b_2) = -L\sqrt{1-\zeta^2}\,F_3^o(1) \qquad \text{(E.8b)}$$

where $L = \dfrac{b_2-b_1}{2}$

The derivation for the expression of the strain energy release rate at the interface crack tip is as follow: From (E.8) we have:

$$\psi_3^o(r) = -\frac{(r+1)^{-\alpha_3}(r-1)^{-\beta_3}e^{i\pi\beta_3}}{\sqrt{1-\zeta^2}}\left[\frac{1}{\rho_3}\frac{1}{2G_{xy}}k_2 - i\sqrt{\frac{\rho_4}{\rho_1\rho_2\rho_3}}\frac{1-\nu_{xy}\nu_{yx}}{2E_x}k_1\right]$$

$$= -\frac{1}{\sqrt{1-\zeta^2}}\left[\frac{1}{\rho_3}\frac{1}{2G_{xy}}k_2 - i\sqrt{\frac{\rho_4}{\rho_1\rho_2\rho_3}}\frac{1-\nu_{xy}\nu_{yx}}{2E_x}k_1\right]\left(\frac{1-r}{1+r}\right)^{i\omega}\frac{1}{\sqrt{1-r^2}} \qquad |r|<1 \qquad \text{(E.9)}$$

and from eqn (E.7):

$$\frac{1}{\rho_3}\frac{1}{2G_{xy}}\sigma_{xy} - i\frac{1-\nu_{xy}\nu_{yx}}{2E_x}\sqrt{\frac{\rho_4}{\rho_1\rho_2\rho_3}}\sigma_{xx}$$

$$= \lim_{r\to 1}(r+1)^{-\alpha_3}(r-1)^{-\beta_3}\left[\frac{1}{\rho_3}\frac{1}{2G_{xy}}k_2 - i\sqrt{\frac{\rho_4}{\rho_1\rho_2\rho_3}}\frac{1-\nu_{xy}\nu_{yx}}{2E_x}k_1\right]$$

$$= \left[\frac{1}{\rho_3}\frac{1}{2G_{xy}}k_2 - i\sqrt{\frac{\rho_4}{\rho_1\rho_2\rho_3}}\frac{1-\nu_{xy}\nu_{yx}}{2E_x}k_1\right]\left(\frac{r-1}{r+1}\right)^{i\omega}\frac{1}{\sqrt{r^2-1}} \qquad |r|>1 \qquad \text{(E.10)}$$

Let $\eta = r-1$ and assume $\eta \ll 1$ then (E.10) can be approximated by

$$\frac{1}{\rho_3}\frac{1}{2G_{xy}}\sigma_{xy} - i\frac{1-\nu_{xy}\nu_{yx}}{2E_x}\sqrt{\frac{\rho_4}{\rho_1\rho_2\rho_3}}\sigma_{xx}$$

$$\cong [\frac{1}{\rho_3}\frac{1}{2G_{xy}}k_2 - i\sqrt{\frac{\rho_4}{\rho_1\rho_2\rho_3}}\frac{1-\nu_{xy}\nu_{yx}}{2E_x}k_1]$$

$$\times\frac{1}{\sqrt{2}\sqrt{\eta}}[\cos(\omega\log(\frac{\eta}{2})) + i\sin(\omega\log(\frac{\eta}{2}))] \qquad (E.11)$$

Similarly, let $\varsigma = 1-r$ and assume that $\varsigma \ll 1$, then (E.9) can be expressed as:

$$\psi_3^o(\varsigma) \cong -\frac{1}{\sqrt{1-\zeta^2}}[\frac{1}{\rho_3}\frac{1}{2G_{xy}}k_2 - i\sqrt{\frac{\rho_4}{\rho_1\rho_2\rho_3}}\frac{1-\nu_{xy}\nu_{yx}}{2E_x}k_1]$$

$$\times\frac{1}{\sqrt{2}\sqrt{\varsigma}}[\cos(\omega\log(\frac{\varsigma}{2})) + i\sin(\omega\log(\frac{\varsigma}{2}))] \qquad (E.12)$$

Since $\psi_3^o(r) = \frac{1}{2}\frac{\partial}{\partial r}[(v_1-v_2) - i\sqrt{\frac{\eta_1}{\eta_2}}(u_1-u_2)]$ therefore

$$\psi_3^o(\varsigma) = -\frac{1}{2}\frac{\partial}{\partial \varsigma}[(v_1-v_2) - i\sqrt{\frac{\eta_1}{\eta_2}}(u_1-u_2)]$$

$$\cong -\frac{1}{\sqrt{1-\zeta^2}}[\frac{1}{\rho_3}\frac{1}{2G_{xy}}k_2 - i\sqrt{\frac{\rho_4}{\rho_1\rho_2\rho_3}}\frac{1-\nu_{xy}\nu_{yx}}{2E_x}k_1]$$

$$\times\frac{1}{\sqrt{2}\sqrt{\varsigma}}[\cos(\omega\log(\frac{\varsigma}{2})) + i\sin(\omega\log(\frac{\varsigma}{2}))] \qquad (E.12^*)$$

The oscillatory behaviors in eqns (E.11) and (E.12*) can be removed using the techniques given in [40,42]. Considering the fact that the stress intensity factors and the displacement derivatives just away from the interface crack tips should have definite values. Therefore we can chose η and ς in such a way, so that

$$\omega\log(\frac{\eta}{2}) \cong 0 \text{ and } \omega\log(\frac{\varsigma}{2}) \cong 0.$$

In fact, for most material combinations, that above two quantities are indeed very small [43].Then from eqns (E.11) and (E.12*), we have:

$$\sigma_{xy} \cong \frac{1}{\sqrt{2}\sqrt{\eta}} k_2 , \qquad \sigma_{xx} \cong \frac{1}{\sqrt{2}\sqrt{\eta}} k_1$$

$$\Delta v = (v_1 - v_2) \cong 2\sqrt{2} \frac{1}{\sqrt{1-\zeta^2}} \frac{1}{\rho_3} \frac{1}{2G_{xy}} \sqrt{\varsigma} k_2$$

and $$\Delta u = (u_1 - u_2) \cong 2\sqrt{2} \frac{1}{\sqrt{1-\zeta^2}} \frac{1}{\rho_2} \frac{1-\nu_{xy}\nu_{yx}}{2E_x} \sqrt{\varsigma} k_1$$

Assume the crack front was closed along the interface by an amount of Δy, then using the method given in [37], we obtain the increment of the strain energy:

$$\Delta E = 2\int_r^{r+\Delta y} \frac{1}{2} [\sigma_{xx} \Delta u(r-\Delta y) + \sigma_{xy} \Delta v(r-\Delta y)] dr$$

$$= 2\frac{1}{\sqrt{1-\zeta^2}} \left[\frac{1}{\rho_2} \frac{1-\nu_{xy}\nu_{yx}}{2E_x} k_1^2 + \frac{1}{\rho_3} \frac{1}{2G_{xy}} k_2^2 \right] \int_r^{r+\Delta y} \frac{\sqrt{1+\Delta y - r}}{\sqrt{r-1}} dr$$

$$= 2\frac{1}{\sqrt{1-\zeta^2}} \left[\frac{1}{\rho_2} \frac{1-\nu_{xy}\nu_{yx}}{2E_x} k_1^2 + \frac{1}{\rho_3} \frac{1}{2G_{xy}} k_2^2 \right] \frac{\pi}{2} \Delta y$$

Therefore, the strain energy release rate will be:

$$\frac{\Delta E}{\Delta y} = \frac{\pi}{\sqrt{1-\zeta^2}} \left[\frac{1}{\rho_2} \frac{1-\nu_{xy}\nu_{yx}}{2E_x} k_1^2 + \frac{1}{\rho_3} \frac{1}{2G_{xy}} k_2^2 \right] \qquad \text{(E.13)}$$

For Isotropic materials we have:

$$\frac{1}{\rho_2} \frac{1-\nu_{xy}\nu_{yx}}{2E_x} = \frac{1}{\rho_3} \frac{1}{2G_{xy}}$$

then $$\frac{\Delta E}{\Delta y} = \frac{\pi}{\sqrt{1-\zeta^2}} \frac{1}{\rho_3} \frac{1}{2G_{xy}} [k_1^2 + k_2^2] \qquad \text{(E.13*)}$$

ii) Case of transverse crack touching the interface

Define the stress intensity factor:

$$k(a_1) = \lim_{x_2 \to -H_2} 2^{\gamma}(x_2+H_2)^{\gamma}\sigma_{2y}(x_2,0) \tag{E.14}$$

from eqn (3.29b), we have

$$\sigma_{2y}(x_1,0) = \frac{2\gamma_{14}E_y}{\pi(1-\nu_{xy}\nu_{yx})}\int_{-H_1}^{H_1} K_{21s}(x_2,t)\phi_1(t)dt + \sigma^{\circ}_{2y}(x_2,0) \tag{E.15}$$

where $\sigma^{\circ}_{2y}(x_2,0)$ is bounded function and

$$\phi_1(t) = \frac{F_1(t)}{(H_1^{\,2}-t^2)^{\gamma}} = \frac{F_1(t)e^{i\gamma}}{(t-H_1)^{\gamma}(t+H_1)^{\gamma}}$$

Again define: $\varphi(z) = \frac{1}{\pi}\int_{-H_1}^{H_1}\frac{\phi_1(t)}{t-z}dt$ then we have:

$$\varphi(z) = \frac{F_1(-H_1)e^{i\pi\gamma}}{(2H_1)^{\gamma}\sin\pi\gamma(z+H_1)^{\gamma}} - \frac{F_1(H_1)}{(2H_1)^{\gamma}\sin\pi\gamma(z-H_1)^{\gamma}} + \varphi_o(z) \tag{E.16}$$

Substituting (E.16) back into (E.15), and then from the definition of (E.14), we have:

$$k(a_1) = \frac{(H_1)^{2\gamma}\gamma^{*}_{14}E^{*}_{y}F^{\circ}_1(1)}{(1-\nu^{*}_{xy}\nu^{*}_{yx})\sin(\pi\gamma)}\left[\lambda_{101}\frac{|w_1|/\beta_5}{\left[|w_1^{*}||w_1|/\beta_5\right]^{\gamma}} + \lambda_{102}\frac{|w_1|/\beta_5}{\left[|w_3^{*}||w_1|/\beta_5\right]^{\gamma}}\right.$$

$$\left. + \lambda_{103}\frac{|w_3|/\beta_5}{\left[|w_3||w_1^{*}|/\beta_5\right]^{\gamma}} + \lambda_{101}\frac{|w_3|/\beta_5}{\left[|w_3||w_3^{*}|/\beta_5\right]^{\gamma}}\right] \tag{E.17}$$

The stress intensity factors and the strain energy release rate at the interface crack tip remain the same.

iii) H-shaped cracks

The derivation of stress intensity factors at the interface remains the same as given in eqns (E.8ab) with L = b_2, and the strain energy release rate at the interface crack tip is also given by eqns (E.13).

Appendix F Determination of singularities for different crack geometry

The stress singularity at the crack tip varies for different crack geometry. The index of singularity for the following crack geometries have been considered:

a) Embedded cracks ($|a_1|< H_1$, $|a_2|< H_2$ and $b_1> 0$)

For embedded cracks, the crack density functions are of the following forms:

$$\phi_1^\circ(t)=\frac{F_1^\circ(t)}{(1+t)^{\alpha_1}(1-t)^{\beta_1}},\quad \phi_2^\circ(t)=\frac{F_2^\circ(t)}{(1+t)^{\alpha_2}(1-t)^{\beta_2}}$$

$$\psi_3^\circ(t)=\frac{F_3^\circ(t)}{(1+t)^{\alpha_3}(1-t)^{\beta_3}},\quad \psi_4^\circ(t)=\frac{F_4^\circ(t)}{(1+t)^{\alpha_4}(1-t)^{\beta_4}} \qquad \text{(F.1abcd)}$$

where $F_i^\circ(t)$ (i=1,2,3,4) are bounded at crack tips. and because of symmetry $\alpha_1=\beta_1$ and $\alpha_2=\beta_2$.

Substituting eqns (F.abcd) into eqns (3.29abcd) and using the following formula:

$$\psi_n(z)=\frac{1}{\pi}\int_{z_1}^{z_2}\frac{\phi_n(t)}{t-z}dt=\frac{1}{\pi}\int_{z_1}^{z_2}\frac{F_n(t)}{(t-z_1)^{\alpha_n}(z_2-t)^{\beta_n}(t-z)}dt$$

$$=\frac{F_n(z_1)\cot(\pi\alpha_n)}{(z_2-z_1)^{\beta_n}(z-z_1)^{\alpha_n}}-\frac{F_n(z_2)\cot(\pi\beta_n)}{(z_2-z_1)^{\alpha_n}(z_2-z)^{\beta_n}}+G_n(z) \qquad \text{(F.2)}$$

where $G_n(z)$ is bounded at crack tips.

then we have:

$$\frac{F_1^\circ(-1)\cot(\pi\alpha_1)}{(2)^{\alpha_1}(r+1)^{\alpha_1}}-\frac{F_1^\circ(1)\cot(\pi\alpha_1)}{(2)^{\alpha_1}(1-r)^{\alpha_1}}=-\frac{(1-\nu_{xy}\nu_{yx})}{2\gamma_{14}E_y}p_1(r)+\text{bounded terms} \qquad \text{(F.3)}$$

$$\frac{F_2^\circ(-1)\cot(\pi\alpha_2)}{(2)^{\alpha_2}(r+1)^{\alpha_2}}-\frac{F_2^\circ(1)\cot(\pi\alpha_2)}{(2)^{\alpha_2}(1-r)^{\alpha_2}}=-\frac{\pi(1-\nu_{xy}^*\nu_{yx}^*)}{2\gamma_{14}^*E_y^*}p_2(r)+\text{bounded terms} \qquad \text{(F.4)}$$

$$\frac{F_3^\circ(r)}{(1+r)^{\alpha_3}(1-r)^{\beta_3}}+\frac{\zeta^{-1}}{i}\left[\frac{F_3^\circ(-1)\cot(\pi\alpha_3)}{(2)^{\beta_3}(1+r)^{\alpha_3}}-\frac{F_3^\circ(1)\cot(\pi\beta_3)}{(2)^{\alpha_3}(1-r)^{\beta_3}}\right]$$

$$=m_1p_3(r)+im_2p_4(r)+\text{bounded terms}\qquad b_1<y<b_2$$

(F.5)

$$\frac{F_4(r)}{(1+r)^{\alpha_4}(1-r)^{\beta_4}}-\frac{\zeta^{-1}}{i}\left[\frac{F_4^\circ(-1)\cot(\pi\alpha_4)}{(2)^{\beta_4}(1+r)^{\alpha_4}}-\frac{F_4^\circ(1)\cot(\pi\beta_4)}{(2)^{\alpha_4}(1-r)^{\beta_4}}\right]$$

$$= -\,im_1p_3(r) - m_2p_4(r) + \text{bounded terms} \qquad b_1 < y < b_2 \tag{F.6}$$

From eqns (F.3) and (F.4), it can be easily shown that:

$$\alpha_1 = \beta_1 = \frac{1}{2}, \qquad \alpha_2 = \beta_2 = \frac{1}{2} \tag{F.7}$$

These are the known results for cracks perpendicular to interface [22].

Similarly, from eqns (F.5) and (F.6) we can derive:

$$\cot(\pi\alpha_3) = -\,i\zeta = -\,i\sqrt{\frac{\rho_1\rho_4}{\rho_2\rho_3}}, \qquad \cot(\pi\beta_3) = i\zeta = i\sqrt{\frac{\rho_1\rho_4}{\rho_2\rho_3}}$$

$$\cot(\pi\alpha_4) = i\zeta = i\sqrt{\frac{\rho_1\rho_4}{\rho_2\rho_3}}, \qquad \cot(\pi\beta_4) = -\,i\zeta = -\,i\sqrt{\frac{\rho_1\rho_4}{\rho_2\rho_3}}$$

Using the formula:

$$\cot^{-1}(z) = \frac{1}{2i}\log\frac{z+i}{z-i} \tag{F.8}$$

We then have:

$$\alpha_3 = \frac{1}{2} + i\omega, \quad \beta_3 = \frac{1}{2} - i\omega,$$

$$\alpha_4 = \frac{1}{2} - i\omega, \quad \beta_4 = \frac{1}{2} + i\omega, \tag{F.9abcd}$$

where $$\omega = \frac{1}{2\pi}\log\left(\frac{1+\zeta}{1-\zeta}\right)$$

Eqn (F.9abcd) are of the same form as often seen in interface cracks between two isotropic media [38,44-47].

b) Matrix crack tip touching the interface($a_1=H_1, b_1>0$ and $a_2<H_2$)

In this case, as x_1 and t approach to H_1, the kernel $k_{11}(x_1,t)$ becomes unbounded.

Let $k^{\circ}_{11s}(r,s)$ be the normalized kernel of $k_{11S}(x_1,t)$, that is:

$$k^{\circ}_{11s}(r,s) = \lambda_{85}\frac{H_1(1-s)\beta_5/|w_1| + H_1|w_1|}{[H_1(1-s)\beta_5/|w_1| + H_1|w_1|]^2 - H_1^2(w_1r)^2}$$

$$+\lambda_{86}\frac{H_1(1-s)\beta_5/|w_1|+H_1|w_3|}{[H_1(1-s)\beta_5/|w_1|+H_1|w_3|]^2-H_1^2(w_3r)^2}$$

$$+\lambda_{87}\frac{H_1(1-s)\beta_5/|w_3|+H_1|w_1|}{[H_1(1-s)\beta_5/|w_3|+H_1|w_1|]^2-H_1^2(w_1r)^2}$$

$$+\lambda_{88}\frac{H_1(1-s)\beta_5/|w_3|+H_1|w_3|}{[H_1(1-s)\beta_5/|w_3|+H_1|w_3|]^2-H_1^2(w_3r)^2}$$

$$=\frac{\lambda_{85}|w_1|}{2\beta_5}\left[\frac{1}{H_1(1-s+(1+r)\frac{|w_1|^2}{\beta_5})}+\frac{1}{H_1(1-s+(1-r)\frac{|w_1|^2}{\beta_5})}\right]$$

$$\frac{\lambda_{86}|w_1|}{2\beta_5}\left[\frac{1}{H_1(1-s+(1+r)\frac{|w_1||w_3|}{\beta_5})}+\frac{1}{H_1(1-s+(1-r)\frac{|w_1||w_3|}{\beta_5})}\right]$$

$$\frac{\lambda_{87}|w_3|}{2\beta_5}\left[\frac{1}{H_1(1-s+(1+r)\frac{|w_1||w_3|}{\beta_5})}+\frac{1}{H_1(1-s+(1-r)\frac{|w_1||w_3|}{\beta_5})}\right]$$

$$\frac{\lambda_{88}|w_3|}{2\beta_5}\left[\frac{1}{H_1(1-s+(1+r)\frac{|w_3|^2}{\beta_5})}+\frac{1}{H_1(1-s+(1-r)\frac{|w_3|^2}{\beta_5})}\right] \qquad \text{(F.10)}$$

Substituting eqn(F.10) into eqn(3.29a) and move the bounded terms to the right hand side of the equation, we have:

$$\frac{1}{\pi}\int_{-1}^{1}\left\{\frac{1}{s-r}+\pi H_1\frac{\lambda_{85}|w_1|}{2\beta_5}\left[\frac{1}{H_1(1-s+(1+r)\frac{|w_1|^2}{\beta_5})}+\frac{1}{H_1(1-s+(1-r)\frac{|w_1|^2}{\beta_5})}\right]\right.$$

$$+\pi H_1\frac{\lambda_{86}|w_1|}{2\beta_5}\left[\frac{1}{H_1(1-s+(1+r)\frac{|w_1||w_3|}{\beta_5})}+\frac{1}{H_1(1-s+(1-r)\frac{|w_1||w_3|}{\beta_5})}\right]$$

$$\left.+\pi H_1\frac{\lambda_{87}|w_3|}{2\beta_5}\left[\frac{1}{H_1(1-s+(1+r)\frac{|w_1||w_3|}{\beta_5})}+\frac{1}{H_1(1-s+(1-r)\frac{|w_1||w_3|}{\beta_5})}\right]\right.$$

$$+\pi H_1\frac{\lambda_{88}|w_3|}{2\beta_5}\left[\frac{1}{H_1(1-s+(1+r)\frac{|w_3|^2}{\beta_5})}+\frac{1}{H_1(1-s+(1-r)\frac{|w_3|^2}{\beta_5})}\right]\}\phi_1^o(s)ds$$

$$=\frac{1-\nu_{xy}\nu_{yx}}{2\gamma_{14}E_y}p_1(r)+\quad\text{bounded terms}\tag{F.11}$$

Applying eqns (F.1a) and (F.2) to (F.11), and let $\alpha_1=\beta_1=\gamma$, we have:

$$\frac{F_1^o(-1)\cot(\pi\gamma)}{(2)^\gamma(1+r)^\gamma}-\frac{F_1^o(1)\cot(\pi\gamma)}{(2)^\gamma(1-r)^\gamma}+\frac{\lambda_{85}}{2}\frac{|w_1|}{\beta_5}\frac{F_1^o(1)}{(2)^\gamma\sin(\pi\gamma)\left[\frac{w_1^2}{\beta_5}\right]^\gamma}\left[\frac{1}{(1+r)^\gamma}+\frac{1}{(1-r)^\gamma}\right]$$

$$+\frac{\lambda_{86}}{2}\frac{|w_1|}{\beta_5}\frac{F_1^o(1)}{(2)^\gamma\sin(\pi\gamma)\left[\frac{|w_1||w_3|}{\beta_5}\right]^\gamma}\left[\frac{1}{(1+r)^\gamma}+\frac{1}{(1-r)^\gamma}\right.$$

$$+\frac{\lambda_{87}}{2}\frac{|w_3|}{\beta_5}\frac{F_1^o(1)}{(2)^\gamma\sin(\pi\gamma)\left[\frac{|w_1||w_3|}{\beta_5}\right]^\gamma}\left[\frac{1}{(1+r)^\gamma}+\frac{1}{(1-r)^\gamma}\right]$$

$$+\frac{\lambda_{88}}{2}\frac{|w_3|}{\beta_5}\frac{F_1^o(1)}{(2)^\gamma\sin(\pi\gamma)\left[\frac{w_3^2}{\beta_5}\right]^\gamma}\left[\frac{1}{(1+r)^\gamma}+\frac{1}{(1-r)^\gamma}\right]$$

$$=\frac{1-\nu_{xy}\nu_{yx}}{2\gamma_{14}E_y}p_1(r)+\quad\text{bounded terms}\tag{F.12}$$

Multiplying both sides of eqn (F.12) by $(1+r)^\gamma$ and let $r\to -1$, we have:

$$-2\cos(\pi\gamma)+\lambda_{85}\frac{|w_1|}{\beta_5}\frac{1}{\left[\frac{w_1^2}{\beta_5}\right]^\gamma}+\lambda_{86}\frac{|w_1|}{\beta_5}\frac{1}{\left[\frac{|w_1||w_3|}{\beta_5}\right]^\gamma}$$
$$+\lambda_{87}\frac{|w_3|}{\beta_5}\frac{1}{\left[\frac{|w_1||w_3|}{\beta_5}\right]^\gamma}+\lambda_{88}\frac{|w_3|}{\beta_5}\frac{1}{\left[\frac{w_3^2}{\beta_5}\right]^\gamma}=0\tag{F.13}$$

This result is the same as given in [22].

c) H-shaped cracks ($a_1=H_1$, $b_1=0$ and $a_2>0$)

As $a_1 \rightarrow H_1$ and $b_1 \rightarrow 0$, the transverse crack intersects with the interface crack and the kernels K_{11}, K_{13}, K_{14}, K_{31} and K_{41} become unbounded. Let α be the index of singularity at the point of intersection, then we have:

$$\phi_1(t)=\frac{F_1(t)}{(H_1^2-t^2)^{\alpha}}, \qquad \phi_3(t)=\frac{F_3(t)}{t^{\alpha}(H_1-t)^{\beta_3}} \quad \text{and} \quad \phi_4(s)=\frac{F_4(t)}{t^{\alpha}(H_1-t)^{\beta_4}}$$

Substituting above expressions into eqns (3.29acd), we have:

$$\frac{1}{\pi}\int_{-H_1}^{H_1}\{\frac{1}{t-x_1}+\pi\frac{\lambda_{85}|w_1|}{2\beta_5}[\frac{1}{(H_1-t+(H_1+x_1)\frac{|w_1|^2}{\beta_5})}+\frac{1}{(H_1-t+(H_1-x_1)\frac{|w_1|^2}{\beta_5})}]$$

$$+\pi\frac{\lambda_{86}|w_1|}{2\beta_5}[\frac{1}{(H_1-t+(H_1+x_1)\frac{|w_1||w_3|}{\beta_5})}+\frac{1}{(H_1-t+(H_1-x_1)\frac{|w_1||w_3|}{\beta_5})}]$$

$$+\pi\frac{\lambda_{87}|w_3|}{2\beta_5}[\frac{1}{(H_1-t+(H_1+x_1)\frac{|w_1||w_3|}{\beta_5})}+\frac{1}{(H_1-t+(H_1-x_1)\frac{|w_1||w_3|}{\beta_5})}]$$

$$+\pi\frac{\lambda_{88}|w_3|}{2\beta_5}[\frac{1}{(H_1-t+(H_1+x_1)\frac{|w_3|^2}{\beta_5})}+\frac{1}{(H_1-t+(H_1-x_1)\frac{|w_3|^2}{\beta_5})}\}\frac{F_1(t)}{(H_1^2-t^2)^{\alpha}}dt$$

$$+\int_0^{b_2}[\rho_{13}\frac{|w_1|(H_1-x_1)}{|w_1|^2(H_1-x_1)^2+t^2}+\rho_{14}\frac{|w_3|(H_1-x_1)}{|w_3|^2(H_1-x_1)^2+t^2}]\frac{F_3(t)}{t^{\alpha}(b_2-t)^{\beta_3}}dt$$

$$+\int_0^{b_2}[\rho_{15}\frac{|t}{|w_1|^2(H_1-x_1)^2+t^2}+\rho_{16}\frac{t}{|w_3|^2(H_1-x_1)^2+t^2}]\frac{F_4(t)}{t^{\alpha}(b_2-t)^{\beta_4}}dt$$

$$= \frac{1-\nu_{xy}\nu_{yx}}{2\gamma_{14}E_x} p_1(r) + \text{bounded terms} \qquad \text{(F.14)}$$

$$\int_{-H_1}^{H_1} \{\frac{1}{2\gamma_{13}\pi}[-\gamma_1 \frac{H_1-t}{\frac{|w_1|^2 y^2}{\beta_5^2}+(H_1-t)^2} + \frac{\gamma_2\gamma_{11}}{\gamma_{12}} \frac{H_1-t}{\frac{|w_3|^2 y^2}{\beta_5^2}+(H_1-t)^2}]$$

$$+ \rho_5 \frac{\frac{(H_1-t)\beta_5}{|w_1|}}{\frac{(H_1-t)^2\beta_5^2}{|w_1|^2}+y^2} + \rho_6 \frac{\frac{(H_1-t)\beta_5}{|w_3|}}{\frac{(H_1-t)^2\beta_5^2}{|w_3|^2}+y^2}\} \frac{F_1(t)}{(H_1^2-t^2)^\alpha} dt$$

$$+\frac{\rho_1}{2}\phi_3(y) + \frac{\rho_2}{2\pi}\int_0^{b_2} (\frac{1}{t-y}+\frac{1}{t+y}) \frac{F_4(t)}{t^\alpha (b_2-t)^{\beta_4}} dt$$

$$= \frac{1-\nu_{xy}\nu_{yx}}{2E_x} p_3(y) \quad + \quad \text{bounded terms} \qquad \text{(F.15)}$$

$$\int_{-H_1}^{H_1} \{\frac{\gamma_{11}}{2\gamma_{13}\pi}[\frac{\frac{|w_1|y}{\beta_5}}{\frac{|w_1|^2 y^2}{\beta_5^2}+(H_1-t)^2} + \frac{\frac{|w_3|y}{\beta_5}}{\frac{|w_3|^2 y^2}{\beta_5^2}+(H_1-t)^2}]$$

$$+ \rho_9 \frac{y}{\frac{(H_1-t)^2\beta_5^2}{|w_1|^2}+y^2} + \rho_{10} \frac{y}{\frac{(H_1-t)^2\beta_5^2}{|w_3|^2}+y^2}\} \frac{F_1(t)}{(H_1^2-t^2)^\alpha} dt$$

$$+\frac{\rho_4}{2}\phi_4(y) + \frac{\rho_3}{2\pi}\int_0^{b_2} (-\frac{1}{t-y}+\frac{1}{t+y}) \frac{F_3(t)}{t^\alpha (b_2-t)^{\beta_3}} dt$$

$$= \frac{1}{2G_{xy}} p_4(y) \quad + \quad \text{bounded terms} \qquad \text{(F.16)}$$

Multiplying both sides of eqns (F.14-16) by t^α and let $t \to 0$, we then have the following three algebraic equations for $F_1(H_1)$, $F_3(0)$ and $F_4(0)$ with α yet to be determined:

$$\{-\frac{\cot(\pi\alpha)}{(2H_1)^\alpha} + \frac{\lambda_{85}}{2}\frac{|w_1|}{\beta_5}\frac{1}{(2H_1)^\alpha \sin(\pi\alpha)[\frac{w_1^2}{\beta_5}]^\alpha} + \frac{\lambda_{86}}{2}\frac{|w_1|}{\beta_5}\frac{1}{(2H_1)^\alpha \sin(\pi\alpha)[\frac{|w_1||w_3|}{\beta_5}]^\alpha}$$

$$+\frac{\lambda_{87}}{2}\frac{|w_3|}{\beta_5}\frac{1}{(2H_1)^\alpha \sin(\pi\alpha)[\frac{|w_1||w_3|}{\beta_5}]^\alpha}+\frac{\lambda_{88}}{2}\frac{|w_3|}{\beta_5}\frac{1}{(2H_1)^\alpha \sin(\pi\alpha)[\frac{w_3^2}{\beta_5}]^\alpha}\}F_1(H_1)$$

$$+\frac{\pi}{2b_2^\beta \cos(\frac{\pi\alpha}{2})}[\frac{\rho_{13}}{|w_1|^\alpha}+\frac{\rho_{14}}{|w_3|^\alpha}]F_3(0)+\frac{\pi}{2b_2^\beta \sin(\frac{\pi\alpha}{2})}[\frac{\rho_{15}}{|w_1|^\alpha}+\frac{\rho_{16}}{|w_3|^\alpha}]F_4(0)=0 \qquad \text{(F.17a)}$$

$$-\{\frac{1}{2\gamma_{13}}[-\gamma_1(\frac{\beta_5}{|w_1|})^\alpha+\gamma_2\frac{\gamma_{11}}{\gamma_{12}}(\frac{\beta_5}{|w_3|})^\alpha]+$$

$$\pi[\rho_5\frac{|w_1|}{\beta_5}(\frac{\beta_5}{|w_1|})^\alpha+\rho_6\frac{|w_3|}{\beta_5}(\frac{\beta_5}{|w_3|})^\alpha]\}\frac{1}{(2H_1)^\alpha \sin(\frac{\pi\alpha}{2})}F_1(H_1)+\frac{\rho_1}{b_2^\beta}F_3(0)$$

$$+\frac{\rho_2}{b_2^\beta}[\cot(\pi\alpha)+\frac{1}{\sin(\pi\alpha)}]F_4(0)=0 \qquad \text{(F.17b)}$$

$$-\{\frac{\gamma_{11}}{2\gamma_{13}}[(\frac{\beta_5}{|w_1|})^\alpha+(\frac{\beta_5}{|w_3|})^\alpha]+\pi[\rho_9\frac{|w_1|}{\beta_5}(\frac{\beta_5}{|w_1|})^\alpha+\rho_{10}\frac{|w_3|}{\beta_5}(\frac{\beta_5}{|w_3|})^\alpha]\}\frac{1}{(2H_1)^\alpha \cos(\frac{\pi\alpha}{2})}F_1(H_1)$$

$$+\frac{\rho_3}{b_2^\beta}[-\cot(\pi\alpha)+\frac{1}{\sin(\pi\alpha)}]F_3(0)+\frac{\rho_4}{b_2^\beta}F_4(0)=0 \qquad \text{(F.17c)}$$

Since $F_1(H_1)$, $F_3(0)$ and $F_4(0)$ are generally assumed nonzero, therefore the characteristic equation associated with eqns (F.17abc) has to be zero. Numerical calculations indicate that α is 0 as expected.

REFERENCES

[1] B. M. Liaw, S. J. Zhang and F. Delale, "An Experimental Technique for Tensile Testing of Ceramic Matrix Composites in SEM at Elevated Temperature," *Advances in Experimental Mechanics and Biomimetics*, AD-Vol. 29/AMD-Vol. 146, ed. by W. F. Jones and J. M. Whitney, The American Society of Mechanical Engineers, New York, 1992, pp. 1-12.

[2] Schioler, L. J. and Stiglich, J. J., Jr. "Ceramic matrix composites: a literature review. *Ceramic Bull.* **65**, 289-292, 1986.

[3] Cornie, J. A., Chiang, Y., M., Uhlmann, D. R., Mortensen, A. and Collins, J. M. "Processing of metal and ceramic matrix composites." *Ceramic Bull.* **65**, 293-304, 1986.

[4] Ichinose, N. (Editor) *Introduction to Fine Ceramics Applications in Engineering.* Wiley, New York, 1987.

[5] Wachtman, J. B., Jr (Editor) *Structural Ceramics, Treatise on Materials Science and Technology*, Vol. 29, 1989. Academic Press, New York.

[6] Phillips, D. C. "The fracture energy of carbon-fiber reinforced glass." *J. Mater. Sci.* 7, 1175-1191, 1972.

[7] Gomina, M., Chermant, J. L., Osterstock, F., Bernhart, G. and Mace, J. "Applicability of fracture mechanics to fiber-reinforced CVD-ceramic composites." *Fracture Mechanics of Ceramics* (Edited by R. C. Bradt *et al.*), Vol. 7, pp. 17-32, 1986. Plenum Press, New York.

[8] Prewo, K. M. and Brennan, J. J. "High-strength silicon carbide fiber-reinforced glass-matrix composites." *J. Mater. Sci.* **15**, 463-468, 1980.

[9] Brennan, J. J. and Prewo, K. M. "Silicon carbide fiber reinforced glass-ceramic matrix composites exhibiting high strength and toughness." *J. Mater. Sci.* **17**, 2371-2383, 1982.

[10] Mah, T., Mendiretta, M. G., Katz, A. P., Ruh, R. and Mazdiyasni, K. S. "Room-temperature mechanical behavior of fiber-reinforced glass-ceramic-matrix composites." *J. Am. Ceramic Soc.* **68**, C27-C30, 1985.

[11] Mah, T., Mendiretta, M. G., Katz, A. P., Ruh, R. and Mazdiyasni, K. S. "High-temperature mechanical behavior of fiber-reinforced glass-ceramic-matrix composites." *J. Am. Ceramic Soc.* **68**, C248-C251, 1985.

[12] Marshall, D. B. and Evans, A. G. "Failure mechanisms in ceramic-fiber/ceramic-matrix composites. *J. Am. Ceramic Soc.* **68**. 225-231, 1985.

[13] Marshall, D. B. and Evans, A. G. "The tensile strength of uniaxially reinforced ceramic fiber composites." In *Fracture Mechanics of Ceramics* (Edited by R. C. Bradt, *et al.*), Vol. 7, pp. 1-15, 1986. Plenum Press, New York.

[14] Stewart, R. L., Chyung, K., Taylor, M. P. and Cooper, R. F. "Fracture of SiC/glass-ceramic composites as a function of temperature." In *Fracture Mechanics of Ceramics* (Edited by R. C. Bradt, *et al.*), Vol. 7, pp. 33-51, 1986. Plenum Press, New York.

[15] Jenkins, M. G., Kobayashi, A. S., White, K. W. and Bradt, R. C. "Crack initiation and arrest in a SiC whisker/Al_2O_3 matrix composite." *J. Am. Ceramic Soc.* **70**. 393-395. 1987.

[16] Singh, R. N. and Gaddipati, A. R. "Mechanical properties of a uniaxially reinforced mullite-silicon carbide composite," *J. Am. Ceramic Soc.* **71**. C100-C103. 1988.

[17] Xu, Y. L., Delale, F. and Liaw, B. M. "Effect of temperature and fiber distribution on matrix cracking in ceramic matrix composites." *Composites Engng* **2**, 67-79. 1992.

[18] Karandikar, P. and Chou, T. W. "Characterization and Modeling of Microcracking and Elastic Moduli Changes in Nicalon/CAS Composites." *Composites Science and Technology* Vol 46, 253-263, 1993.

[19] Daniel, I. M. and Anastassopoulos, G. "The Behavior of Ceramic Matrix Fiber Composites Under Longitudinal Loading." *Composites Science and Technology* Vol 46, 105-113, 1993.

[20] Barsoum, M. W., Kangutkar, P. and Wang, A. S. D. "Matrix Crack Initiation in Ceramic Matrix Composites Part I: Experiments and Test Results." *Composites Science and Technology* Vol 44, 257-269, 1992.

[21] A. S. D.Wang, X. G. Huang and Michel W. Barsoum, "Matrix Crack Initiation in Ceramic Matrix Composites Part II: Models and Simulation Results." *Composites Science and Technology* Vol 44, 271-282, 1992.

[22] F. Delale, "Fracture of Composite Orthotropic Plate Containing Periodic Buffer Strips," Ph.D. Dissertation, Lehigh University (1976).

[23] F. Erdogan, " Approximate Solutions of Systems of Singular Integal Equations ", *SJAM J. Appl. Math*. Vol. 17, No. 6. November 1969.

[24] F. Erdogan, "Mixed Boundary-Value Problems in Mechanics," *Mechanics Today*, (Edited by S. Nemat-Nasser) Vol. 4, Pergamon Press, Oxford, p. 1, 1978.

[25] M. A. Golberg, " Numerical Solution of Integral Equations", Plenum Press, New York, 1990.

[26] A. H. Stroud and D. Secrest, "Gaussian Quadrature Formulas", Prentice-Hall, Englewood Cliffs, New Jersey, 1966.

[27] P. J. Davis and P. Rabinowitz, " Methods of numerical Integration", Second Edition, Academic Press, New York, New York, 1984.

[28] N. I. Muskhelishvili, " Singular Integral Equations ", Noordhoff, Groningen, Holland, 1953.

[29] A. Ghizzetti and A. Ossicini, "Quadrature Formulae", Academic Press, New York, 1970.

[30] Z. Kopal, "Numerical Alalysis", Second Edition. John Wiley & Sons Inc. New York 1961.

[31] N. I. Ioakimidis and P. S. Theocaris, "On the Numerical Solution of a Class of Singular Integral Equations", *Journal of Mathematical and Physical Sciences*. Vol. 11, pp 219-235, 1977.

[32] P. S. Theocaris and N. I. Ioakimidis, " Numerical Solution of Cauchy Type Singular Equations", Transactions of Academy of Athens. Vol. 40, pp 1-39, 1977.

[33] N. I. Ioakimidis and P. S. Theocaris, "On the Selection of Collocation Points For the Numerical Solution of Singular Integral Equations With Generalized Kernels Appearing in Elasticity Problems", *Computers & Structures*. Vol. 11. pp 289-295. 1978.

[34] N. I. Ioakimidis and P. S. Theocaris, "Numerical Evaluation of a Class of Generalized Stress Intensity Factors by Use of the Lobatto-Jacobi Numerical Integration Rule", *Int. Journal of Fracture*. Vol. 14. pp 469-484. 1978.

[35] M. H. Lewis and V. S. R. Murthy, "Microstructural Characterization of Interfaces in Fibre-Reinforced Ceramics", *Composites Science and Technology*, Vol. 42, pp 221-249, 1991.

[36] A. G. Evans, F. W. Zok annd J. Davis, "The Role of Interaces in Fiber-Reinforced Brittle Matrix Composites", *Composites Science and Technology*, Vol. 42, pp 3-24, 1991.

[37] T. L. Anderson, "Fracture Mechanics: Fundamentals and Applications", CRC Press, Inc. 1991.

[38] F. Erdogan and G.D. Gupta ,"Layered Composites with an interface Flaw," International Journal of Solids and Structures, Vol. 7, p. 1089, 1971.

[39] J. R. Rice and G. C. Sih, "Plane Problems of Cracks in Dissimilar Media", *Transactions of ASME*. June 1965.

[40] B. M. Malyshev and R. L. Salganik, "The Strength of Adhesive Joints Using The Theory of Cracks", *Int. Journal of Fracture Mechanics*. Vol. 1. 114-127 1965.

[41] Tada, H., Paris, P. C., and Irwin, G. R., "The stress Analysis of Cracks Handbook", (2nd Ed.) Paris Productions, Inc, St. Louis, 1985.

[42] J. R. Rice, "Elastic Fracture Mechanics Concepts for Interface Cracks", *Transactions of ASME*. Vol 55, Marcch 1988.

[43] G. P. Cherepanov, "Mechanics of Brittle Fracture", McGra-Hill, New York, 1979.

[44] F. Erdogan and G.D. Gupta, "The Stress Analysis of Multi-Layered Composites with a Flaw," *International Journal of Solids and Structures*, Vol. 7, p. 39, 1971.

[45] M.C. Lu and F. Erdogan, "Stress Intensity Factors in Two Bonded Elastic Layers Containing cracks Perpendicular to and on the Interface, Part I. Analysis," *Engineering Fracture Mechanics*, Vol. 18, pp. 491-506, 1983.

[46] M.C. Lu and F. Erdogan, "Stress Intensity Factors in Two Bonded Elastic Layers Containing cracks Perpendicular to and on the Interface, Part II. Solution and Results," *Engineering Fracture Mechanics*, Vol. 18, pp. 507-528, 1983.

[47] M. C. Lu, "A Composite of Two Bounded Strips Containing Perpendicular Cracks And An Interface Crack ", Ph.D. Dissertation, Lehigh University (1978).

VITA

Mr. Shaojin Zhang was born on June 8, 1958 in the city of Taiyuan, P.R. China to father Reiwen Zhang and mother Liqing Xia. He graduated from Taiyuan No. 29 middle school in Fall 1975. Two years later, after the ending of the turmoil of the "Cultural Revolution" in China, Mr. Zhang was enrolled in Taiyuan Heavy Machinery Institute majoring in Machine Design and he received the Bachelor of Engineering in Mechanical Engineering in February 1982.

From March 1982 to July 1985, Mr. Zhang was employed by Taiyuan Heavy Machinery Institute as a lecturer in the Mining Machinery Section, Department of Mechanical Engineering. He then came to America to pursue graduate study.

Mr. Zhang received the Master of Engineering degree at the City College of New York in September, 1987. He is currently a Research Assistant and an Adjunct Lecturer in the Department of Mechanical Engineering at CUNY City College campus.